Kwame Nkrumah University of Science and Technology
College of Engineering
Department of Geomatic Engineering

Retrieval of Integrated Water Vapour from GNSS Signals for Numerical Weather Predictions

by

Akwasi Afrifa Acheampong, MPhil, MGhIE

Thesis submitted in partial fulfilment for the award of the degree of Doctor of Philosophy in GEOMATIC ENGINEERING

August 2015

Supervisors: **Prof. Collins Fosu**
Department of Geomatic Engineering, KNUST, Kumasi - GHANA

Dr. Leonard Kofitse Amekudzi
Department of Physics, KNUST, Kumasi - GHANA

Prof. Eigil Kaas
Niels Bohr Institute, Univ. of Copenhagen

Declaration of Authorship

I, *Akwasi Afrifa Acheampong*, declare that this thesis titled, *'Retrieval of Integrated Water Vapour from GNSS Signals for Numerical Weather Predictions'* and the work presented in it are my own. I confirm that:

This work was done wholly while in candidature for a research degree at this University and no part of this thesis has previously been submitted for a degree or any other qualification at this University or any other institution.

Where I have consulted the published work of others, due acknowledgements and citations have been provided. With the exception of such quotations, this thesis is entirely my own work.

Signed: .... Date: ....

Akwasi Afrifa Acheampong

(PhD Candidate)

Signed: .... Date: ....

Prof. Collins Fosu

(Supervisor)

Signed: .... Date: ....

Dr. Isaac Dadzie

(Internal Examiner)

"Life is a stage, rise up early, prepare well and act your part with honesty and diligence and leave the rest to Tweduanpon"

Kwasi Acheampong Atta-Badu

Abstract

Atmospheric Water vapour is an important greenhouse gas and contributes greatly in maintaining the Earth's energy balance. This critical meteorological parameter is not sensed by any facility in Ghana contributing weather data to the Global Telecommunication System of WMO. This thesis presents a highly precise tool for water vapour sensing based on the concept of Global Navigation Satellite Systems (GNSS) meteorology and tests the computed results against global reanalysis data. Conventional approaches used to sense the atmospheric water vapour or precipitable water (PW) or Integrated Water Vapour such as radiosondes, hygrometers, microwave radiometers or sun photometers are affected by meteorological conditions, expensive and have coverage limitations. However, GNSS meteorological concept offers an easier, inexpensive and all-weather technique to retrieve PW or IWV from Zenith Tropospheric Delays over a reference station with very high temporal resolutions. This study employed precise point positioning (PPP) techniques to quantify the extent of delays on the signal due to the troposphere and stratosphere media where the atmospheric water vapour resides. The KNUST GPS Base station was used to log dual-frequency signals for approximately 260days between the months of February 2013 to December 2014. Stringent processing criteria were set using an elevation cut-off of 5^{o}, precise orbital and clock products, Antex files, nominal tropospheric correction and mapping functions. The delays which were originally slanted are mapped unto the zenith direction and integrated with surface meteorological parameters to retrieve PW or IWV. This research work investigated the applications of ground-based GNSS to meteorology and gives all correction models implemented in PPP and for Tropospheric delay estimation.The gLAB software was used for ZTD computations. PW values obtained were compared with ERA-Interim, Japanese Meteorological Agency Reanalysis (JRA) and National Centres for Environmental Prediction (NCEP) global reanalysis data. Correlation analysis were run on computed PW from logged GNSS datasets and downscaled reanalysis data. The obtained results show stronger correlation between the retrieved PW values and those provided by the ERAinterim. The computed amount of ZTDs varies perfectly with weather pattern in the country. Again, a linear-model was derived that could predict PW based on ZTD with standard errors of 6.01mm for JRA, 5.40mm for ERA-Interim and 6.34mm for NCEP reanalysis data. Finally, the study results indicate that with a more densified network of GNSS base stations the retrieved PW or IWV will greatly improve numerical weather predictions and more specifically precipitation forecasting in Ghana.

Keywords: *GNSS, PPP, gLAB software, Reanalysis, Integrated Water Vapour, Precipitable Water, ERA-Interim, NCEP, JRA*

Acknowledgements

My greatest appreciation goes to the Lord Almighty for bringing me this far throughout my course. Next, I wish to convey sincere gratitudes to Profs. Collins Fosu, Leonard K. Amekudzi and Eigil Kaas for accepting me as their student. Your support, guidance and valuable suggestions were of immense importance to this dissertation.

Special thanks go to all the staff members of the Geomatic Engineering Department, KNUST, Niels Bohr Institute and Danida Fellowship Center, Copenhagen - Denmark. This thesis benefited greatly from funds, seminars and equipment from the Building Stronger Universities' Environment and Climate Platform under Danish International Development Agency (DANIDA). To the Platform Chairman, Coordinators (both local and abroad) and officers at the International Programs Office of KNUST and DANIDA Fellowship Centre, Copenhagen, I am most grateful.

Last but not the least, I would like to extend special thanks to my family and all my friends. Your company, friendship, support and encouragement in times of need were invaluable. May God richly bless you all.

Contents

List of Figures

List of Tables

Abbreviations

AC	**A**nalysis **C**entre
ECMWF	**E**uropean **C**entre for **M**edium-Range **W**eather **F**orecasts
GRIB	**GRI**dded **B**inary or **G**eneral **R**egularly-distributed **I**nformation in **B**inary
GMet	**G**hana **Met**eorological **A**gency
GNSS	**G**lobal **N**avigation **S**atellite **S**ystem
GPS	**G**lobal **P**ositioning **S**ystem
GUAN	**G**lobal Climate Observing System (GCOS) **U**pper-**A**ir **N**etwork
IGS	**I**nternational **G**NSS **S**ervice
IWV	**I**ntegrated **W**ater **V**apour
JRA	**J**apanese 55-year **R**e**A**nalysis
KNUST	**K**wame **N**krumah **U**niversity of **S**cience and **T**echnology
LEO	**L**ow **E**arth **O**rbit
LIDAR	**LI**ght **D**etection **A**nd **R**anging
NASA	**N**ational **A**eronautics and **S**pace **A**dministration
NCEP	**N**ational **C**enters for **E**nvironmental **P**rediction
NetCDF	**Net**work **C**ommon **D**ata **F**orm
NOAA	**N**ational **O**ceanic and **A**tmospheric **A**dministration
NWP	**N**umerical **W**eather **P**rediction
PNT	**P**ositioning **N**avigational and **T**iming
PPP	**P**recise **P**oint **P**ositioning
PW	**P**recipitable **W**ater
RMS	**R**oot **M**ean **S**quare
RO	**R**adio **O**ccultation
STD	**S**lant **T**otal **D**elay
TOUGH	**T**argeting **O**ptimal **U**se of **G**PS **H**umidity Measurements in Meteorology
WMO	**W**orld **M**eteorological **O**rganization
WV	**W**ater **V**apour
ZHD	**Z**enith **H**ydrostatic **D**elay
ZTD	**Z**enith **T**otal **D**elay
ZWD	**Z**enith **W**et **D**elay

Physical Constants

Speed of Light	c	=	$2.997\,924\,58 \times 10^8\ \mathrm{ms}^{-1}$ (exact)
	Π	=	0.1629
	k_1	=	77.60 ± 0.05 K/hPa
	k_2	=	77.40 ± 2.2 K/hPa
	k_2'	=	22.10 ± 2.2 K/hPa
	k_3	=	$373900 \pm 1200\ \mathrm{K}^2/hPa$
Molar mass of dry air	m_d	=	28.9644 ± 0.0014 g/mol
Molar mass of water vapour	m_w	=	$18.01528\, g/mol$
Universal Gas constant	R	=	$8.314345 \pm 0.00007\ \mathrm{Jmol}^{-1} K^{-1}$

Symbols

ε	satellite elevation angle	*degrees*
e	partial pressure of water vapour	*hPa*
g	gravitational acceleration	m/s^2
g_m	gravitational acceleration at the mass centre	m/s^2
H	surface height above the geoid	m
M_d	molar mass of dry gases	g/mol
M_w	molar mass of water vapour	g/mol
n	atmospheric refractive index	
N	refractivity	*kelvin*
θ	station latitude	*degrees*
P_s	total ground pressure	*hPa*
p_d	partial pressure of dry gases	*hPa*
ρ_w	density of liquid water	kg/m^3
p_v	partial density water vapour	kg/m^3
R	universal gas constant	J/kgK
R_d	specific gas constant for dry constituent	J/kgK
R_w	specific gas constant for water vapour	J/kgK
T	absolute temperature	*kelvin*
T_M	mean temperature	*kelvin*
T_s	surface temperature	*kelvin*
Z_d	compressibility factor for dry gases	
Z_w	compressibility factor for moist air	

To my family...most especially Paapa - tho' you're not with us but my promise to you has seen daylight

Chapter 1

Introduction

Human existence and our quest to adapt comfortably to the natural environment are impacting negatively on climate and weather patterns (Acheampong, 2012). The ultimate challenge for researchers and scientists in meteorology is to appreciate the processes that determine the state of the climate and the varied ways that might have influenced this change in the past and/or will be in the future. Climatic[1] studies and numerical weather predictions entail the use of mathematical models based on systems of differential equations that consider a 3D grid over the surface in question (Buizza, 2002, Lynch, 2008, Shuman, 1978). Climate and weather models are evaluated by studying interactions between the Sun's energy, atmosphere, oceans, land, living things, ice, and its effect on each other (Acheampong, 2012, Baede et al., 2001).

Atmospheric conditions and weather patterns are modelled using wind, heat transfer, radiation, relative humidity and surface hydrological parameters based on the laws of physics and the basic properties of the atmosphere. The developed models are used to describe vividly rising earth surface temperature, increasing greenhouse gases, precipitations, decreasing ice and other geophysical phenomena (Soos, 2010). As stated by Bader et al. (2008) these climate simulations provide a framework for enhanced understanding of climate-relevant processes, especially in projecting temperature changes and

[1] Climatic conditions of an area is established by averaging the weather phenomena for a longer period of time - preferably 30 years

frequency of heavy precipitations resulting from increases in atmospheric concentrations of greenhouse gases. The effectiveness of greenhouse gases influence on climatic patterns depends directly on its atmospheric concentration and their capacities to absorb thermal infra red energy radiated from the Earth (Watson et al., 1990). Water vapour is the single most important greenhouse gas with its atmospheric concentration not significantly influenced by direct anthropogenic emissions and accounting for about 95% of Earth's greenhouse effect (Hieb, 2007, Seidel, 2002, USGS-Eds, 2011). It influences many things like condensation, clouds formation, rains, as well as how hot or cold the surface feels. According to Solomon et al. (2007), an estimated 70% of the recent rises in atmospheric temperature are attributed to water vapour feedback.

The water vapour content of the atmosphere is highly variable both in space and in time due to temperature changes, atmospheric circulation and other micro-physical processes (Hoffman, 2010, Pottiaux, 2010). The atmospheric holding capacity for water vapour doubles for every 10^{o} C rise in temperature (Ahrens, 2012, Carter, 2004). 99% in terms of volume of the total atmospheric water vapour resides in the troposphere, ranging in depth from 9 km at the poles to 16 km at the equator (K¨ampfer, 2013, Tao, 2008). The distribution of water vapour in the horizontal and vertical space is a major parameter in the development of Numerical Weather Prediction (NWP) and the very short-term forecasting or 'nowcasting' community (Emanuel, 1995, Jones, 2010). As reported by Jones et al. (2010) the contribution of water vapour cannot be underestimated and must be measured accurately as it is a key parameter for forecasting extreme weather events and monitoring climate change. Measurement of water vapour by conventional methods using radiosondes, hygrometers and microwave water radiometers according to Wolfe and Gutman (2000) & Solheim and Ware (1997), are inadequate on a global scale. Again they are affected by meteorological conditions and very expensive. Water vapour with its great importance in influencing the weather is under-sampled in current operational meteorological and climate observing systems (Jones et al., 2010)

From Wolfe and Gutman (2000) and Solheim and Ware (1997), existing atmospheric water vapour sensing systems are inadequate on a global scale, hence the need for a sensor that is highly accurate irrespective of adverse meteorological conditions, have modelling capabilities to estimate errors with high temporal and spatial resolution. Plus the added advantages of little or no maintenance requirements and supports operational forecasting of atmospheric conditions. This type of sensor was first proposed by Bevis et al. (1992) based on the concept of GNSS Meteorology and patented by Solheim and Ware (1997). The technique characterizes the propagation delays on the signals caused by the neutral atmosphere (also known as the troposphere), the magnitude of the delayed component is directly proportional to the atmospheric water vapour.

1.1 GNSS Meteorology and Applications

The Global Navigation Satellite System (GNSS), encompassing the US Global Positioning System (GPS), the Russian GLONASS, the European Galileo and the Chinese COMPASS (Beidou), are highly precise, continuous and all-weather system that provide navigation, positioning, surveillance and timing information for ground, marine, aviation and space applications (Enderle, 2003). Microwave signals from the space vehicles propagate through the Earth's atmosphere, and the atmosphere delays the signal resulting in curved and lengthened signal path and speed retardation (Bevis et al., 1992, Businger et al., 1996, Rocken et al., 1995, Wolfe and Gutman, 2000). For geodetic applications the delayed signals due to tropospheric and ionospheric effects are considered as nuisance and an error source but when determined accurately it can be modelled into useful atmospheric parameters (Schu¨ler, 2001).

The concept of GNSS Meteorology uses specialized algorithms, GNSS hardware, atmospheric assumptions and knowledge of the surface meteorological conditions to estimate tropospheric delays and integrated water vapour (IWV) from GNSS Signals (Notarpietro et al., 2012). Sensing meteorological parameters using GNSS signals can be achieved using ground-based surface network of GNSS receivers or space-borne GNSS receivers on board a low Earth orbiting (LEO) satellite (i.e. Radio Occultation techniques) (De Haan, 2008).

Currently ground-based GNSS measurements for characterizing the atmosphere has moved from study and development stage to full operational status around the globe, most importantly the mid-latitude regions. The US initiative is being advanced by the SuomiNet (Ware et al., 2000) and the University Corporation for Atmospheric Research[2]. For Europe the project Targeting Optimal Use of GPS Humidity measurements (TOUGH) was launched in 2003 with major aim of measuring atmospheric delays to obtain high quality atmospheric moisture information from existing networks for European weather prediction assignments (Vedel, 2006). The European National Meteorological Services (EUMETNET) GNSS Water vapour Programme (E-GVAP) was instituted as a follow-up and improvement to the TOUGH project. Under E-GVAP, the approach is geared towards to the use of GPS delay and water vapour measurements for operational meteorology (Vedel et al., 2010). A joint initiative between Japan Meteorological Agency (JMA) and the Geographical Survey Institute is working to deliver IWV products. The framework under the GPS Earth Observation NETwork (GEONET) comprises of approximately one thousand GPS receivers located throughout Japan (Ishihara, 2005).

For effective use of atmospheric moisture information sensed from ground-based GNSS stations, data processing and delivery must be in a timely manner preferably below one hour (Jones et al., 2010). Near real-time delivery latency of approximately 15 minutes is the target of GNSS Meteorological products as an input to NWP models.

Applications - The concept of GNSS Meteorology is used to produce accurate, all weather, global refractive index, pressure and density profiles of the troposphere, ionospheric total electron content (TEC) as well as electron density profiles for use in weather analysis and forecasting, climate change monitoring and monitor ionospheric events (Jin et al., 2010,

[2] http://www2.ucar.edu/

Jin and Komjathy, 2010). Further application is in the field of Earth's surface monitoring using multipath delayed reflections.

1.2 Atmospheric Water Vapour

Water is the only substance in the Earth's environment that exists naturally in significant quantities in all three states: solid(ice), liquid(water) and gas(water vapour) (Brammer et al., 2010, Shakhashiri, 2011). Water in its gaseous phase moves on a global scale transporting enormous amount of latent heat energy to maintain the Earth's energy balance. Water vapour gets to the atmosphere through open-water evaporation (from the ocean, lakes and rivers), land surfaces, sublimation from ice and snow surfaces and evapo-transpiration from vegetation. It then condenses and returns to the earth's surface as precipitation - rain, fog, mist, snow or hail. This cycle takes approximately between 7 to 10 days, the movement includes vertical and horizontal transports, mixing, condensation, precipitation and evaporation (Guerova, 2003). It also serves as an oxidizing agent that cleanses the atmosphere of many air pollutants (Gupta, 2011). Different regions typically contain different amounts of water vapour and this can drastically affect the climate across these regions. Water vapour's distribution and existence is a primary factor behind atmospheric weather systems and climatic conditions. 99.99% of water vapour concentrations come from natural sources and it is by far the dominant player in the Earth's greenhouse gas concentrations (Hieb, 2007).

Water vapour density, water vapour mixing ratio, specific humidity and relative humidity are various definitions used to quantify the amount of water vapour in air (De Haan, 2008). The total amount of water vapour in a vertical column which is widely used in meteorology are expressed using Total Precipitable Water (TPW) or Integrated Precipitable Water (IPW) or Integrated Water Vapour (IWV). The nature and distribution of water vapour affects the vertical stability of the atmosphere, the structure and evolution of storm systems, and the energy balance of the global climate system (Chahine, 1992, Gupta, 2011). Accurate and frequent observations of three-dimensional water vapour would result in significant improvements in weather prediction and climatological research (MacDonald et al., 2002, Notarpietro et al., 2012). This study is aimed at setting the framework for ground-based integrated water vapour extraction or retrieval from tropospheric delay effects on GNSS signals in Ghana.

1.3 Tropospheric Delay

The troposphere is the lowest region of the Earth's atmosphere (see Figure 1.1) and extends from the ground surface up to about 9 km at the poles and exceeds 16 km at the Equator (Brunner and Welsch, 1993, Russell, 2010). It is a thin layer compared to the height of the entire atmosphere but it is also the densest region, containing about 75% of the total atmospheric mass and 99% of its water vapour and aerosols (Januszewski, 2013, Jounot, 1998, Pottiaux, 2010). Almost all atmospheric water vapour or moisture is found in the troposphere. Water vapour concentration varies from trace amounts in polar regions to nearly 4 percent in the tropics (Shrestha, 2003).

GNSS signals which propagate through the Earth's troposphere, are affected significantly due to the variability of the refractive index of the tropospheric medium (Shrestha, 2003). Within the troposphere, all GNSS observables on the carriers and signal information are delayed equally (Kaplan and Hegarty, 2005, Seeber, 2003). The delay is a function of the tropospheric refractive index, which is dependent on the local temperature, pressure, and relative humidity. The variability of tropospheric delay as reported by Jones (2010) is far more difficult to predict, both temporally and spatially as the variable component is directly proportional to atmospheric water vapour. When not mitigated it can introduce range errors equivalent to about 2.3m for a satellite at the zenith (satellite directly overhead), about 9.3m for 15^o elevation angle, and between 20–28m for those at the observer horizon (El-Rabbany, 2002, Leick, 2004).

The tropospheric delay is due to the excess path delay and the bending effects on the radio signal, its computation is done by integrating along the signal path through the troposphere (Mendes, 1999, Shrestha, 2003). The delays associated with the troposphere can be separated into two components- i.e. dry (or hydrostatic) and wet components (Saastamoinen, 1972). The dry component represents about 90% of the total delay and can be predicted accurately using mathematical models since it is entirely dependent on the atmospheric weather characteristics found in the troposphere (El-Rabbany, 2002, Januszewski, 2013). On the other hand, the wet delay is caused solely by water vapour

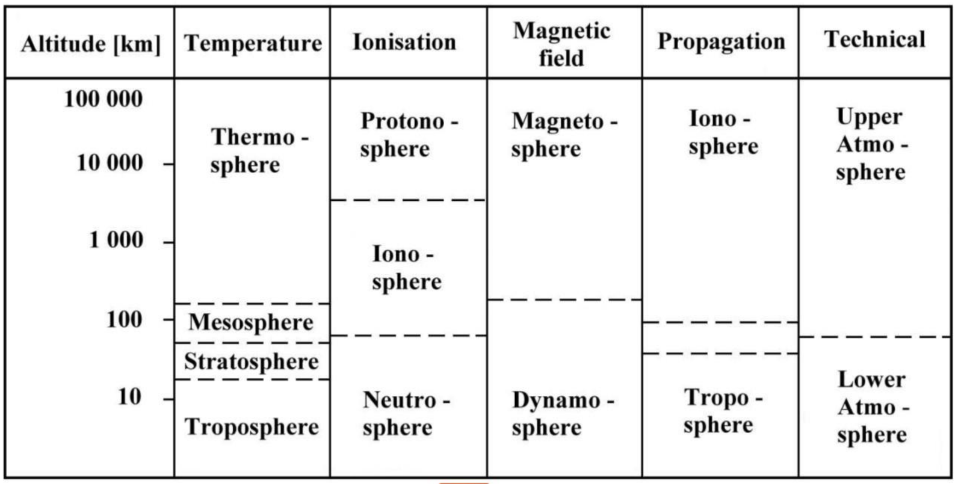

Figure 1.1: Earth's Atmospheric Layers

in the atmosphere which has strong spatial and temporal variabilities (Leick, 2004). By measuring the total delay, and calculating the hydrostatic delay from mathematical models using surface measurements, the remaining wet delay signal, caused by water vapour in the atmosphere, may be recovered for assimilation in Numerical Weather Prediction (NWP) models (Seeber, 2003, Shrestha, 2003).

1.4 Research Problem and Justification

The importance of Water Vapour's quantity and distribution in the atmosphere cannot be underestimated and conventional measurement techniques are expensive, have limited coverage area and affected by weather especially under heavy clouds and precipitation. GNSS meteorological concepts proposed over two decades ago have the potential to overcome all limitations identified in the conventional sensing techniques. However, the much improved network of ground-based GNSS receivers which forms part of the Global Climate Observing System (GCOS) Upper-Air Network (GUAN) (Seidel et al., 2009, Teunissen, 2003), still exhibits substantial data gaps for the African region (refer

Figure 1.2). This research work is aimed at setting the framework for Integrated Water Vapour retrieval using Precise Point Positioning (PPP) techniques for an enhance global weather forecasting by improving coverage and data availability to the GUAN network. Again, GNSS precipitable water (PW) is a useful source of humidity information for Numerical Weather Prediction (NWP) applications (Deblonde et al., 2005, Isioye et al., 2015). However, almost all the studies and projects launched into the exploitation of GNSS for meteorological applications are all in the mid to high latitude regions which has a thinner tropospheric layer than the lower latitude regions closer to the equator.

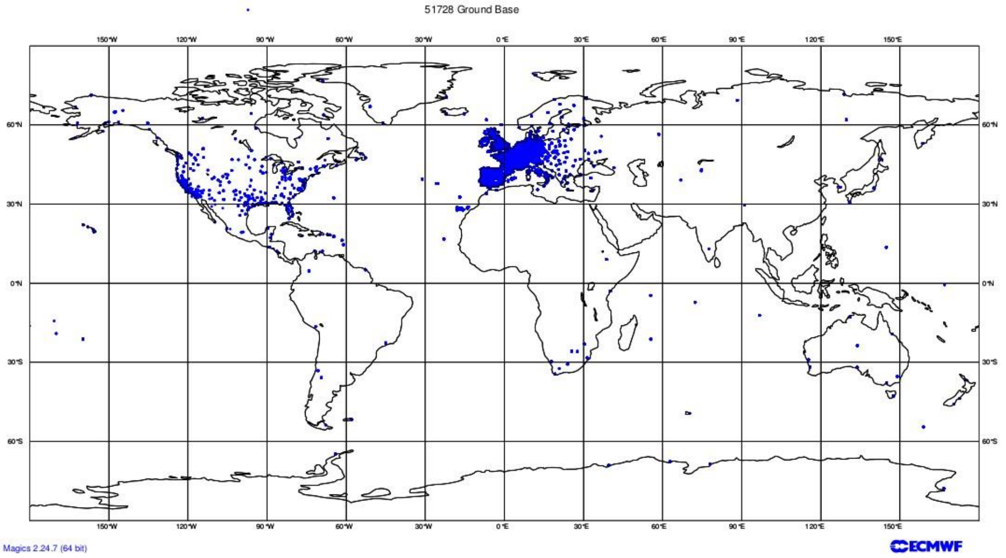

Figure 1.2: Locations of Ground-Based GPS Stations (shown in blue dots) in GUAN. [*ref* : *www.ecmwf.int*]

1.5 Aim and Objectives

This study focuses on the meteorological application of ground-based GNSS for IWV estimations. From the introduction given, GNSS Meteorology has demonstrated improvements in spatial and temporal sampling of atmospheric water vapour.

This study has the following objectives:

(I) Create a database of tropospheric delay products for use by meteorologists and geodesists;

(II) Validate the effectiveness of Global Numerical Weather models at our regional level and

(III) Provide GNSS tropospheric delay estimates for precise positioning applications.

1.6 Thesis Outline

This report is organised in six chapters. This chapter introduces the main work and presents the importance of atmospheric water vapour and the need to measure it accurately as it is a key in assimilating NWP models. The research problem, GNSS meteorological concepts, tropospheric delays on signals propagating through its medium as well as study objectives are outlined in Chapter One.

Chapter Two gives an overview of Global Navigation Satellite Systems, Positioning, PPP correction models and Height systems. The Earth's atmosphere, water vapour and humidity definitions in conjunction with reanalysis data are presented in Chapter Three.

Chapter Four centres mainly on the Methodology and it treats Tropospheric Delays from PPP, Precipitable Water Computations, Processing Techniques and tests conducted on Zenith tropospheric delays. Chapter Five continues with results and discussions, a brief on GNSS Tomography and a proposal for nationwide exploitation of GNSS Meteor is also given. Chapter Six contains a summary of findings and ends by giving some recommendations for future work.

Chapter 2

GNSS, Positioning and Mathematical Models

2.1 GNSS Overview

Global Navigation Satellite Systems (GNSS) is a term used to describe all forms of satellite based navigation systems and encompasses all satellite radio-navigation systems that can be accessed globally and provide signals for navigation, positioning, surveillance and timing information for ground, marine, aviation and space applications (Acheampong, 2009, Hofmann-Wellenhof et al., 2007, Misra and Enge, 2011).

GNSS is composed of two operational space satellite systems, the US Global Positioning System (NAVSTAR GPS), the Russian GLONASS and the upcoming European Global Satellite Navigation System – Galileo and Chinese BieDou (Compass) (Acheampong, 2009). It also includes three operational Satellite Based Augmentation Systems (SBAS); Wide Area Augmentation System (WAAS) of the Federal Aviation Administration – USA, The European Geostationary Navigation Overlay System (EGNOS) and Japanese Multi-functional Satellite Augmentation System (MSAS). These other systems – The Russian System for Differential Corrections and Monitoring (SDCM), Indian GPS and Geostationary Augmented Navigation (GAGAN) and South/Central America and

the Caribbean initiative called Soluci`on de Aumentaci`on para Caribe, Centro y Sudam`erica (SACCSA) are at various stages of development. There are planned proposals and joint venture agreement with the African Union and European Union to develop an SBAS for the African Continent (Scarda, 2010).

GNSS is now a global utility and is affecting all facets of human activities (Gullish and Vaccaro, 2009). The applications scope of GNSS ranges from simple, single benefits for individual users, to enormous, multifaceted benefits for nations of the world (Acheampong, 2009). The scale of these improvements varies from recreational to scientific and safety-of-life applications. Depending on receiver type and tracked signals GNSS usage at any instance depends on:

- Line-of-sight conditions between USER receiver and GNSS constellation
- Receivers Signal-to-Noise-Ratio (SNR) threshold for acquisition and tracking of GNSS signals
- Receiver characteristic for high dynamic environment and the related Doppler frequency shift (Enderle, 2003).

These varied resources and different approaches to use signal-in-space for Positioning Navigational and Timing (PNT) applications are motivated by the fact that GPS and Glonass were originally military systems and can be switched off by system providers in times of combat. With this information, nations are developing systems to retain their navigational capabilities that will not solely be reliant on one GNSS. A more technical motivation is in the combination of multiple signals from different GNSS as a single failure can result in a denial of service to a large number of users. Multiple GNSS do provide greater levels of redundancy and added degree of robustness to GNSS applications (Rizos, 2008).

All GNSS are composed of three (3) main segments: the space, control and user segments. A brief description is given below:-

Space Segment: This segments is basically the space vehicles (SVs) or satellites and provide the platform for atomic clocks, radio transceivers, computers, solar panels for power supply and a propulsion system for orbit adjustments and stability control (Hofmann-Wellenhof et al., 2012). Its main functions are to generate and transmit code and carrier phase signals, and to store and broadcast the navigation message sent to it by the control segment (Misra and Enge, 2011, Subriana et al., 2013).

Control Segment: The tasks of the Control Segment as shown in Subriana et al. (2013), Misra and Enge (2011) and Seeber (2003) are to provide command and control functions in:

- continuously monitoring the whole system
- controlling and maintaining the status and configuration of satellite system
- keeping the corresponding GNSS time scale
- predicting the satellite ephemerides and the behaviour of the satellite clocks
- periodically updating the navigation message for all satellites in the constellation, and
- commanding small manoeuvres to maintain orbit, or relocate to substitute an unhealthy satellite.

User segment: This is mainly the GNSS receivers and information services designed to report constellation status, scheduled outages, and orbital data. User receivers are used to track signals, determine observables (carrier phase, pseudoranges and doppler), solve for navigation equations and compute accurate position, velocity and time (Gaglione, 2015, Rahemi et al., 2014). The basic components of GNSS receivers are: antenna, radio frequency section, microprocessor, power source, data memory storage and user control panel.

2.1.1 Applications of GNSS

The range of applications offered by GNSS is extremely varied with potential spin-offs that has stretched beyond the imaginations of the original system designers. GNSS signals transmitted from satellites in known orbits and tracked by users are used to generate an estimate of position, velocity and time. These applications as identified by Hofmann-

Wellenhof et al. (2007), Kaplan and Hegarty (2005), Misra and Enge (2011) may be classified according to the following:

- Land, Sea and Air Navigation and Tracking:- including way-points as well as precise navigation, collision avoidance, cargo monitoring, vehicle tracking, search and rescue operations, etc.
- Surveying and Mapping, on land, at sea and from the air. Includes geophysical and resource surveys, GIS data capture surveys, engineering and topographic surveys, etc.
- Military Applications: the military systems are generally developed to ”military specifications” and a greater emphasis is placed on system reliability and increased power against interference and jamming.
- Recreational Uses on land, at sea and in the air.
- Timing and Frequency settings:- With the systems' accurate time references, GNSSbased time are used for the synchronization of very accurate clocks and timing standards[3]. Notable uses are in the control of data communications networks, synchronized switching of power grids and timing of race cars.
- Scientic applications: These include using signals for remote sensing of the environment, space weather studies, altitude determination, spacecraft operations
- Other specialised uses are movement of the Earth's Crust, precision agriculture, environmental/crisis management, etc.

Obviously such applications require specially developed systems, often with additional demanding requirements such as real-time operation, etc (Gleason and Gebre-Egziabher, 2009).

[3] Precise Time Reference – http://www.navipedia.net/index.php/Precise Time Reference

2.1.2 GNSS Constellation Status

GPS, GLONASSS, Galileo and Compass are currently four main GNSS systems in different states of development. GPS and GLONASS are in full operation, Galileo is operating a flexible schedule to reach Full Operational Capability (FOC) in 2015, and Compass is upgrading its regional BeiDou-1 to BeiDuo-2 to reach global FOC in 2020. The table below gives a comparison of some of the key features of these different GNSS systems. Detailed information on the status of the various GNSSes can be found in
GPSWorld-Editors (2014).

Table 2.1: GNSS Current Status

		ational	Under-Dev	
	GPS	**Glonass**	**Galileo**	**BeiDuo**
FOC (global)	1994	1994 ; 2011	2016/2017	2020
FOC (regional)	--	--	2014/2015	2012
Political entity	USA	Russia	EU	China
Total planned MEO SVs)	21 + 3	21 + 3	27 + 3 / 18 27 / 4	
Current SVs	30 (3)	24 (5)	4 IOV	9 (5)
Orbit Height (MEO in km)	20240	19100	23222	21150
Orbit Inclination (degrees)	55	64	56	55 ??
Period	11h 58m	11h 18m	14h 6m	12h 36m ??
Frequency bands used	L1, L2	L1, L2	L1, E2, E5	E2, E5b, E6
Frequency bands planned	L5	L3	E1, E6	B1, B2a/b

The numbers in parentheses are satellites in active spares

2.1.3 GNSS Signal and Observables

GNSS are passive[4] one-way down-link satellite ranging systems emitting modulated signals that include the time of transmission to derive ranges as well as the modeling parameters to compute satellite positions at any epoch (Hofmann-Wellenhof et al., 2007). GNSS space vehicles continuously transmit navigation signals at two or more frequencies in L band (Subriana et al., 2013). The fundamental observable is the signal travel time between the satellite antenna and the receiver antenna. The signal travel time is scaled

[4] SVs only transmit signals

into a range measurement using the signal propagation velocity (Seeber, 2003). The observed signal travel time always contains a systematic synchronization error (time bias) due to different clocks on-board SVs and receivers (Raju, 2013). Hence ranges obtained from these time-biased signals are called *pseudoranges* as they are more than the true geometric ranges. The detailed structures of the various GNSS signals can be found in Interface Control Documents published by system providers. The main signal components as identified by Subriana et al. (2011), Misra and Enge (2011) and Seeber (2003) are described as follows:

(a) carrier: radio frequency sinusoidal signal at a given frequency

(b) ranging code: sequences of zeros and ones which allow the receiver to determine the travel time of the radio signal from the satellite to the receiver. They are called the PRN sequences or codes

(c) Navigation data: a binary-coded message providing information on the satellite ephemeris, clock bias parameters, almanac, satellite health status and other complementary information.

Observables: Four basic observables have been identified in Seeber (2003) from GNSS to be the following:

(i) pseudoranges from code measurements,

(ii) pseudorange differences from integrated Doppler counts,

(iii) carrier phases or carrier phase differences, and

(iv) differences in signal travel time from interferometric measurements.

These observables are ranges which are deduced from measured time or phase differences based on a comparison between received signals and receiver-generated signals in the GNSS time scale. The pseudoranges are determined by the multiplication of time shift that is necessary to correlate the incoming code sequence with a code sequence generated in the GPS receiver with the velocity of light (Kaplan and Hegarty, 2005).

The fundamental observation equations for both code pseudoranges and carrier phase as given by Misra and Enge (2011) & Wells et al. (1999) are given below.

1. For code pseudoranges, the basic measurement made by the GNSS receiver is the apparent transit time of the signal from satellite to receiver. The value obtained is biased due to non-synchronized clocks of the satellite and receiver clocks, atmospheric propagation delays and environmental effects, hence the name pseudoranges.

$$\rho(t) = R + c[\delta t_r - \delta t^s] + I_\rho + T_\rho + \varepsilon_\rho \tag{2.1}$$

   where, ρ, is pseudorange, R is the true range, I_ρ and T_ρ are the delays associated with signal transmission through the ionosphere and troposphere delays, ε_ρ are measurement noise, c is speed of light in vacuum, $(\delta t_r - \delta t^s)$ are receiver and satellite clock biases respectively.

2. For carrier phases the receiver meassures the difference between the phases of the receiver-generated carrier signal and the carrier received from satellites at the instant of the measurement. For carrier phases to be measured, the receiver needs to acquires phase lock with the satellite signal, measures the initial fractional phase difference, count full cycles and tracks changes of the fractional cylce at each epoch (Misra and Enge, 2011). The carrier phase is given as:

$$\phi = \lambda^{-1}\left[R + I_\rho + T_\rho\right] + \frac{c}{\lambda}\left[\delta t_r - \delta t^s\right] + N + \varepsilon_\rho \tag{2.2}$$

   where, φ, is carrier phase, λ is wavelength, N is interger ambiguity. The fundamental difference between both observables is the ambiguity term in Equations (2.1) and (2.2).

As with all measurements GNSS code pseudoranges and carrier phase are affected by systematic errors or biases and random noises as well (Hofmann-Wellenhof et al., 2007, Misra and Enge, 2011, Seeber, 2003, Subriana et al., 2011). These errors can be grouped into three classes, namely satellite-related errors, propagation-medium-related errors, and receiver-related errors. Table 2.2 gives a summary of the various components. Aside

Table 2.2: Measurement Biases

Source	Effect
Satellite	Clock bias and Orbital errors
Signal propagation	Tropospheric refraction ionospheric refraction
Receiver	Antenna phase center variation Clock bias and Multipath

these biases GNSS's are subjected to various limitations including:

1. Interoperability;
2. Signal attenuation or jamming;
3. Geometric heights as compared to physical heights and
4. Satellites Geometrics

The range error resulting from residual satellite clock bias, satellite orbit bias, receiver clock error, ionospheric and tropospheric refraction delays can vary from a few metres to as much as 15*m* in single-point positioning.

To overcome, reduce or correct for these errors/biases, various strategies and positioning methods must be employed, examples are given below:

- In the case of satellite clock bias, using precise ephemeris as generated by the International GNSS Service[5] (IGS) is an option.
- For receiver clock error, the clock bias should be treated as an additional parameter in the pseudo-range navigation model.
- The ionospheric delay on a signal is a function of the frequency, hence dualfrequency receiver are used to mitigate this effect. Moreover, coefficients of correction formulas are transmitted within the satellite navigation message to reduce the effect.

[5] International GNSS Service is a worldwide agencies that pool resources from over 200 permanent GPS & GLONASS station data to generate precise GPS & GLONASS products Services. www.igs.org

- Tropospheric effects depends on the air density profile along the signal path and can be accounted for by avoiding low elevation satellites and treating the residual bias as a parameter in the final navigation solution (Olynik, 2002).

- On the effects of Multipath and its dependency on the antenna's environment, data differencing techniques cannot be used in its elimination. Hence, these measures must be adhered to:

  (a) Sites free of reflective surfaces must be selected for antenna sites/monuments,

  (b) Use of multipath resistance quality antennas,

  (c) Use of receivers with capabilities of internally digitally filtering multipath disturbances and

  (d) Avoid low elevation satellite signals which are highly susceptible to multipath

  Multipath effects are frequency/wavelength dependent and as such carrier phases are less affected than code ranges (Leick, 2004).

2.2 Positioning

With the right receiver users have access to the four different observables provided by GNSS thus making it possible to use the signals in a variety of configurations for user satisfaction. All GNSS are designed to offer two levels of positioning services; the highly accurate service, which is available only to authorized users, and a Standard Positioning Service (SPS), a less accurate positioning and timing service which is available to all users (FAA-Editors, 2015, ROB-Editors, 2010). From the SPS, Position, Velocity and Timing (PVT) solutions can be derived by using the receivers in either autonomous or relative modes.

Autonomous or Single Point Positioning: involves the use of only a single GNSS receiver to collect data from multiple satellites in order to determine the user's geographical position and navigational output based the GNSS referenced frame. The performance of stand-alone GNSS is sufficient only for a limited number of applications especially those requiring lower accuracies. However, with applications that demand improved and higher accuracies the signals are often combined with other sensors, signals and rigorous algorithms. Centimetre-level accuracies are achievable when carrier phase measurements from dual frequency receivers are combined with precise orbits and satellite clock corrections products from IGS servers (Ghoddousi-Fard and Dare, 2006). Absolute positioning is the most widely used military and civilian/commercial GPS positioning method for real-time navigation and location (USACE-Editors, 2003).

Relative or Differential Positioning: This requires at least two receivers set up at more than one station (with at least one location known) to observe/measure satellite data simultaneously in order to determine coordinate differences. This method positions the receivers relative to each other and provides improved accuracies. It can also be described as a process of determining the relative differences in coordinates between two receiver points, each of which is simultaneously maintains lock unto satellites measuring code ranges and/or carrier phases from GNSS constellation (USACE-Editors, 2003). The reference station calculates corrections which are transmitted to the remote receiver in real time via a data link or stored to be applied later. Differential systems gives better accuracies than stand-alone positioning modes and also provides information on the position integrity (Gleason and Gebre-Egziabher, 2009). Differential techniques are further classified, depending on the status of the rover receiver and the period of observation as static, fast-static, kinematic or real-time kinematic (RTK). Its design can be implemented from local, regional or global areas.

2.2.1 Reference Systems

As indicated by Cross et al. (2002) and Torge (2001), one of the basic aims of geodesy is to determine the positions of points on (or above or below) the surface of the earth. Point positioning are done by taking measurements such as angles, distances, azimuths, radial velocity (in satellite Doppler), gravity differences, etc. between the points of interest and process to determine a set of coordinates. Solutions from the computed raw measurements aide in the establishment of geodetic networks, prediction of satellite orbits, determination of the earth's shape and its crustal motions. The resulting values or computational results are based on a chosen reference system with a clearly defined location of the origin, the orientation of the three axes and ellipsoidal parameters. GNSS has revolutionized positioning capabilities for terrestrial observers at all scales (i.e. local, regional, national, and international levels). This revolution is making countries and continents around the world to revise, re-define and update their fundamental networks to take advantage of the high accuracy, the ease of establishing and densifying the control, and homogeneity afforded by GNSS (Jekeli, 2006).

For ease of use and coordinates integration amongst the various GNSSes, the International Terrestrial Reference Frame (ITRF)[6] has been adopted. The International Earth Rotation Service (IERS) introduced ITRF to support scientific activities that require highly accurate positional data (Hu, 2009). The IERS works in collaboration with institutions using a combination of worldwide tracking technologies such as Very Long Baseline Interferometry (VLBI), Satellite Laser Ranging (SLR), Doppler Orbitography by Radio-positioning Integrated on Satellite (DORIS) and GPS. The IERS output or computational products are in various forms notable amongst them are station coordinates and their velocities.

The initial realization was called ITRF of 1988 (ITRF88). The current and fully functional realization is the ITRF2008 which coincides perfectly with the WGS84 of the US GPS. All current realizations are revision of published positions and velocities in addition to newly established sites Soler and Snay (2004). With all satellite navigation systems basically aligning to the ITRF it is advantageous to adopt it as a national reference system in order to make the use of GNSS data easier in Ghana (Poku-Gyamfi, 2009).

[6] ITRF:- http://www.iers.org/IERS/EN/DataProducts/ITRF/itrf.html

2.2.2 Time

Time, is one of the seven basic units of measurements. The rest are *meter, kilogram, ampere, kelvin, mole, and candela*. The unit of time is second. The definition of *Second* as agreed on the 13th Conference of the International Committee of Weights and Measures in Paris, 1967, states that:

> *The second is the duration of 9 192 631 770 periods of the radiation corresponding to the transition between the two hyperfine levels of the ground state of the Cesium 133 atom*.

All other measurements (e.g., force, velocity, area and integrated water vapour) are expressed in terms of the aforementioned seven basic units. Time unlike other measured quantities, is always changing, it flows and sometimes it even flies (Misra and Enge, 2011). The idea behind all timekeeping is to observe a periodic process and count the periods/cycles. Time is a fundamental quantity in GNSS code phase measurements, that is the signal flight time.

In ages past people conceive time based on the motion of the sun and were able to reckon time well enough not to miss a planting season (Rogers, 2008). With advances in technology, applications reliant on time need highly precise, uniform and well-defined time scales. These time references are defined and adopted, based on associated periodic processes, examples being earth's rotation, celestial mechanics or energy level transitions in atomic oscillators. Hofmann-Wellenhof et al. (2007) and Burhanpurwala et al. (2008) summarises the various time systems as well their associated periodic process in Table 2.3.

Table 2.3: Time Systems

Periodic Process	Representative time systems
Earth Rotation	Universal time (UT) Greenwich sidereal time
Earth Revolution	Terrestrial dynamic time (TDT) Barycentric dynamic time (BDT)
Atomic oscillations	International atomic time (TAI) Coordinated UT (UTC) GNSS Reference times

Currently the precision of time measurements have been improved to nanoseconds ($10^{-9}s$) and picoseconds ($10^{-12}s$) levels. Signal flight time is the core off GNSS measurements and as such requires highly precise clocks on board satellites and equally good ones in the user receivers. This is so because a synchronization error of $1\mu s$ in a satellite clock will introduce an error of $\approx 300m$ in the pseudorange, with a corresponding error in the position estimate (Seeber, 2003). For meter-level position estimates, the clock synchronization among the satellites must be maintained within a few nano-seconds (Misra and Enge, 2011). The various GNSS maintain their own time scales which is an offset from the Universal Coordinated Time (UTC). UTC is a composite time implemented to serve as a compromise between periodic earth rotation and atomic oscillations. Integer leap seconds are inserted at distinct epochs hence UTC is not a continuous time scale (Hofmann-Wellenhof et al., 2007). UTC is obtained using specialized algorithms to assure uniform time based on about 250 cesium clocks and hydrogen masers in 65 different laboratories, spread around the world (Subriana et al., 2013). Subriana et al. (2011) give a summary in Table 2.4. With the exception of Glonass, the remaining

Table 2.4: Time References of the various GNSS

GNSS	Time Reference
GPS	GPS Time (GPST) is a continuous time scale on atomic clocks at the Monitoring Stations and onboard the satellites. GPS time is synchronised with the UTC and kept within $25ns$. The relation between UTC and GPS time as included in time bulletins of the US Naval Observatory and satellite navigation message is: $GPST = UTC_{2014} + 16s$
GLONASS	GLONASS Time (GLONASST) is generated by their Central Synchroniser and the difference between the UTC and GLONASST is kept within $1ms$ plus three hours: $GLONASST = UTC + 3^h - \tau$, where $\lvert\tau\rvert < 1ms$
Galileo	Galileo System Time (GST) is a continuous time scale maintained by the Galileo Central Segment and synchronised with International Atomic Time (TAI) with a nominal offset below $50ns$. The starting epoch is 0^h UTC on Sunday, 22 August 1999
Beidou	BeiDou Time (BDT) is a continuous time scale starting at 0^h UTC on January 1st, 2006 and is synchronised with UTC within $100ns$

systems do not implement leap second making their differences between UTC always increasing (Seeber, 2003). study. For Differential or Relative Positioning references can be made to (Acheampong, 2009, Hofmann-Wellenhof et al., 2007, Seeber, 2003, USACE-Editors, 2003). PPP technique uses undifferenced single or dual frequency pseudorange and carrier phase observations of a receiver operating in autonomous mode along with precise orbit and clocks products to achieve a cm-level accuracy (Karabati´c and Weber, 2009, Kouba, 2009). The estimation of accurate receiver coordinates and centimetrelevel precision have been possible due to these factors:

1. the availability of highly accurate orbit and clock estimates, for GPS and Glonass satellites, by means of a dense global network of receivers and analysis centres (Dow et al., 2009, Kouba, 2009), and
2. rigorous algorithms designed to handle multiple frequencies, combined signals, estimate parameters and eliminate errors (Gao and Chen, 2004, Juan et al., 2012).

Recent developments and the modernization of GNSS have greatly improve the satellite geometries and more signals deployed to allow redundancy in observables. Newer signals and varied frequencies have enhanced effects of improving convergence time, positional accuracies, signal integrity, availability and continuity. Juan et al. (2012) and Grinter and Roberts (2011) identified that the major drawback is the large convergence time needed to get a good estimation of the ionospheric-free carrier phase ambiguity. This limitation can be overcome by using of ionospheric corrections computed and broadcast by a dedicated PPP Central Processing Facility, satellites broadcasting fractional part of ambiguities and multi-constellation and multi-frequency observable (Juan et al., 2012).

Researchers worldwide have taken opportunities offered by PPP techniques to develop centralized geodetic positioning services that require users to complete a request form and submit valid GNSS observation files for accurate solutions (Banville et al., 2014, Ghoddousi-Fard and Dare, 2006, Mireault et al., 2008). Other applications obtained from PPP techniques are time-transfer, ionospheric and tropospheric characterization and biases calibration (Tegedor et al., 2014).

Following Subriana et al. (2013) & Karabati´c et al. (2011), the PPP dual-frequency functional model for code, $P_{r,i}{}^{s}$, and phase, $\Phi^{s}{}_{r,i}$, as given in un-differenced observables measured in metric units:

$$P_{r,i}^{s} = \rho + c\Delta t_r - c\Delta t_s + \Delta d_{iono,i} + \Delta d_{trop,i} + \Delta\rho_{rel} + \Delta d_{mp,i} + c\beta_r + c\beta_s + \varepsilon_{P,i} \quad (2.3)$$

$$\Phi^{s}_{r,i} = \rho + c\Delta t_r - c\Delta t_s + \Delta d_{iono,i} + \Delta d_{trop,i} + \Delta\rho_{rel} + \Delta d_{mp,i} + c\alpha_r + c\alpha_s + \Delta d_{pcv,i}$$
$$+ \lambda_i\omega + \lambda_i\alpha_{r,i} + \lambda_i\alpha_i^s + \lambda_i N_i + \varepsilon_{\Phi,i} \quad (2.4)$$

ρ, as indicated in Equations 2.3 and 2.4 is the true geometric distance between satellite, s, and receiver, r, which is equal to $\vec{R}_r(t_r) - \vec{R}^s(t_r - \tau_r^s)$ ( )). Where, R_r is the station geocentric vector at the time of signal reception t_r, $\vec{R}^s$ is the geocentric vector to the satellite at the time of signal emission ($t_r - \tau_r^s) = t^s$ and τ_r^s is the signal travel time between s and r. i is the carrier frequency. The speed of light is represented by c.

ρ can hardly be obtained as its adulterated with offsets caused by satellite and receiver clocks, $c\Delta t_r$ and $c\Delta t^s$, ionospheric and tropospheric delays, d_{iono} and d_{trop}, β_r and β^s are code biases for the receiver and the satellite, $\alpha_{r,i}$ and α_i^s are phase biases for receiver and satellite, $\Delta\rho_{rel}$ is range correction due to relativistic effects, ω is a phase wind-up correction, λ is wavelength, N is ambiguity for the carrier frequency. $\Delta d_{pcv,i}$ is frequency dependent delay due to the phase center variations, Δd_{mp} is delay due to multipath, $\varepsilon_{P,i}$ and $\varepsilon_{\Phi,i}$ are the remaining un-modelled errors in the measurements.

2.2.3 PPP Correction Models

PPP models are solved by holding fix and tightly constraining satellites positions on the assumption of no orbital errors. In addition, satellite clock corrections provided by global analysis centres [7] are introduced in the models as known. The accuracies of these clock corrections and orbital products applied dictate the accuracy of PPP solutions [see Table 2.5 culled from Kouba (2009) and IGS-Webmasters (2015). One major caution is that

[7] Examples of the Analysis Centres are International GNSS Service (http://beta.igs.org/), GFZ German Research Centre for Geosciences (http://www.gfz-potsdam.de/startseite/), Shanghai Astronomical Observatory (http://english.shao.cas.cn/), Korea Astronomy and Space Science Institute (http://www.kasi.re.kr/english/), Crustal Dynamics Data Information System (http://cddis.nasa.gov/), Scripps Orbit and Permanent Array Center (http://sopac.ucsd.edu/), Institut G´eographique National France International (http://www.ignfi.fr/en)

precise clock and orbital products from the same analysis centre must be used and not mixed up (Subriana et al., 2013).

Table 2.5: IGS orbits and clock products: accuracy, latency and sampling rates

Products	Broadcast	Ultra-rapid		Rapid	Final
		Predicted	Observed		
(latency)	(real time)	(real time)	(3-9 h)	(17-41 h)	(12-18 d)
Orbit GPS	~ 100 cm	~ 5 cm	~ 3 cm	~ 2.5 cm	~ 2.5 cm
(sampling)	(~ 2 h)	(15 min)	(15 min)	(15 min)	(15 min)
(Glonass) (sampling)					~ 5 cm (15 min)
Clock GPS (sampling)	~ 5 ns (daily)	~ 3 ns (15 min)	~ 150 cm (15 min)	~ 75 ps (5 min)	~ 75 cm (30 s)
(Glonass) (sampling)					N/A

2.2.3.1 Antenna Phase Center Variations

This is represented by $\Delta d_{pcv,i}$ in the PPP dual-frequency functional model for carrier phase, $\Phi^s_{r,i}$, (2.4). This correction must be effected because the models used for the satellite orbits are made with references to the earth and satellites centres of mass, but the signals emanates from the satellite's antenna phase centre. Since, measurements are

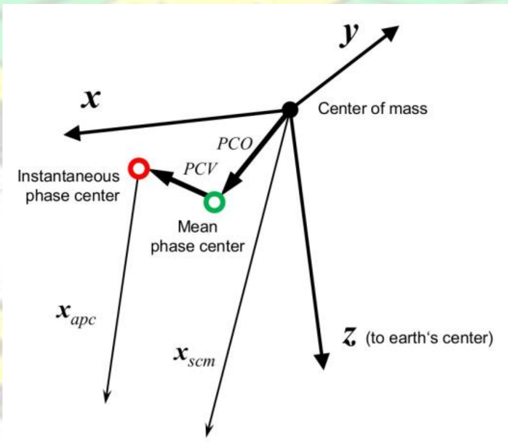

Figure 2.1: Offsets in satellite's centre of mass and antenna phase center, where, PCO and PCV are phase centre offsets and variations (Karabati´c, 2011)

made to the antenna phase center, satellite phase center offsets must be known and the orientation vectors must be monitored as the satellite orbits the Earth (Subriana et al.,

2011).
gLAB[r] implements this corrections by using ANTEX [8] files. The antenna phase center offset (PCO) has to be known for each satellite and receiver antenna types, and it is usually accounted for in the calculation using a publicly available antenna information file (example of the current ANTEX file is igs08.atx available for the International GNSS Service servers).

2.2.3.2 Phase Wind-up Effects

Wind-up effects are represented by ω, in $\Phi^{s}_{r,i}$, (2.4), and affects only carrier phase measurements. This effects on phase measurements are as result of changes in the relative orientations of transmitting and receiving antenna due to the right circularly polarized nature of the radio wave (Karabati´c, 2011, Kouba, 2009, Subriana et al., 2011). Movements of satellites in the orbital plane and adjustments of on-board solar panels as well as kinematic surveys do cause these errors. For stationary receiver the effects are considered only at the satellites side. Wu et al. (1993) studies on wind-up effects concluded that its effects are negligible even in the most precise differential positioning on baselines/networks covering up to a few hundred kilometers. However, in cases of baselines reaching 4000 km the value can size to 4 cm.

The model for computing wind-up corrections based on Wu et al. (1993) for static PPP based on an evaluation of dot (·) and vector (×) product are:

$$\omega = \delta\phi + 2N\pi, \quad N = nint\left[\frac{\omega_{prev} - \delta\phi}{2\pi}\right] \tag{2.5}$$

where $\delta\varphi$ is the fractional part of the cycle, N is the integer number which is initialized as zero, ω_{prev} is previous value of the phase correction and *nint* is the nearest integer.

2.2.3.3 Relativistic Effects

[8] Antenna Exchange Format http://igscb.jpl.nasa.gov/igscb/station/general/antex14.txt

GNSS are built to use accurate, stable atomic clocks in satellites and user receivers to provide world-wide PNT solutions. Clocks [9] aboard these systems have gravitational and motional frequency shifts which can be so large that when not treated carefully gives rise to numerous relativistic effects causing the system to malfunction (Ashby, 2003).

A fundamental requisite for smooth operation of the system is that the various clocks must be in sync, but this is hardly the case because time transfer between satellite and user receivers are affected by relativistic effects, $\Delta\rho_{rel}$, (Subriana et al., 2013). According to Karabati´c (2011), Kouba (2009), Misra and Enge (2011) the receiver time, t_r, (after applying the clock corrections) is given as:

$$t_r = t^s - \Delta\rho_{rel} \tag{2.6}$$

$\Delta\rho_{rel}$ is further divided into a constant, $\Delta\rho_{rel,con}$ and a periodic $\Delta\rho_{rel,per}$ correction terms, i.e.

$$\Delta\rho_{rel} = \Delta\rho_{rel,con} + \Delta\rho_{rel,per}$$

$\Delta\rho_{rel,con}$ components are caused by the gravitational field and the speed of satellites causing clock displacements. These effects forces the frequency to shift from the nominal frequency, f_0 = 10.23MHz, introducing errors in the PNT solutions. An integration of the shifts over one day yields the clock correction value of 38.58 μs and in order to deal with this effect the satellite-transmitted nominal frequency, f_0, are adjusted lower in frequency to 10.22999999543MHz (Karabati´c, 2011). A note of caution is that these adjustments are not the same for all satellites.

The periodic component, $\Delta\rho_{rel,per}$, is due to the orbit eccentricity as well as effects of effect of orbital perturbation and must be applied at the user site specifically in the processing software. $\Delta\rho_{rel,per}$ varies with the satellite's position in its orbital plane.

This effect as reported by Ashby (2003) has an amplitude of 46ns for GPS satellites with maximum eccentricities of 0.02. The correction is derived as follows:

[9] Satellite clocks are much more stable than ground receiver clocks by a factor of ≈ 1000, except in the case of ground hydrogen maser clocks (Karabati´c, 2011)

$$\Delta\rho_{rel,per} = \frac{2\sqrt{GM_E a}}{c^2} e\sin(E) = 4.4428 \cdot 10^{-10} e\sin(E(t_{el}))a \tag{2.7}$$

where, G is gravitational constant, M_E is the mass of the earth, a is semi-major axis of satellites, t_{el} is elapsed time, e is satellite eccentricity and E is the eccentric anomaly.

2.2.3.4 Ionospheric Delays

The ionospheric delay, Δd_{iono}, depends on the electron content along the signal path through the atmosphere at altitudes 60–2000km and on the frequency used (Hoque and Jakowski, 2010). Solar activities and the Earth's geomagnetic field are major parameters affecting the ionised particles in the medium (Seeber, 2003). Interactions of free electrons in the ionosphere make electromagnetic signals passing through experience delays or advancement in relation to vacuum medium. Ionospheric influences can introduce range errors varying from less than 1m to more than 100m (Klobuchar, 1996). However, ionospheric effects on user receivers vary from signal frequency, geographic location and time. The ionized gas is dispersive for radio waves and highly dependent on the carrier frequency. Linear combinations of code or carrier measurements using multiple frequencies are employed to mitigate Δd_{iono} in the PPP solution model (Subriana et al., 2013). The models for ionosphere-free linear combination for code, P, and carrier,Φ, phases are given below:

$$P_{iono-free} = \frac{f_1^2\, p_{L_1} - f_2^2\, p_{L_2}}{f_1^2 - f_2^2} \tag{2.8}$$

$$\Phi_{iono-free} = \frac{f_1^2\, \Phi_{L_1} - f_2^2\, \Phi_{L_2}}{f_1^2 - f_2^2} \tag{2.9}$$

where f_1,f_2 are carrier frequencies on the $L1$ and $L2$ signals, p_{L1},p_{L2} are pseudorange measurements and Φ_{L1},Φ_{L2} are carrier phase measurements. Comprehensive discussions on ionospheric propagation effects on GNSS signals can be found in (Hofmann-Wellenhof et al., 2007, Klobuchar, 1996, Misra and Enge, 2011, Seeber, 2003).

2.2.3.5 Tropospheric Delays

Referring §1.3, the atmospheric layer also refract GNSS signals, unlike the ionosphere, it is non-dispersive for radio waves (i.e., the refractive index is independent of the signals' frequency). Measurements of code and carrier phases at the various frequencies experience a common delay (Misra and Enge, 2011). The tropospheric medium slows the speed of propagation of the signal making range measurements to satellites longer. The tropospheric effects can introduce errors from 2.5 m to as high as 25 m depending on the elevation of the satellite (Seeber, 2003). Richardus (1984) calculated the total delays based elevation angles and its presented in Table 2.6. The tropospheric delays,

Table 2.6: Influence of the tropospheric refraction on measured ranges (m)

Elevation Angle	90^o	20^o	15^o	10^o	5^o
Δd_{trop_d}	2.31	6.71	8.81	12.90	23.61
Δd_{trop_w}	0.20	0.58	0.77	1.14	2.21
Δd_{trop}	2.51	7.29	9.58	14.04	25.82

Δd_{trop}, cannot be estimated from GNSS observables and as such its effects are mitigated by using models. Δd_{trop} on range measurements to satellites are made up of two components: the dry component and the wet component. Hence, Δd_{trop} can further be defined as:

$$\Delta d_{trop} = \Delta d_{trop_d} + \Delta d_{trop_w}$$

where, Δd_{tropd} is the dry or hydrostatic component and Δd_{tropw} is the wet component. Δd_{tropw}, which comprises only 10% of total tropospheric refraction, depends on the distribution of water vapour in the atmosphere and the hardest of the two components to model (Schu¨ler, 2001, Seeber, 2003). Whereas, Δd_{tropd} can be precisely described within an accuracy of ±1% by tropospheric models. Wet delays on the other hand, according to Langley (1996) can be modelled using precise surface meteorological parameters with an accuracy not better than 2 cm.

Models for tropospheric refraction are based on functions of meteorological parameters and refractive index of air mass along signal path. Following Hartmann and Leitinger (1984), Thayer (1974) an empirical formula for computing the reduced index of tropospheric refraction, *N*, and is given below:

$$N = k_1 \frac{p_d}{T} Z_d^{-1} + k_2 \frac{e}{T} Z_w^{-1} + k_3 \frac{e}{T^2} Z_w^{-1} \quad \Rightarrow \quad N(s) = [n(s) - 1] \cdot 10^6 \tag{2.10}$$

where p_d and e are partial pressures of the dry gases and water vapour in hPa, T is absolute temperature in Kelvins; Z_d^{-1} and Z_w^{-1} are inverse are compressibility factors for dry and moist air respectively and are used to describe the deviation of the atmospheric constituents from an ideal gas; k_1, k_2 and k_3 are constants based on laboratories estimates and Bevis et al. (1994) found them to be $k_1 = 77.60 \pm 0.05$ K/hPa, $k_2 = 77.40 \pm 2.2$ K/hPa, $k_3 = 373900 \pm 1200$ K^2/hPa and $k_2' = 22.10 \pm 2.2$ K/hPa.

Equation (2.10) can further be expressed in terms of integrals of the two components and ignoring all other terms which are zero in the zenith direction, Δd_{trop} becomes:

$$\Delta d_{trop} = 10^{-6} \int_{atm} N(s) \cdot ds = 10^{-6} \int_{atm} [\Delta d_{tropd}(s) + \Delta d_{tropw}(s)] \cdot ds \qquad (2.11)$$

Most tropospheric delays estimations are based on average meteorological conditions at the antenna location from models of the *standard atmosphere* using the day of the year, latitude and altitude (Misra and Enge, 2011). Two approaches that are used to estimate Δd_{trop} are:

1. Estimation of the Zenith tropospheric delay (ZTD) in terms of the corresponding dry (ZHD) and wet delays (ZWD); $ZTD = ZHD + ZWD$
2. Define a mapping function to scale the ZTD as a function of the elevation angle (ε).

$$\Delta d_{trop}(\varepsilon) = \Delta d_{trop_{z,d}} \cdot m_d(\varepsilon) + \Delta d_{trop_{z,w}} \cdot m_w(\varepsilon)$$

where m_d and m_w are mapping functions for the dry and wet components. Simple models normally use a common mapping function for both the dry and wet components ignoring the atmospheric profile differences (Misra and Enge, 2011).

There are various tropospheric models that been developed based on the assumptions of changes in temperature and water vapour with altitude. Berrada et al. (1988), Davis et al. (1985), Goad and Goodman (1974), Hopfield (1969), Saastamoinen (1972) give further details and algorithms of models developed and named after them. *gLAB*^{r}, the software used for this thesis uses a model that does not require any surface meteorological data

(Hernandez-Pajares et al., 2010). The model shown below also uses the Niell mapping functions that considers different obliquity factors for the wet and dry components (Niell, 1996):

$$T_{z,dry} = a\ e^{-b\,H}$$
$$T_{z,wet} = T_{z_0,wet} + \Delta T_{z,wet} \qquad (2.12)$$

where $a = 2.3m$, $b = 0.116 \cdot 10^{-3}$, and H is station height above sea level, in meters. $T_{z0,wet} = 0.1\ m$ and $\Delta T_{z,wet}$ [10] is estimated as a random-walk process using Kalman filtering together with the station coordinates, and other parameters (Subriana et al., 2013). There is a caution that this model has a huge simplification for the vertical delays.

2.2.3.6 Mapping Functions

Mapping functions (also referred to as obliquity factors) are models used to convert the slant tropospheric delays to zenith delays. These functions make computations of total tropospheric delays easier as signals arrive at the antenna location from various angles.

The simplest model for both dry (hydrostatic) and wet delays according to Misra and Enge (2011) is $1/\sin el$. This model works well when the earth is considered to be flat and satellites are above 15^o elevation angles (el). Several models have been developed to counter the effects of the earth's curvature and low-elevation satellites. Examples can be seen in Davis et al. (1985), Herring (1992), Hopfield (1969), Ifadis (1986), Niell (1996), Saastamoinen (1972), Spilker (1996). However for this study the mapping function implemented in *gLAB*r is based on a modified Niell (1996) model using the Marini (1972) model normalized to unity at the zenith. The models are presented below, where *E* is the elevation angle and *H* is receiver's height adove sea level in km:

Dry or *Hydrostatic* mapping function:

[10] This estimate takes care of the mis-modelling of the dry component

$$M_{dry}(E,H) = m(E, a_d, b_d, c_d) + \Delta m(E,H)$$
$$with, \quad \Delta m(E,H) = \left[\frac{1}{sinE} - m(E, a_{ht}, b_{ht}, c_{ht})\right] \cdot H \tag{2.13}$$

Wet mapping function:

$$M_{wet}(E) = m(E, a_w, b_w, c_w) \tag{2.14}$$
$$m(E,a,b,c) = \frac{1 + \frac{a}{1+\frac{b}{1+c}}}{\sin E + \frac{a}{\sin E + \frac{b}{\sin E + c}}} \tag{2.15}$$

Following Subriana et al. (2013) and Niell (1996), the hydrostatic parameters a_d, b_d, c_d are time (t) and latitude (θ) dependent and can be evaluated using the expression

$$\xi(\theta,t) = \xi_{avg}(\theta) - \xi_{amp}(\theta)\cos\left(2\pi\frac{t-T_0}{365.25}\right)$$

where t is the time from January 0.0, in days, and T_0 is taken as Day of Year (DoY). The parameters $\xi_{avg}(\theta_i)$ and $\xi_{amp}(\theta_i)$ are linearly interpolated from Table 2.7 using a_{ht}, b_{ht}, c_{ht} as constants. On the other hand the wet components, a_w, b_w, c_w, are only

Table 2.7: Coefficients of hydrostatic mapping function

Coefficient (ξ)	Latitude (θ) 15°	30°	45°	60°	75°
	Average				
a	1.2769934e-3	1.2683230e-3	1.2465397e-3	1.219604e-3	1.2045996e-3
b	2.9153695e-3	2.9152299e-3	2.9288445e-3	2.9022565e-3	2.9024912e-3
c	62.61055e-3	62.837393e-3	63.721774e-3	63.824265e-3	64.258455e-3
	Amplitude				
a	0.0	1.2709626e-5	2.652366e-5	3.4000452e-5	4.1202191e-5
b	0.0	2.1414979e-5	2.6523662e-5	7.2562722e-5	11.723375e-5
c	0.0	9.0128400e-5	3.0160779e-5	84.795348e-5	170.37206e-5
	Height Correction				
a_{ht}	2.53e-5				
b_{ht}	5.49e-3				

Cht	1.14e-5

dependent on latitudes and the linear interpolations are done using values from Table 2.8.

Table 2.8: Coefficients of the wet mapping function

Coefficient (ξ)	Latitude (θ)				
	15^o	30^o	45^o	60^o	75^o
a	5.8021897e-4	5.6794847e-4	5.8118019e-4	5.9727542e-4	6.1641693e-4
b	1.4275268e-3	1.5138625e-3	1.4572752e-3	1.5007428e-3	2.9024912e-3
c	4.3472961e-2	4.6729510e-2	4.3908931e-2	4.4626982e-2	64.258455e-2

2.3 Height Systems

Geometric heights obtained from GNSS which are based on their reference ellipsoids can only be used in NWP modelling and data assimilation when they are converted to geopotential heights (Vedel, 2000). This is the case because almoast all NWP models use pressure as their vertical coordinates. Geopotential [11] heights are also referred to as dynamic heights in meteorology and climatology. To convert geometric heights to geopotential heights, this two-step procedure must be followed:

1. conversion from GNSS ellipsoids to Earth Geoidal Model (EGM2008 or EGM96) orthometric heights (Pavlis et al., 2012);
2. conversion of orthometric heights above the geoidal surface to geopotential heights (Odumosu et al., 2015, Vedel, 2000, Yilmaz, 2008).

The transformation between geometric and geopotential heights are dependent on altitude and lattitude of the station. Following Schu¨ler (2001) and based on the definition by (Heiskanen and Moritz, 1993) which states that geopotential heights describe a height system that is linked to potential layers and defined by the difference in geopotential at mean sea level (geoidal surface) and the geopotential at point *P*. This difference in

[11] Geopotential are actual heights of a pressure surface above mean sea-level (Barthelmes, 2013, WW2010, 2015).

geopotential is scaled by the normal gravity at a latitude of $\varphi = 45^o$. The geopotential at point, *P*, denoted by W_P is given by

$$W_P = W_O - \int_O^P g \cdot ds \quad \Rightarrow h_{gp} = \frac{1}{g_O} \int_O^P g \cdot ds \tag{2.16}$$

where h_{gp} is the geopotential height at P, g_0 in gravitational acceleration at mean sea level or geoidal surface. Weast et al. (1989) give the approximate expression for the value of acceleration due to gravity, g, at the geoid surface as function of latitude as

$$g_s \approx g_e(1 + a_1 \sin^2 \theta + a_2 \sin^2 2\theta) \tag{2.17}$$

where θ is the latitude, $g_e = 9.780356\ m/s^2$, $a_1 = 5.2885 \cdot 10^{-3}$ and $a_2 = -5.9 \cdot 10^{-6}$.

For the variation of g with heights, this expression may be used

$$g \approx g_s(\frac{R_s}{R_s + h_P})^2, \qquad R_s \approx \frac{R_e}{\sqrt{(R_e/R_p)^2 \sin^2 \theta + \cos^2 \theta}} \tag{2.18}$$

where $R_e \approx 6378.1\ km$ is the average equatorial radius and the average polar radius, $R_p \approx R_e - 21.5\ km$.

Merging Equations 2.16 and 2.18 geopotential heights can be computed by:

$$h_{gp} = \frac{g_s}{g_O} \int_O^P \frac{R_s}{R_s + h_P} \cdot ds \quad = \frac{g_s}{g_O} \frac{h_P}{1 + h_P/R_s} \tag{2.19}$$

Concluding Remarks: this chapter gives account on the general overview of the various GNSS, the observables and PNT solutions that can be derived from the tracked signals. It goes further to explain the mathematical models involved and gives greater emphasis to PPP, the errors involved and how they can be mitigated. In addition, heights systems as used in NWP models are treated because these models use pressure levels as their vertical coordinates.

Chapter 3

Atmosphere, Water Vapour and Reanalysis Data

3.1 Composition of Earth's atmosphere

The atmosphere envelops the Earth and is composed of different gas constituents which can be grouped under three main categories: dry air, water substance, and aerosols (Iribarne and Godson, 1981, P¨oschl, 2005, Salby, 2003). In addition to climatic processes, precipitation, temperature, currents, and electrical discharges, most meteorological studies are on the atmosphere. The Earth's atmosphere consists of five (5) different layers according to their thermal state (Leinweber, 2010) refer Figure 3.1. Each layer is distinct and can be identified mainly by how temperatures change with increasing height and chemical composition. The layers are bounded by four (4) ”pauses” where appreciable changes in thermal characteristics, chemical compositions, movements, and densities occur.

The lowest layer called the troposphere is characterized by a decreasing temperature with respect to height up to the tropopause (≈ 16km) . On top of the troposphere is the stratosphere that is characterized by an increase in temperature up to 50km due to very strong ozone absorption. Next is the Mesosphere with a ceiling of between 90

– 100km in altitude, temperature decreases with height in this medium. Thermosphere comes next rising from 90km to 1000km. Temperatures in this layer can reach up to 2000^{o} K or higher (UCAR, 2008). The uppermost layer is the Exosphere, its extremely thin layer compared to the other four and gradually fades into the vacuum of space.

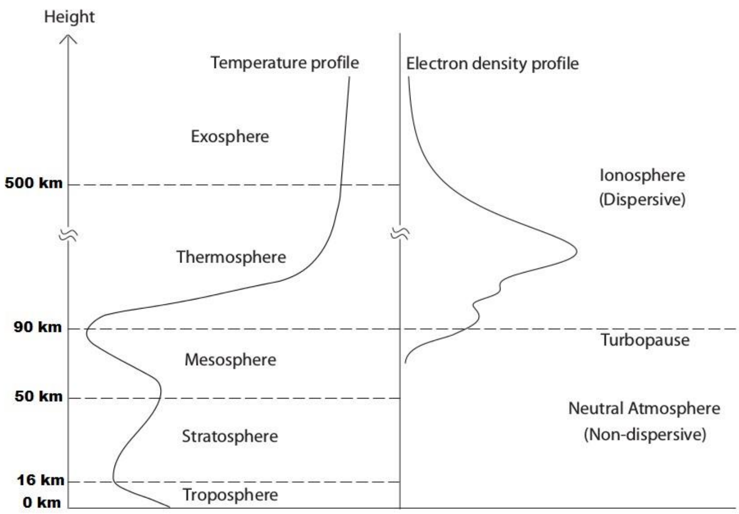

Figure 3.1: Atmospheric structure and subdivision (Pottiaux, 2010)

The Atmosphere plays the lead role in determining climate conditions such as the distribution of solar radiation, the Earth's surface temperatures, the hydrological cycle, and the distribution of nutrients in the oceans (Wallace and Hobbs, 2006). At ordinary pressure and temperature, the weight of a sample of air near the earth's surface is about 1/800 of the weight of an equal volume of water (Jutze and Foster, 1967). This weight exerts a pressure amounting to about 101.3 kPa on the Earth's surface. This pressure is used as the standard unit of atmospheric measurements and is called 1 atmosphere. The Earth's atmosphere is relatively transparent to incoming ultra-violet solar radiation and opaque to outgoing infra-red radiation emitted by the Earth's surface. This atmospheric property of scattering radiation or signals propagating through it's medium (especially the troposphere) is the motivation for this study.

90% of the weight of atmosphere lies between the ground surface up to the tropopause. Almost all weather phenomenon occurs in the lowest atmospheric layer, troposphere, this region. contains most of the atmosphere's water vapour and aerosols (Pottiaux, 2010). The tropospheric layer which is based on temperature distribution classification is considered for this thesis. The troposphere is the lowest layer of the atmosphere and characterized by a constant decrease of the temperature with atmospheric lapse rate of 6.5^{o} C/km (Wallace and Hobbs, 2006). The tropopause, which is the upper boundary of the troposphere, is a region where temperature ceases to decrease with increasing height. The height of the tropopause is not constant and changes depending on where you are on the globe (Grace, 2015). It averages 16km over the equator, 11km in middle latitudes and 8km over the Polar Regions. The troposphere is relatively unstable with frequent occurrence of vertical mixing, leading to condensation, clouds formation and precipitation (Andrews, 2010).

3.2 Water Vapour

Water is the only substance in the Earth's environment that exists naturally in significant quantities in all three states: solid(ice), liquid(water) and gas(water vapour). Water in its gaseous phase moves on a global scale transporting enormous amount of latent heat energy to maintain the Earth's energy balance (refer §1.2 on page 5). Water vapour gets to the atmosphere through open-water evaporation (from the ocean, lakes and rivers), land surfaces, sublimation from ice and snow surfaces and evapo-transpiration from vegetation. It then condenses for clouds developments and some returns to the earth's surface as precipitation - rain, fog, mist, snow or hail (Ramanathan et al., 1989). This cycle takes approximately between 7 to 10 days, the movement includes vertical and horizontal transports, mixing, condensation, precipitation and evaporation (Guerova, 2003). It also serves as an oxidizing agent that cleanses the atmosphere of many air pollutants (refer §1.2 on page 5). Different regions typically contain different rainable amount of water vapour and this can drastically affect the climate across these regions

(Kaufman and Gao, 1992).

Although very small in volume, water vapour is the most important gaseous source of infra-red capacity in the atmosphere accounting for about 60% of the natural greenhouse effect for clear skies (Courcoux and Schr¨oder, 2015, Kiehl and Trenberth, 1997). Due to it's strong feedback mechanisms for global warming (Soden et al., 2002), water vapour is one of the key prognostic variables in numerical weather prediction (NWP) models as well for climate models (Leinweber, 2010). NWP systems' accuracies are driven by the quality of data used to determine the present state of the atmosphere and how best the physical processes in the atmosphere are modelled (Bauer et al., 2007).

Water vapour has a high temporal and spatial variability (Leinweber, 2010, Vogelmann et al., 2015). Therefore accurate measurements in highly temporal and spatial resolutions are essential for the initialization of NWP models for accurate predictions/forecasting. According to Starr and Melfi (1991), water vapour plays important role in the Earth's energy balance and the general circulation of the atmosphere system. Hence the need to monitor closely water vapour contents using an approach that is highly accurate, with global coverage and capable of producing better temporal and spatial resolutions. GNSS Meteorology provides the techniques and specifications that meets the above requirements.

3.2.1 Relationship between Humidity and Water Vapour

Water vapour is a gaseous substance and its concentration in the air is defined by its partial pressure, *e*. The sum of the partial pressures of all atmospheric gases yields to the air pressure of the atmosphere

$$P_{air} = e + p_d$$

with p_d: the partial pressure of dry air.

The equilibrium vapour pressure, e_s, is the partial pressure for which the water vapour is in thermodynamic equilibrium state with its condensed phase. Bolton (1980) gives the equilibrium vapour pressure as a function of temperature, T, in Kelvin as:

$$e_s(T) = 0.6112 \cdot exp\left(\frac{17.67 \cdot T}{T + 243.5}\right)$$

The **Relative Humidity** (RH) is defined as a ratio (%) between the water vapour's partial pressure and the equilibrium vapour pressure:

$$RH = \frac{e}{e_s} \cdot 100\% \qquad (3.1)$$

RH describes how close the concentration of water vapour is to saturation or condensation. The humidity of the air can further be defined in terms of the mixing ratio, *r* in *g/kg* of an air parcel:

$$r = 1000 \cdot \frac{m_w}{m_d} \tag{3.2}$$

where m_w, denotes the mass of water vapour and m_d is the mass of dry air. The mixing ratio can be expressed in terms of partial pressure as

$$r = 1000 \cdot \frac{M_{vap}}{M_{air}} \frac{e}{P_{air} - e}$$

with M_{vap} and M_{air} as the molar weight of water vapour and dry air respectively. Another definition is the specific humidity, *SH* which describes the part (in mass) of water vapour in an air particle.

$$SH = 1000 \cdot \frac{m_w}{m_a} \quad g/kg \tag{3.3}$$

with m_w, the mass of water vapour and m_a, the mass of the whole humid air, in the air parcel.

Further, is the definition of **Absolute Humidity**, *AH* which is mass of water vapour in a given volume of air

$$AH = \frac{m_w}{V_a} = e \cdot \frac{M_w}{RT} \quad kg/m^3 \tag{3.4}$$

3.2.2 Integrated Water Vapour

Integrated water vapour, IWV denotes the amount of water vapour in a column between two levels of height or pressure. The units of IWV is kg/m^2 and the expression between the altitudes h_1 and h_2 is:

$$IWV(h_1, h_2) = \int_{h_1}^{h_2} AH(h)dh \tag{3.5}$$

In terms of two pressure levels, P_1 and P_2.

$$IWV(P_1, P_2) = \int_{P_1}^{P_2} \frac{AH(P)}{\rho_{air}(P) \cdot g} dP = \frac{1}{1000g} \int_{P_1}^{P_2} SH(P)dP \tag{3.6}$$

where, g is the Earth's gravity and ρ_{air} is air density. It can also be expressed in terms of water vapour's partial pressure and temperature.

$$\Delta IWV(h_1, h_2) = \int_{h_1}^{h_2} \frac{e(h) \cdot M_w}{RT(h)} dh \tag{3.7}$$

with $R = 8.314472\ JK^{-1}mol^{-1}$ is the ideal gas constant and T is air temperature.

Finally, Table 3.1 gives the various units and conversions for IWV.

Table 3.1: IWV Unit conversion matrix

	mm	cm	$\frac{g}{cm^2}$	$\frac{kg}{m^2}$
mm	1			
cm	0.1	1		
$\frac{g}{cm^2}$	0.1	1	1	
$\frac{kg}{m^2}$	1	10	10	1

3.3 Meteorological Observations and Techniques

Measurements are made in the atmosphere for a variety of reasons. The measurement data are gathered from a large number of onshore and offshore stations across the globe. Onshore, weather stations are located so as to provide adequate coverage of the areas of interest. Offshore observations are made by vessels, aircraft, buoys, and satellites to cover interested locations (MSI, 2012). Data recorded at offshore locations are sent by radio or satellite uplink to national meteorological centres and research centres where they are collated and fed into the computer forecast models.

Weather observations are normally taken on the major synoptic hours (0000, 0600, 1200, and 1800 UTC), but three-hourly intermediate observations are necessary at some instances (NWS-Editors, 2010, Uppala et al., 2005). Data retrieved from satellites must be compared with actual reports of surface variables to confirm developing patterns

(MSI, 2012). Forecasts can only be as good as the data and models used in predictions. High-quality observations are essential for the creation of reliable forecasts (Allen, 2015). Table 3.2 gives the various observation techniques and the parameters that can be sensed.

Forecasts are released from agencies at periodic scales – small or local scales to larger or

Table 3.2: Meteorological Observational Techniques

Observing Techniques	**Weather Parameters**
Surface Measurements	Temperature, pressure, wind speed, precipitation wind direction, humidity, dew point
Radiosonde	Upper air data
Ground Weather Radar	Precipitation and water droplet motions
Water Vapour Radiometer	Vertical humidity profile
Light Detection and Ranging (LIDAR)	atmospheric gases, clouds, and aerosols
Aircraft Meteorological Data Relay (AMDAR)	Air temperature, wind speed and direction, Pressure, Turbulence, Water Vapour
Global Navigation Satellite System (GNSS)	Precipitable water vapour or Integrated water vapour
Satellites	Radiance, Humidity, cloud cover, temperature heat balance, weather fronts, storm locations
Ships and Buoys	Air temperature, barometric pressure, aerosols wind speed and direction, water vapour, trace gases

broad scales. Time scales for local measurements are in minutes, that of synoptic scales are in days and for climatology a year to a decade or longer times are used (Hallett, 2003). As pointed out by Stankov (1998), there are several meteorological quantities that can be derived by combinations of independent measurements from separate instruments at areas of interest or from regions which have highly correlated physical ground conditions. Data observations can be divided into three categories: in-situ measurements, remote sensing from satellite platforms and remote sensing from ground station. Most widelyused in-situ observations are wind speed and direction, pressure, temperature, humidity. These data can be obtained from the National Weather Services' surface network. For Ghana, this service is provided by the Ghana Meteorological Agency (GMet).

Surface meteorological data used in tropospheric monitoring and integrated water vapour computation comprises total pressure, temperature, relative humidity (or partial water vapor pressure) and dew point (Bock et al., 2013, Hagemann et al., 2003, Hordyniec, 2014). Nave (2012) has given detailed explanations of these variables and how they are related. Surface pressure is of greater importance for the determination of zenith hydrostatic delays. An uncertainty in the measurement of pressure in the order of 0.5hPa to a maximum of 1hPa will correspond to 1.5mm to 3mm error in ZHD (Schu¨ler, 2001).

Surface temperatures are used in mean atmospheric temperature model for conversion of ZWD into precipitable water (PW) (§4.2 on page 54). Relative humidity and temperature are input into wet delay models and these models are subsequently used in predicting tropospheric delays.

For highly precise water vapour retrieval, the exact pressure and temperature at the GNSS sensor stations must be known or carefully extrapolated from nearby weather stations to separate the hydrostatic part from the total delays (Karabati´c, 2011). For this study data from the weather station located on KNUST Campus and operated by the Energy Centre[12] were used. Temperature, dew point and humidity measured at this station have a temporal resolution of 10 minutes, whereas barometric pressure and precipitation are measured hourly.

Models have been developed that can be used to extrapolate surface variables from nearby weather stations in case there are no such facilities at the GNSS base station. The pressure at the GNSS station (P_{GNSS}) can be extrapolated from the pressure measured at weather station, P_{MET},by this equation:

$$P_{GNSS} = P_{MET} \left(\frac{T_{MET} - \gamma(H_{GNSS} - H_{MET})}{T_{MET}} \right)^{\frac{g}{\gamma}} \tag{3.8}$$

T_{MET} denotes the temperature at the weather station, H_{GNSS} and H_{MET} are the orthometric heights of the GNSS and weather station and γ represents the temperature gradient. The gravitational parameter g is computed from Karabati´c (2011) as follows:

$$g(h,\varphi) = 9.8063(1 - 10^{-7}h)(1 - 0.0026373\cos(2\varphi) + 5.9 \cdot 10^{-6}\cos^2(2\varphi))$$

[12] the setup is an Automatic Weather Station (AWS) equipped with Barometric Pressure, temperature, humidity, wind, sun hour, precipitation sensors customized by Sutron Corp., USA

g is dependent on the station height h and the latitude φ.

3.4 Weather Forecasting

Weather and its changes are of great and immediate concern to people, plants, animals, living creatures as well as structures and installations because it affects lives, survival and sustenance daily. The impact of weather can be very dire if warnings are not given in time and the rate of change are not reported periodically. Almost all weather phenomenon occur in the tropospheric layer of the atmosphere. The atmosphere as been defined by Buizza (2002) is dynamical system with many degrees of freedom and predicting its state is very difficult. Again the atmospheric state is described by the tri-dimensional spatial distribution of wind, temperature, pressure, humidity and other weather variables (Taylor and Buizza, 2006). To forecast the weather and how the atmospheric variables evolve in time requires a complete understanding of physical principles and a comprehensive set of observations of the atmosphere (Pasini, 2005). Lai et al. (2004) and Oyediran and Adeyemo (2013) identified weather forecasting as a continuous, data-intensive, multidimensional and chaotic process. This implies that there is the need for good observations so that theories can be tested, the atmospheric state can be modelled and its evolution be predicted with greater certainty.

Weather forecasting is simply the application of science and state-of-art ICT to predict the state of the atmosphere at a location in future. For true and reliable forecasts of the weather, information must be gathered for a wider area and from different sources in order to understand the state of the atmosphere and identify the weather systems it contains and their motions. Forecasting of weather phenomena has evolved from an exercise in extrapolation to specific predictions of the evolution of weather systems to computer simulations that accurately forecast the evolution of weather systems (Coiffer, 2004). Below are techniques and approaches in forecasting the weather:

Persistence Technique:- works best for some regions in the world than others and the assumption is that weather now will persist for the next period. Examples are if the skies are clear in the morning, expect clear skies all day or if the pressure tendency is falling, expect low pressure coming through. Persistence techniques are most accurate for time scales of minutes to hours and computers are not used extensively (Wang, 2007).

Analogue Technique:- a compilation of previous weather events are used, with this a search is conducted into the analogous data to find weather phenomenon similar to what is happening today. Forecasting is done by using the event that happens in the ensuing days of the analogous database. Pattern recognition serves as the main guide in this approach (Stimac, 2006). This technique is useful method for longer-term forecasts (3 days – months) (Atkins, 2006).

Trend Technique:- if a phenomenon is in steady state, or is moving at constant speed then trend technique can be used. Weather systems such as fronts and cyclones move predictably, so if distance covered by cold front is known over a given time period, its position can be extrapolated in time (Smart, 2015). Predictions of this kind are limited to a few hours (Allaby, 2009).

Numerical Weather Prediction Technique:- with this approach given today's weather observations, the complex physical process in the atmosphere is simulated using numerical models on highly powerful computers to predict how the atmosphere will evolve in time. With Numerical Weather Prediction (NWP), predictions of the weather can be made for several days in advance with high degrees of confidence as greater insights have been gained into the factors causing changes in the atmosphere, and their likely timing and severity (Lynch, 2008). Because of the chaotic nature and non-linearity of the atmospheric processes, time integrations of the NWP models are treated as an initial-value problem (Kalnay, 2003). NWP models solve these by making sure the models used are realistic representation of the atmosphere and that the initial conditions fed into them are accurate.

The massive strides in weather forecasting during the past years have been due in large part to advances in technology and the growing understanding of the nature and dynamics of atmospheric phenomena (Dunn, 2003). Weather forecast irrespective of the technique used involves three steps: observation and analysis, extrapolation to find the future state of the atmosphere, and prediction of particular variables (Huffman, 2015). The best possible forecast can be obtained by a systematic combination of NWP products with conventional observations, radar imagery, satellite imagery and other data (Lynch, 2008).

3.4.1 Importance of Weather Data

Weather data comes in a variety of forms and can be obtained from human reports, insitu instruments, or remote sensors. For every facet of our lives, from the clothes we wear through to rocket launches, weather data has a critical role in decision making (Kann, 2005). Data associated with extreme weather events such as severe storms, hurricanes, dust storms and winter storms that can result in potential loss of lives and destruction to properties are carefully monitored and early warnings issued. Long records of weather data are compiled to create databases for climatologists to examine climate variability. These same data are used by modellers for model initialization and verification. Weather data is also use to monitor the spread of diseases (especially the communicable ones) and assist farmers in the applications of fertilizers and chemicals (Clark et al., 2001, Harmon, 2009). Kann (2005) and Muthike (2014) give comprehensive uses of weather data.

3.5 Ghana and Its Climate

Ghana is situated on the southern coast of the West African bulge with a total area of 238,540 sq km. From its southernmost tip at Cape Three Points, which lies on latitude 4^o 30^0 north of the equator to its northernmost point, 11^o North latitude, the country extends about 676km. The distance across the widest part, between longitude 1^o 12^0 east and longitude 3^o 15^0 west, measures about 563km (Oppong and Oppong, 2003). Bordered on the east by Togo, on the south by the Atlantic Ocean (Gulf of Guinea), on the west by Cˆote d´Ivoire, and on the north by Burkina Faso, Ghana has a total boundary length of 2,633km, of which 539km is coastline (Gall and Hobby, 2007). Ghana’s population in the mid-2015 was around 27.7million and it is projected to be 37.7million in the mid 2030 according to estimates provided Population Reference Bureau.[13] (Haub et al., 2015)

Ghana's coastline is mostly of a low sandy shore behind which stretches the coastal plain, except in the west, where the forest comes down to the sea. Ghana is mainly lowland with about half the country lying below 152m above sea level in elevation. The forest belt, which extends northward from the western coast to about 320km and eastward for a maximum of about 270km, is broken up into heavily wooded hills and steep ridges and it is drained by several rivers and streams. On top of the forest is undulating low scrub and grassy plains commonly referred to as the savannah belt and drained by the Black Volta and White Volta rivers (Gall and Hobby, 2007).

Climate

Ghana's location is in the tropics. Due to its location so close to the equator, the country receives an abundant supply of sunlight year-round. The major elements that influence the country's climate are prevailing air masses, latitudinal location and closeness to the sea. The climate is dominated by the interaction of the Inter-Tropical Discontinuity (ITD) and the West African Monsoon (Stanturf et al., 2011). Flamant et al. (2007) define ITD as the interface between the cool moist south-westerly monsoon flow and the warm, dry and aerosol-laden north-easterly harmattan flow. Climatic differences between various parts of the country are affected by the suns journey north or south of the equator and the corresponding position of ITD. Bordering the ITD are a series of low-pressure systems that produce precipitation. The ITD[14] migrates all year round, its location occurs nearer the coast during the months of December – January and gradually moves north by July and August. It then returns southwards more rapidly between September and December. Much of Ghana experiences two rainy periods based on the annual oscillation of ITD.

[13] *http://www.prb.org*

[14] The ITD is the demarcation line between north/north-eastern winds from the Sahara (hot, dry and dusty) and south/south-western winds from Atlantic Ocean (cool and moist)

Wet seasons - With exception of the northern part of Ghana, between the months of April to November the southern parts experiences two rainy seasons, from April – June and September – November. This situation occurs when warm and moist mT air mass intensifies and covers much of the country based on the northward or southward movement of the ITD (Flamant et al., 2007, Sultan and Janicot, 2003). The northward movement of the ITD brings much of the southern part of the country under the influence of humid, maritime tropical air resulting in the production of heavy precipitation associated with the rainy season. Squalls occur in the north during March and April, followed by occasional rain until August and September, where the rainfall reaches its peak. Average temperatures range between 21 – 32 ^{o}C, with relative humidity between 50% and 80%. Rainfall ranges from 830 – 2200 mm a year over Ghana (Gall and Hobby, 2007).

Dry seasons - The rains start to decline after September with total cessation at the end of October. The dry northeast trade-winds takes over and begins to dominate resulting in the so called Harmattan season (Manzanas et al., 2014). The dry and sometimes dusty tropical continental air mass originating over the Sahara Desert prevails over much of the country from November until March. Humidity is lowered causing hot days and cool nights during this period.

Temperature variation between day and night are relatively small in the south, but greater in the north, especially in January. During the dry season, many bush fires (both wild and of human orchestrated) are common throughout much of the country, particularly the northern part.

3.6 Reanalysis Data

Data from global reanalysis models were used for data validation as data from conventional water vapour sensing schemes and methods were not available. Reanalysis are comprehensive records of weather and climatic trends over time (CIRES, 2014). In it are observations and numerical models that simulates one or more aspects of the Earth system. Reanalysis data are created by ingesting all available observations at constant time intervals over the period being analysed using unchanging data assimilation schemes and models (Dee et al., 2014). The combinations are done objectively to generate a synthesized estimate of the state of the Earth system. Reanalysis and its products have become an integral part of Earth system science research across many disciplines (Bosilovich et al., 2012).

Reanalysis data have timespan of several decades, global coverage and can be obtained in either of these WMO approved formats - GRIB, netCDF and WMO BUFR (CIRES, 2014). The vertical resolution is from Earth's surface to well above the stratosphere. Reanalysis products are used extensively in climate research and services, monitoring climate variations and for predictions. Even though there have been massive improvements in their developments making research into areas of climatology and weather which were not possible previously (Rienecker et al., 2011), few challenges do exists. As pointed out by Dee et al. (2011a), the challenges are consistency in time, biases in observations and models.

A brief overview of some global reanalysis models used in this study are given below. Table 3.3 as adapted from CSIL Research Data Archive [15] gives summary of other reanalysis products.

NCEP: is operated by the National Center for Environmental Prediction-National Center for Atmospheric Research (NCEP-NCAR) of the United States (Kistler et al., 2001). The reanalysis datasets have 6-hourly temporal coverage, Daily and monthly values for the periods starting from 1979/01 to present (PSD, 2013). Products and forecasts from NCEP reanalysis are available at 0.2, 0.5, 1.0, and 2.5 degree horizontal resolutions (Dattore et al., 2015). 49 meteorological variables can be accessed from NCEP datasets.

[15] Research Data Archive is managed by the Data Support Section of the Computational and Information Systems Laboratory at the National Center for Atmospheric Research (http://rda.ucar.edu/)

ERA-Interim is an initiative of by European Centre for Medium-Range Weather Forecasts (ECMWF). ERA-Interim is a global atmospheric reanalysis from 1979 with real time updates. The data assimilation system used to produce ERA-Interim is based on a 2006 release of the IFS (Cy31r2) (Dee et al., 2011b). The spatial resolution of the data set is approximately 80 km (T255 spectral) on 60 vertical levels from the surface up to 0.1 hPa. Global atmospheric and surface parameters from 1979 to date, at T255 spectral resolution (≈80 km) on 60 vertical levels can be accessed (Berrisford et al., 2011).

JRA-55 is the second Japanese global atmospheric reanalysis project having a temporal range between 1957 to 2015. Its an improved model compared to its predecessor - JRA-25 (Ebita et al., 2011, Stepaniak et al., 2013). JRA-55 implemented a new data assimilation and prediction system with higher spatial resolution (TL319L60), new radiation scheme and a 4D-Variational bias correction for satellite radiances (Kobayashi et al., 2015). The entire JRA-55 production was completed in 2013, and updates are being added on real time basis. There are 43 variables in the JRA-55 model datasets from air temperature, vorticity, precipitable water among others (Harada et al., 2015).

Table 3.3: Overview of Reanalysis Models

Name	Developers	Time steps	Model Resolution
Climate Forecast System Reanalysis (CFSR)	NCEP	Sub-daily, Monthly	0.5^o x 0.5^o & 2.5^o x 2.5^o, 0.266 hPA top
ERA-Interim	ECMWF	Sub-daily, Monthly	0.75^o x 0.75^o x 60 lev 0.1 hPA top
JRA-55	Japanese Meteorological Agency	Sub-daily, Monthly	0.562^o x 0.562^o x 60 levels 0.1 hPA top
NASA MERRA	NASA	Sub-daily, Monthly	0.5^o x 0.667^o x 72 levels 0.1 hPA top
NCEP Reanalysis (R2)	NCEP, DOE	Sub-daily, Monthly	2.5^o x 2.5^o x 28 levels 3 hPA top
NCEP Reanalysis (R1)	NCEP, NCAR	Sub-daily, Month1y	1.875^o x 1.935^o x 28 levels 3 hPA top

Data from ERA-Interim, NCEP Reanalysis and JRA-55 were selected because they contain Precipitable Water (PW), have global coverage and with current time spans that were in sync with logged base station data.

Chapter 4

Tropospheric Delays from PPP

Computations of the slant tropospheric delays and subsequent mapping unto the zenith are discussed and the methodology for computing PW also given. In addition, the choice of Precise Point Positioning (PPP) as against Double-Differencing for tropospheric delay estimation in this thesis have been treated in this Chapter. Dispersion and central tendency test scenarios using online PPP servers computed ZTD were performed to assess the performance of *gLAB*[r] software before proceeding to computed the PW

4.1 Tropospheric Delay Model

The earth's atmosphere affects microwave or radio signals passing through it in three ways:

(i) it causes propagation delays;

(ii) it causes ray bending; and

(iii) signal absorption (Kleijer, 2004).

Propagation delays and ray bending effects on the neutral atmosphere were considered for this study and from literature the total delays depends on the refractivity along the travelled path (Adegoke and Onasanya, 2008, Petrov, 2014, Solheim et al., 1999). This refractivity is a function of pressure and temperature at the receiving station. From Fermat's principle[16] and following Kleijer (2004), the geometric distance of ray is given by:

$$L = \int_l dl, \tag{4.1}$$

where L is the geometrical distance and l is geometrical path. The excess path length becomes

$$\Delta L_a^i(\varepsilon) \doteq S - L = \int_s (n(s) - 1)ds + \{\int_s ds - \int_l dl\}, \tag{4.2}$$

where $\Delta L_a^i(\varepsilon)$ is excess path length (Delay) in the slant direction for a signal from satellite, i to receiver's antenna, a, at elevation angle, ε. $\int_s (n(s) - 1)ds$ on the righthand side is the excess path length caused by the propagation delay and $\{\int_s ds - \int_l dl\}$ is the excess path length caused by ray bending. This research considered the delay caused by excess path length and treated it as a distance parameter. The aspects caused by ray bending are negligible at higher satellite elevations based on the **dg.v1** model by (Mendes, 1999). The dg.v1 model is given by $a\exp^{-\varepsilon/b}$, where a = 2.256 ± 0.0092 m and b = 2.072 ± 0.0054^o. A resultant plot based on the dg.v1 model on elevation angles is shown in Figure 4.1

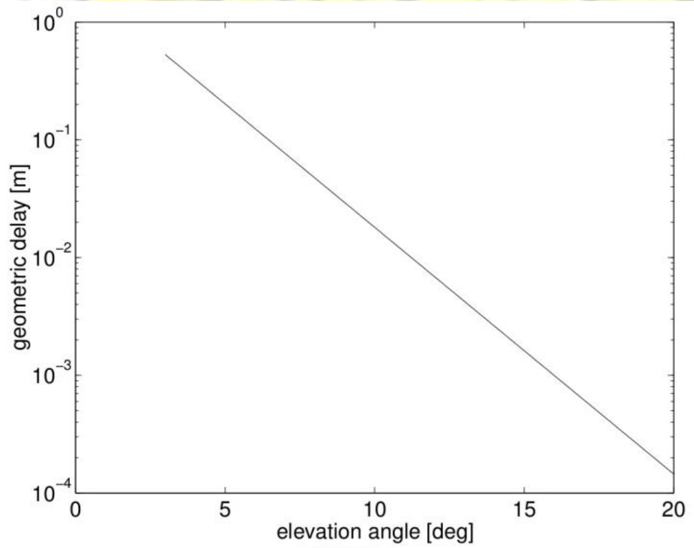

Figure 4.1: Ray bending effects on a radio signal

[16] electro-magnetic waves follow the path between two points involving the least travel time

Expressing $\int_s (n(s)-1)ds$ in terms of refractivity, $N(s)$ (refer Equation (2.10) on page 30), which is the sum of refractivities of the dry gases and water vapour in the atmosphere, and ignoring all other terms which are zero in the zenith direction. The compressibility factor as shown in Nilsson et al. (2013) for ideal gas, Z = 1, and other j^{th} constituent of air is given by:

$$Z_j = \frac{pM_j}{\rho_j RT}, \tag{4.3}$$

where is M_j is the molar mass and R is the universal gas constant. From equation (2.10) the first term is ZHD, caused by the induced dipole moment of the dry gases and the remaining terms are ZWD, caused by the water vapour molecules (Ning, 2012). Nilsson et al. (2013) went on to state that the refractivity of the atmosphere is a function of its temperature, pressure, water pressure and independent to microwave frequencies below 40GHz. Hence, GNSS signals propagating through the neutral atmosphere are also affected irrespective of the frequencies.

From the equation of state for ideal gases, we found out that $p_d/T = R_d\rho_d$, where, R_d is the specific gas constant of the dry constituent, ($R_d = R/M_d$, R is the universal gas constant and M_d is the molar mass of the dry gases). Using simple approximations and the assumption of hydrostatic equation being valid for total pressure and not for partial pressures, Davis et al. (1985) reformatted equation (2.10) to be:

$$N = k_1 R_d \rho + k_2' \frac{e}{T} + k_3 \frac{e}{T^2}, \tag{4.4}$$

k_2', which has been given earlier is derived by the expression $k_2' = k_2 - (M_w/M_d)k_1$, where M_w is the molar mass of water vapour; ρ is the total density of dry air and water vapour.

When all the slant delays are mapped onto the zenith direction, zenith hydrostatic delays, ZHD = ΔL^z_d can be obtained by considering the assumption that hydrostatic equilibrium have been satisfied (Davis et al., 1985);

$$\frac{dp}{dh} = -\rho(h)g(h) \tag{4.5}$$

where g is the acceleration due to gravity in the vertical direction; p is the total pressure. The resultant integration of the first term in Equation (4.4) gives:

$$\Delta L_d^z = (10^{-6} k_1 R_d g_m^{-1}) \cdot P_s \tag{4.6}$$

where P_s is the total ground pressure in hPa, g_m is gravitational acceleration at the mass centre of a vertical column of the atmosphere. Saastamoinen (1972) defines g_m = $(9.784 \pm 0.001 m/s^2) \cdot f(\theta,H)$, and $f(\theta,H) = (1 - 2.66 \cdot 10^{-3} \cos(2\theta) - 2.8 \cdot 10^{-7} H)$. The parameters θ and H are the latitude of the site in degrees and surface height above the geoid in meters respectively.

Substituting all the constants in Equation (4.6), the expression for solving ZHD in units of length becomes:

$$ZHD = \Delta L^z_d = 0.002277(1 + 0.0026\cos 2\theta + 0.00028H) \cdot P_s \tag{4.7}$$

4.2 Precipitable Water Computation

The software *gLAB*ʳ (Hernandez-Pajares et al., 2010) outputs the slant delays mapped onto the zenith. With *ZTD* already computed and knowledge of the precise coordinates of the antenna position (θ,H) and surface pressure values from nearby weather station, $ZWD = \Delta L_w^z$ can be computed using $ZTD = ZHD + ZWD$ and Equation (4.7). Two parameters are used to refer to the atmospheric water vapour content. These are Integrated Water Vapour (IWV) in units of kg/m^2 which refers to the quantity of the atmospheric water vapour over a specific location and Precipitable Water (PW) used to express the height of an equivalent column of liquid water in units of length. Bevis et al. (1992) gives IWV as:

$$IWV = \int_0^\infty p_v(h)dh = \frac{1}{R_w}\int_0^\infty \frac{e(h)}{T(h)}dh \tag{4.8}$$

where p_v is the partial density of water vapour in kg/m^3; the height h in metres and R_w is the specific gas constant for water vapour in $J/(kgK)$. PW relates to IWV by diving with the density of liquid water, ρ_w. $PW = IWV/\rho_w$. Again IWV is related to the ZWD using a dimensionless quantity as conversion factor, Π:

$$IWV = \frac{\Delta L_w^z}{\Pi}, \quad PW = \frac{\Delta L_w^z}{\rho_w \cdot \Pi} \tag{4.9}$$

From Equation (2.11) and considering the second and third terms of Equation (4.4), the wet delays becomes:

$$\Delta L_w^z = 10^{-6} \int_z (k_2' \frac{e(z)}{T(z)} + k_3 \frac{e(z)}{T(z)^2}) dz \tag{4.10}$$

substituting the constants and introducing a mean temperature, T_m, which is defined by Bevis et al. (1992) as: $T_M = 0.72T_s + 70.2$, where T_s is the surface temperature. The conversion factor finally becomes:

$$\Pi = 10^{-6} \rho_w R_w (k_2' + \frac{k_3}{T_m}) \tag{4.11}$$

Bevis et al. (1994) computed Π to be approximately 0.15. This dimensionless constant is a function of season, location, and weather. The minimum and maximum values can have a range with variation of over 20% (Liou et al., 2001). Computed Π ranged between 0.1598 to 0.1665, with an average value of 0.1629 and a standard deviation of 0.0013.

4.3 Observation Data

A single GPS base station on top of the New Engineering building at KNUST, Kumasi was used for logging GPS signals and subsequently retrieval of IWV. Sample shots of the Base station antenna and the receiver is shown in Figure 4.2. The location of the study site on the West African[17] map is shown in Figure 4.3.

[17] Google Maps:- https://maps.google.com.gh/

The Base station equipment is a 12-channel dual frequency survey-grade Sokkia receiver with an SOK600 L1/L2 GPS Antenna using Pinwheel Technology from Novatel Inc. Canada. It was used to log 24-hour GPS datasets at 30-sec logging rate between these periods:

Figure 4.2: KNUST Base Station and *Sokkia*^{r} GSR 2600 used for data logging

Figure 4.3: Kumasi, study area for this study (Google, 2015)

1) Feb, 2013 to May, 2013

2) Sept, 2013 to May, 2014

3) Sept, 2014 to Dec, 2014

The logged data were processed using the *gLAB*^{r} software (Hernandez-Pajares et al., 2010) in PPP mode. The PPP mode was chosen because this study involved the collection of GNSS datasets from a single base station. The logged datasets were converted from *Sokkia*^{r} *.pdc format to RINEX (Gurtner and Estey, 2007) format. Sample Rinex header of the base station observation file is given in Appendix B.

4.4 Processing Techniques

GPS datasets were processed using the gLAB software version 2.0.0 (Hernandez-Pajares et al., 2010) in PPP mode. PPP implementation in GNSS data processing is based on carrier phases (Kouba and H´eroux, 2001). PPP techniques have short processing cycles without significant loss in accuracy. Again knowledge of the precise coordinates of the reference receiver, inter-station distance limitation and simultaneous observations in double-differenced differential techniques are not needed in PPP(Karabati´c, 2011). These advantages made PPP the perfect technique for this study. The *gLAB*ʳ software package, an open-source tool, which offers the user flexibility in parameter manipulations and customized script coding.

Data used in *gLAB*ʳ were decimated to 300 secs and an elevation mask[18] of 5^o was

set. Other parameters set were L1-C1 difference used for cycle-slips detection (Subriana et al., 2013). Receiver antenna phase center and reference point corrections (§2.2.3.1 on page 25) were applied based on values and parameters in IGS ANTEX file (Rothacher and Schmid, 2010). The Klobuchar model was used for ionospheric delay elimination

(Klobuchar, 1987). Phase wind up, relativistic path and clock correction were applied (§2.2.3.3 on page 27). The UNB-3 (Collins and Langley, 1999) tropospheric model was used as well as the Simple Mapping function based on an obliquity factor, $M(\varepsilon)$, as described in Black and Eisner (1984), Subriana et al. (2013) and valid for satellites with elevations greater than 5^o above the horizon. The Simple mapping function which is common for both dry and wet components is shown below:

$$M_{dry}(\varepsilon) = M_{wet}(\varepsilon) = M(\varepsilon) = \frac{1.001}{\sqrt{0.002001 + \sin^2(\varepsilon)}} \tag{4.12}$$

In addition, precise clocks and orbital products were used (Caissy et al., 2012, Kouba, 2009, Noll et al., 2009). The final orbits and clock corrections were downloaded from the

[18] Observations at low elevations are susceptible to tropospheric refraction and multipath effects than those at high elevations but advantageous in enhancing satellite geometry and reliable decorrelation of ZWD estimates

servers of the International GNSS Service (IGS-Webmasters, 2015). Prior to processing, data cleaning and quality checks were made with the TEQC software (Estey and Meertens, 1999). The checks were done for data completeness, cycle slips and multipath detection.

4.5 Coordinates of Antenna Position

An a priori or possibly the precise knowledge of the Base station's antenna position must be known in a specific reference datum. For this study the ITRF2008 reference frame was used (Altamimi et al., 2011). The delays caused by the neutral atmospheric can be estimated very accurately by using a geodetic-grade receiver to log signal for a longer session (Dach et al., 2007, Lichten et al., 2005). The coordinates of the KNUST Base station used for IWV retrieval was computed using three different methods. They were (i) online PPP services, (ii) online DGPS service and (iii) manual computations using gLAB. Data used had 24-hour session lengths and they were picked randomly between the months of October to December 2013. In all 22 days of data were processed for determination of the precise antenna position. The online GNSS processing servers used were:

(i) Canadian Spatial Reference System Precise Point Positioning (CSRS-PPP) a division of Natural Resources Canada (CSRS, 2015, Mireault et al., 2008, T´etreault et al., 2005);

(ii) The Automatic Precise Positioning Service (APPS) of the Global Differential GPS (GDGPS) System from Jet Propulsion Laboratory, California Institute of Technology (APPS, 2015);

(iii) GPS Analysis and Positioning Software from Dept of Geodesy and Geomatics Engineering, University of New Brunswick (GAPS, 2015) and

(iv) AUSPOS - Online GPS Processing Service from Geoscience Australia a division of Department of Resources, Energy and Tourism (AUSPOS, 2015)

Five different sets of results were obtained. The results from the four online services were compared with the output from gLAB. A T-statistic test (MATLAB, 2015) were done on the computed means for all four groups against gLAB. A summary report on the t-test is shown in Table 4.1.

At the 5% significance level all four services show mixed results in terms of significant differences between the computed means. With no two sets of computed results agreeing

Table 4.1: T-test @ 5% Significance level or 95% Confidence Interval

		APPS			CSRS-PPP		
		X	Y	Z	X	Y	Z
gLAB	**t-stat**	-2.6352	0.3838	2.3455	-6.3981	-1.405	-0.0485
	$h_{0\ or\ 1}$	1	0	1	1	0	0
		degree of freedom (*df*) = 40			*df* = 40		
		GAPS			**AUSPOS**		
		X	Y	Z	X	Y	Z
gLAB	**t-stat**	18.0326	-1.9425	-4.526	-5.6474	-4.9568	4.9431
	$h_{0\ or\ 1}$	1	0	1	1	1	1
		df = 41			*df* = 42		

to have no significant difference in all three axes, the results from gLAB were used for the final antenna position. Table 4.2 shows the final antenna position written to the Rinex headers and used for IWV retrieval. The orthometric height was obtained based on the Earth Gravitational Model 2008 (EGM2008) (Pavlis et al., 2012) using the GeoidEval utility from Karney (2014).

Table 4.2: Final Computed Coordinates of the Antenna Position

	ITRF08 (m)		UTM (Zone 30N)	WGS 84
X	6333147.8021 ± 0.0022	E	658546.1868 m	Lat (φ) 6^o 40^0 21.73425″
Y	-173104.3697 ± 0.0012	N	737798.3009 m	Lon (λ) -1^o 33^0 56.44693″
Z	736230.3926 ± 0.0010	h_{ellip}	296.528 m	H_{ortho} 269.526 m

Processed results of all the online services are given in the Appendix A

4.6 Tests on Computed ZTD

In order to evaluate the potential of PPP techniques to derive the ZWD estimates using *gLAB*[r] with satisfactory accuracies, time resolution and delivery formats fit for operational

NWP, test calculations on computed ZTD using online PPP servers were performed. Descriptive statistics and correlation analysis were done on ZTD estimates computed with gLAB, APPS and CSRS online PPP services (§4.5 on page 58). 24-hourly data for the months of September to December in 2014 were used and uploaded to the online PPP services. Positional coordinates, station clocks and ZTDs from the resulting outputs were downloaded from the servers and used. Hourly data were extracted from the three (3) different processing software for the ZTD comparison tests. CSRS-PPP computes its results per every 30 secs whilst APPS and gLAB write their solutions every 300 secs. Sample output files are given in Appendix B on page 126. Figure 4.4 shows plot of computed ZTD values from the three services against day of the year (DOY). The plot

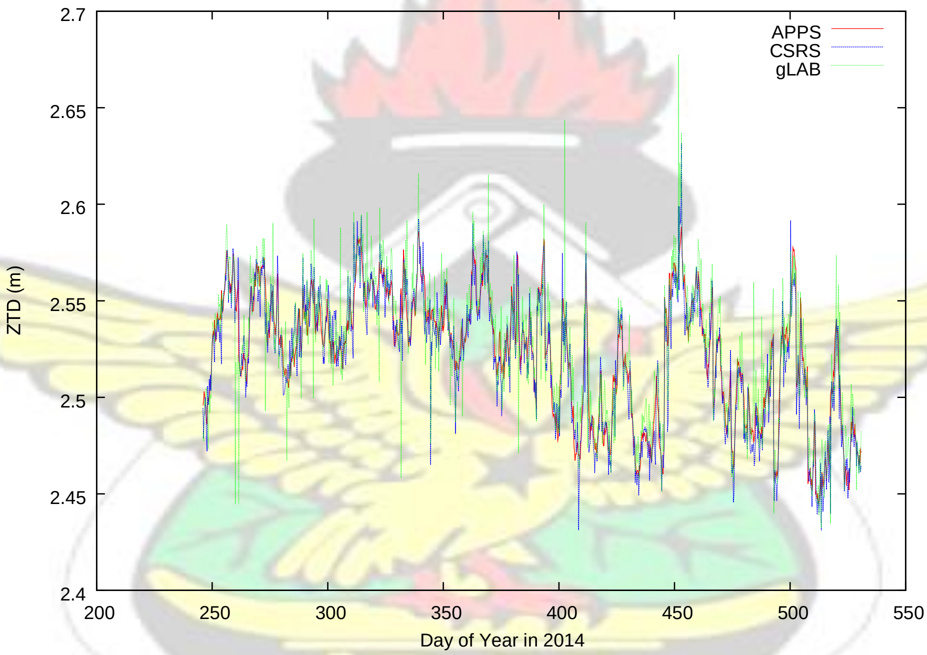

Figure 4.4: ZTD plot against Day-of-Year for online PPP server values and gLAB computations

in general shows agreement in pattern for all three computed results except the gLAB values which depicts occasional spikes at the start of each day due to extra time required for carrier-phase ambiguities resolutions. A descriptive statistics with μ as mean, σ as the standard deviation and ε as standard errors were run on the ZTD data gave values in Table 4.3. In addition, a box plot indicating the minimum, maximum, inter-quartile range and possible outliers are presented in Figure 4.5. Further analysis were conducted

Table 4.3: Descriptive Statistics on computed ZTD

	APPS	**CSRS**	**gLAB**

μ	2.52328	2.52097	2.52616
σ	0.032179	0.03424	0.035185
ε	0.000953	0.001014	0.001042
Range	0.1438	0.2706	0.3815

to compute the correlation coefficients between gLAB ZTD values and ZTDs from APPS

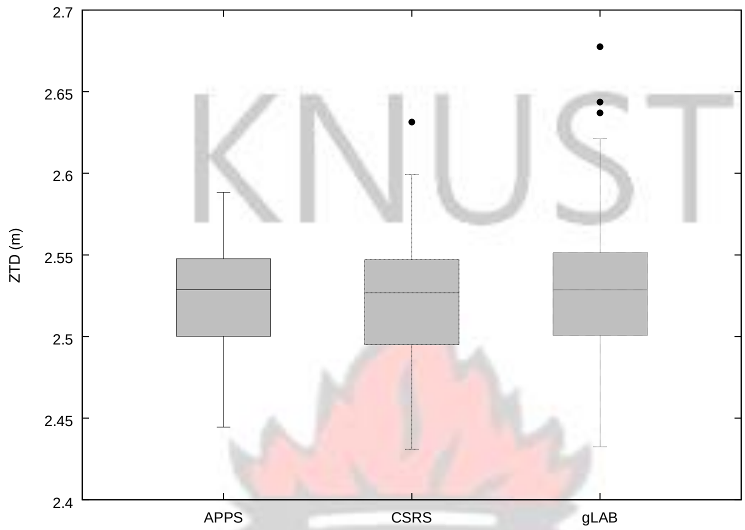

Figure 4.5: Box plot showing data distribution of computed ZTD from the 3 processing approaches

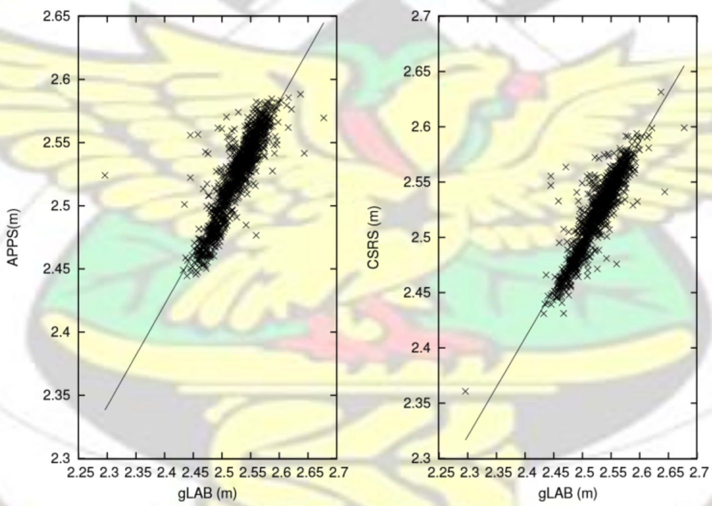

Figure 4.6: Correlation plot APPS and CSRS values against gLAB

and CSRS servers. The results were 0.912 for APPS and 0.878 for CSRS (Figure 4.6), these values clearly show that gLAB, APPS and CSRS are positively correlated. The differences in values may be attributed to different tropospheric models, elevation masks set and surface meteorological values implemented in the various software. The statistics and resulting values indicate that gLAB compares favourably with APPS which uses the GIPSY/OASIS (Lichten et al., 2005) processing engine than CSRS-PPP ver. 1.05 (T´etreault et al., 2005). Hence it can be concluded that gLAB–computed ZTDs can be used for ZWD estimates and further retrieval of Integrated Water Vapour (IWV) or Precipitable Water (PW) or Total Column Water Vapour.

Chapter 5

Results and Discussions

This chapter is devoted to presenting results and analysis on the computed IWV or PW values based on formulas and approach described in §2.2.3.5 on page 29 and §4.1 on page 51. GPS data logs starting from the February 2013 to December 2014, with breaks in the months of June to September 2013 and 2014, were used for ZTD computations from gLAB software. Next step was the calculations of ZHD using surface pressure, station latitude and height, having obtained these ZHD values simple arithmetic subtractions from ZTD at the same timestamps gives ZWD values. PW values are then retrieved from ZWD by multiplying them with the dimensionless constant, $\Pi = 0.1629$, computed in §4.2 on page 54.

Tests and analysis done in this chapter were based on computed PW from delays caused by the troposphere on GNSS signals and PW downloaded from global reanalysis models. Data from three (3) global reanalysis models namely ERA-Interim (Dee et al., 2011b), NCEP Reanalysis (Kistler et al., 2001) and JRA-55 (Ebita et al., 2011) were used (refer §3.6 on page 48). The climate data operators (CDO) (Schulzweida et al., 2009) routines/commands were run at the Linux terminal to read and extract the PW values from proprietary NetCDF and GRIB weather data formats. Details on the usage of CDO software are given in Appendix C. Moreover an investigation into the seasonal variations of precipitable water sampled over the study area has been conducted. A proposal has been given in exploiting the full-scaled deployment of GNSS Meteorology based

on GMet synoptic stations location and the planned Continuous Operating Reference Stations (CORS) to be set-up by Survey and Mapping Division of the Ghana Lands Commission. Lastly a single-station GNSS Tomography (Bender et al., 2011, Benevides et al., 2014, Rohm and Bosy, 2009, Troller et al., 2006) was reviewed for possible replication in the event data from a network of GNSS stations can be accessed real-time in Ghana.

5.1 PW Comparisions

The ZHD values that were used to compute PW were based on two (2) approaches; one that uses surface variables and the other with no weather data (refer Equations (2.12) & (4.7)–(4.11) in Sections §2.2.3.5 and §4.1 respectively). A plot comparing the PW computed with no surface variables against PW or total column water vapour from global reanalysis models is shown in Figure 5.1. Correlation analysis conducted gave these, *r*, values of 0.541 for JRA, 0.598 for ERA-Interim and 0.458 for NCEP. Correlation plots are shown in Figure 5.2. The results clearly show that the model without weather data correlates positively with the global reanalysis products but gave values that under-sampled the total PW in the atmosphere as indicated by the NWP models.

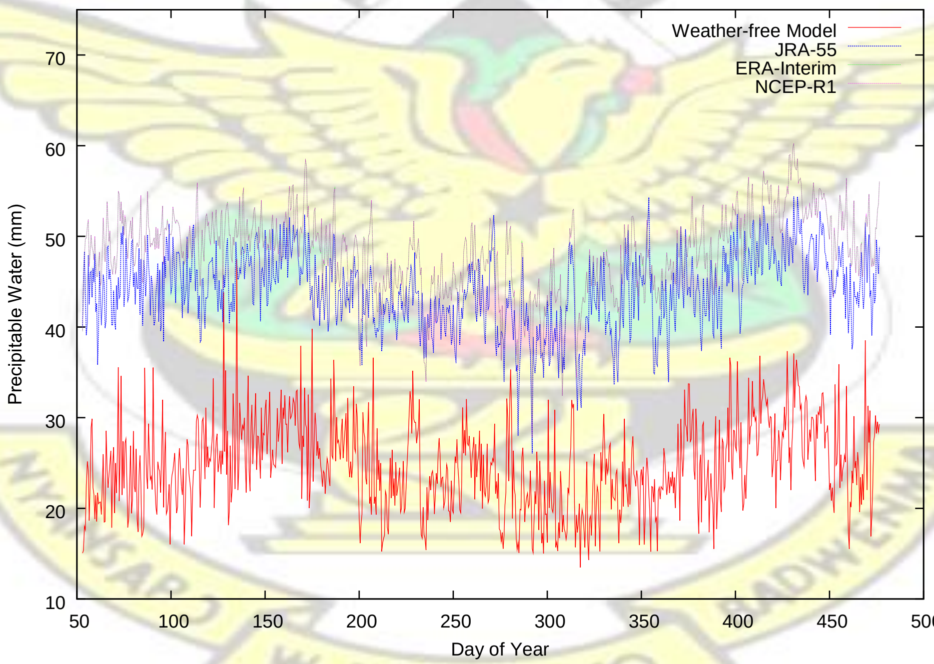

Figure 5.1: Plot of Computed PW from Weather-free Model and Retrieved from Reanalysis Models against DoY

Further computations were done using surface weather variables (i.e. pressure, temperature & water vapour pressure) to retrieve PW and compared with the global reanalysis products in Figure 5.3 the computed correlation using bootstrapping[19] and 95% Confidence Interval (CI) is showed in Figure 5.4. Results indicate stronger positive correlations than those computed using the weather-free model. The findings show that retrieved PW from the KNUST GPS station correlates better with ERA-Interim, with an *r*–value of 0.8345 whilst JRA and NCEP-R1 gave, *r*, of 0.7729 and 0.6491 respectively. Similar study done by Motell et al. (2002) comparing GPS derived PW with Advanced Very High Resolution Radiometer (AVHRR) split-window techniques and radiosondes over Hawaii resulted in $R = 0.64$. Gutman et al. (2003) working at a site in North Central Oklahoma, compared rawinsonde with GPS water vapour retrievals and recorded correlation coefficient of 0.993. Other assignments have been carried out in the past (Bokoye et al. (2003), Mims et al. (2011), Motell et al. (2002), Yoshihara et al. (2000)) all geared towards the comparisons of PW values retrieved from GPS, radiosonde, sun photometers, radiometers and other sensing approaches, they all reported positive correlations.

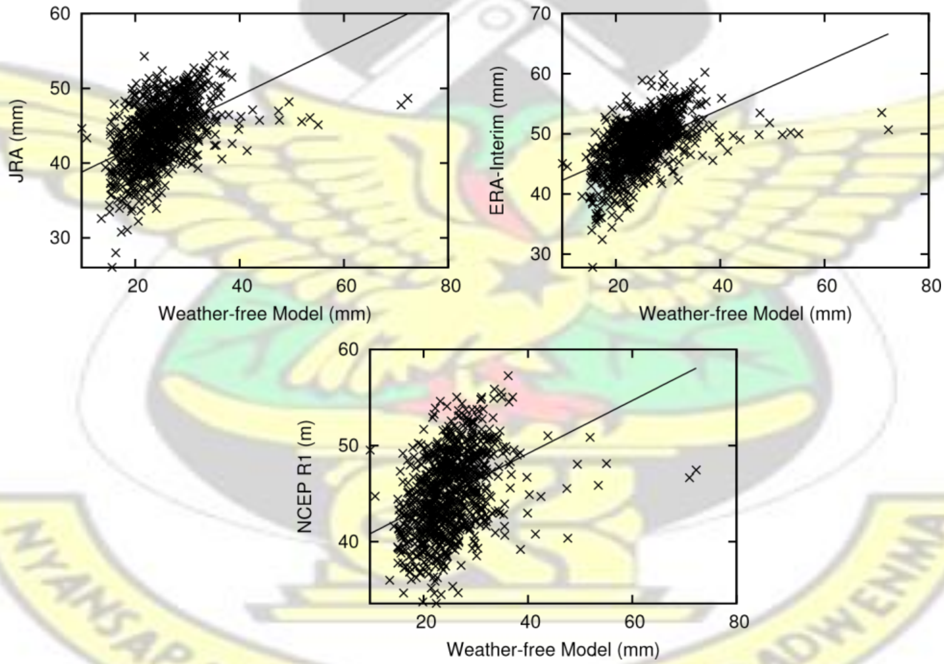

Figure 5.2: Linear-fit plots for Correlation values for computed PW from Weatherfree model and Reanalysis models resulted in 0.541 for JRA, 0.598 for ERA-Interim and 0.458 for NCEP-R1

[19] Bootstrapping is a statistical approach that uses random sampling with replacement to assign measures of accuracy to sample estimates (Boos et al., 2003)

5.1.1 Curve Fitting and Model for Prediction

Considering all the variables and quantities used in computing and retrieving PW, analyses were done to develop a model for predicting PW based on the independent variable(s) used. First, correlation coefficients[2] were computed and results are shown in Table 5.1. PW and ZTD gave the highest *r* of 0.9444 in linear relationship, hence all model-fitting tests were based on these two quantities. The normalized linear, linear and logarithmic model fitting were considered. Plots of the three linear-fitting models including residuals, R^2 and RMSE values are shown in Figure 5.5. A bigger and clearer plots of Figure 5.5 are shown in §Appendix A

From the linear-fitting modelling, the linear model gave better results in terms of R^2 and *RMSE* values. This model was then used to compute PW values and compared with

[2] correlation coefficient sometimes referred to as *r*, *R*, or *Pearson's r*, is a measure of the strength and direction of the linear relationship between two variables

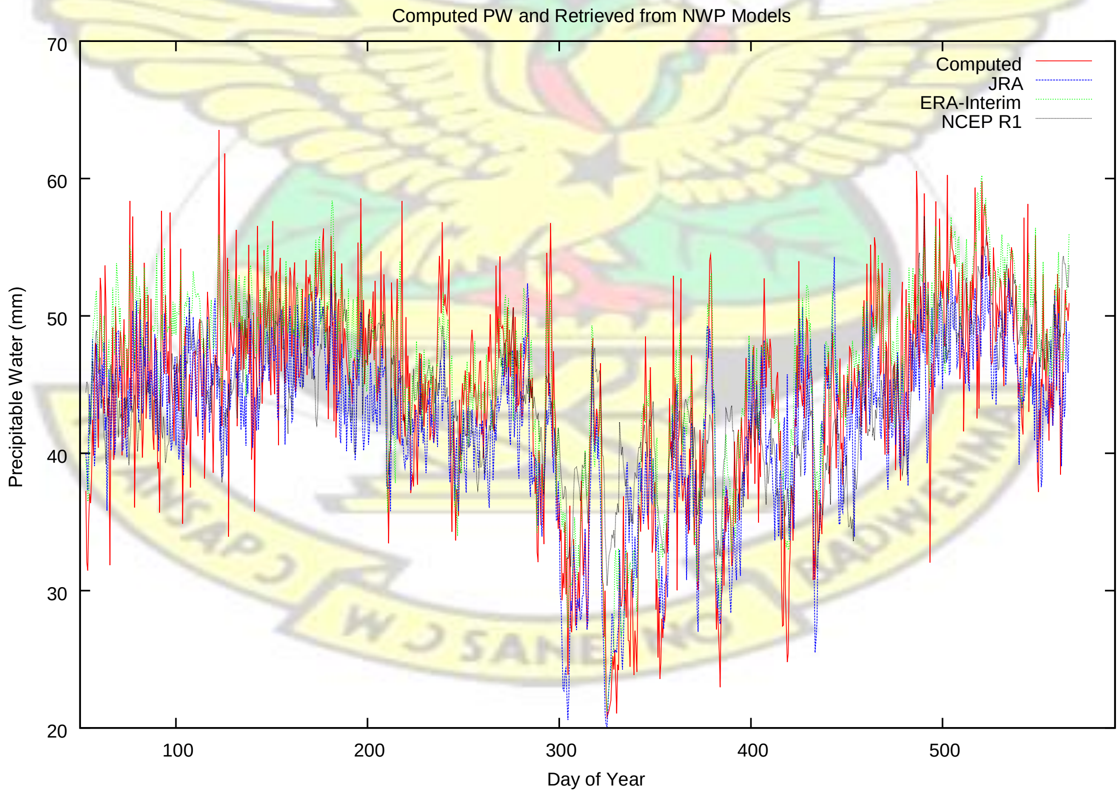

Figure 5.3: Plot of Computed PW using Weather data and PW Retrieved from Reanalysis Models against DoY

the Reanalysis data. The resultant plots including residuals, R^2 and *RMSE* values are shown in Figure 5.6 and Table 5.2. Results in Figures 5.4 & 5.6 and Table 5.2 clearly indicate that the linear model predicted the Total Column Water Vapour (TCWV) or PW sampled by ERA-Interim better when the 3 global reanalysis products are compared

A bigger and clearer plots of Figure 5.6 are shown in §Appendix A

Table 5.1: Correlation coefficients, *r*, for Station Heights, PW, ZTD and surface weather variables

	PW (mm)	ZTD (m)	BP (hPA)	T (K)	RH (%)	Hgt (m)
PW	1.0000	0.9444	0.0281	0.0465	0.2395	-0.1882
ZTD	0.9444	1.0000	0.1140	-0.0274	0.2812	-0.2884
BP	0.0281	0.1140	1.0000	-0.2806	0.2570	0.0035
T	0.0465	-0.0274	-0.2806	1.0000	-0.8038	-0.0753
RH	0.2395	0.2812	0.2570	-0.8038	1.0000	0.0090
Hgt	-0.1882	-0.2884	0.0035	-0.0753	0.0090	1.0000

BP is Barometric Pressure, RH is Relative Humidity, T is Temperature,
Hgt is Station Ellipsoidal heights

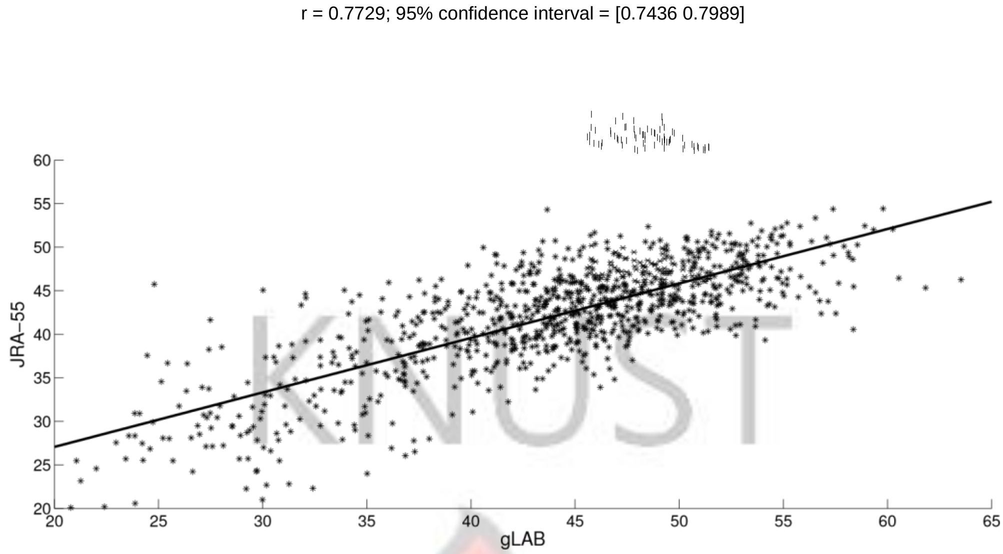

(a) Computed PW against JRA

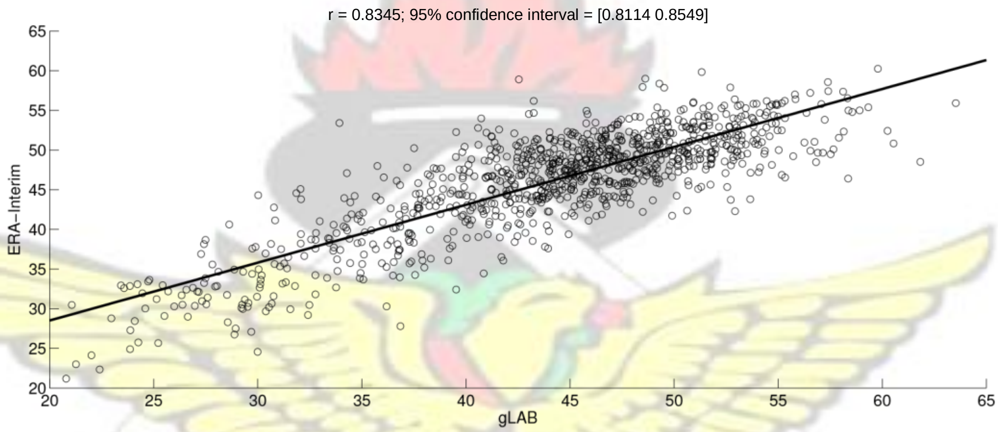

(b) Computed PW against ERA-Interim

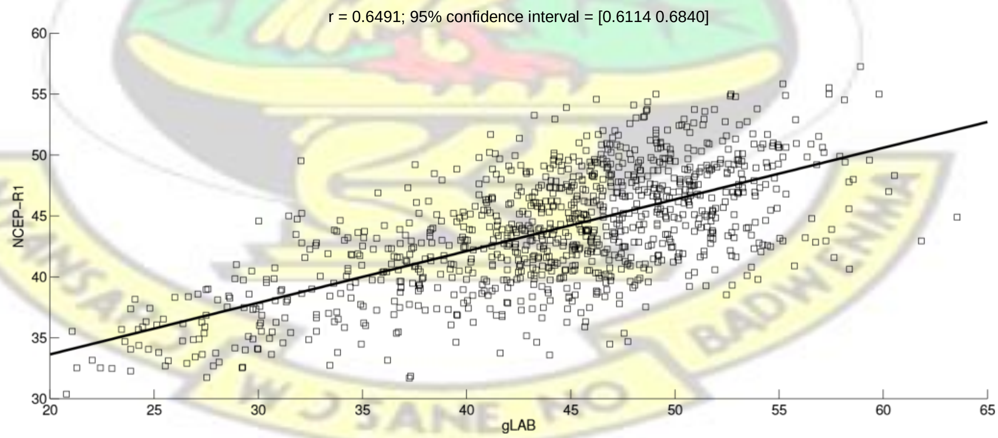

(c) Computed PW against NCEP-R1

Figure 5.4: Correlation Plots using Bootstrapping and 95% CI tests resulted in r values of 0.7729 for JRA, 0.8345 for ERA-Interim and 0.6491 for NCEP-R1

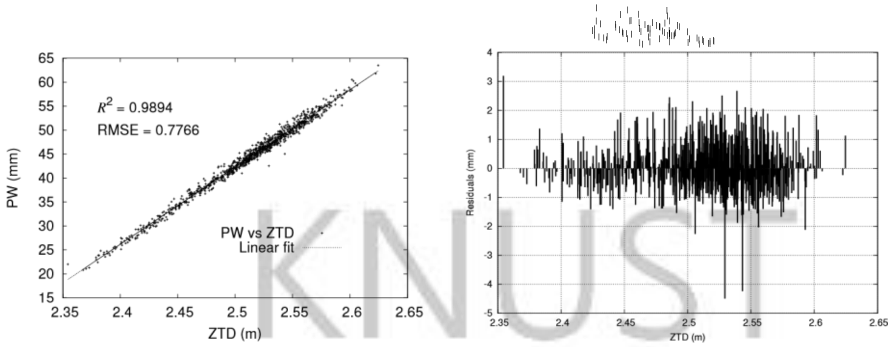

(a) Linear fit with R^2 = 0.9894 and $RMSE$ = 0.7766 yielding $F(x)$ = 161.2(x) − 360.7

(b)

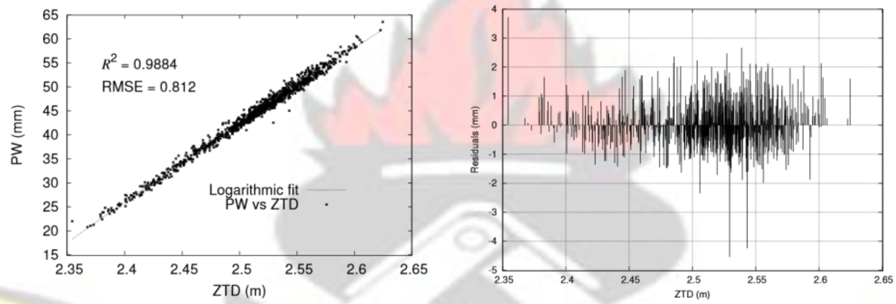

(c) Logarithmic fit with R^2 = 0.9884 and $RMSE$ = 0.812 yielding $F(x) = 401.35 \cdot ln(x) - 325.37$

(d)

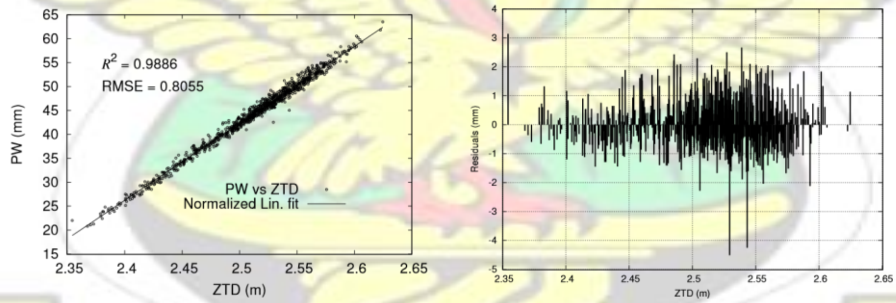

(e) Normalized-Linear fit with R^2 = 0.9886 and $RMSE$ = 0.8055 yielding $F(x)$ = 7.49(z)+44.09, where $z = \frac{x-\mu}{\sigma}$, μ = 2.511 & σ = 0.04653

(f)

Figure 5.5: Linear-fitting models

Table 5.2: Standard Error of Estimate and R^2 between predicted PW and Reanalysis models

	SE	R_2
PW_{JRA}	6.0139	0.7729
PW_{ERA}	5.398	0.8345
PW_{NCEP}	6.338	0.6491

5.1.2 Seasonal Variations of PW

Considering the climatic seasons and rainfall patterns in Ghana, [Kumasi area to be precise], tests were conducted to determine how retrieved PW vary with meteorological

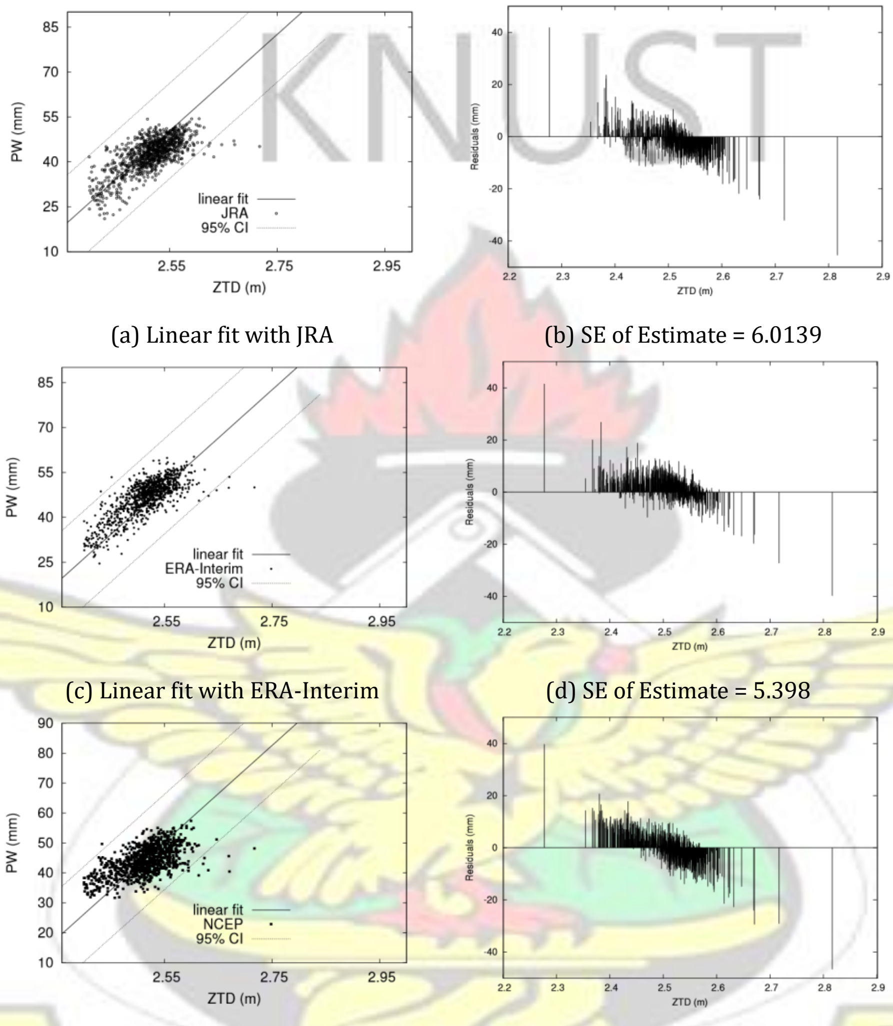

(a) Linear fit with JRA (b) SE of Estimate = 6.0139

(c) Linear fit with ERA-Interim (d) SE of Estimate = 5.398

(e) Linear fit with NCEP-R1 (f) SE of Estimate = 6.338

Figure 5.6: Linear model trendline with 95% C.I. bounds and Reanalysis Data comparison

seasons. Data were grouped based on the two seasons (i.e. wet and dry seasons) and rainfall patterns within the southern climatological zone of Ghana (Manzanas et al., 2014, McSweeney et al., 2010, Owusu and Waylen, 2009, GMet editors, 2013). Table 5.3 gives the descriptive statistics of the computed PW using signals from GNSS. Figure 5.7 shows a plot of the computed PW and Predicted PW with associated R^2 and *RMSE* values.

The results show that the amount of atmospheric water vapour agrees with the study area's weather pattern. PW increases in the rainy seasons of April to June and from

September to November whereas there are decreases in the water vapour contents in the dry seasons. The results compare favourably with similar work carried-out by Wang et al. (2013) in Chengdu, that analysed changes PW have with the strength of zonal and meridional winds as well as the East Asian monsoon system. Again, studies by Jade et al. (2005) using annual variations of water vapour based on Indian seasons in a three-year period using NCEP models, observed meteorological data and GPS signals gave similar results matching local weather patterns.

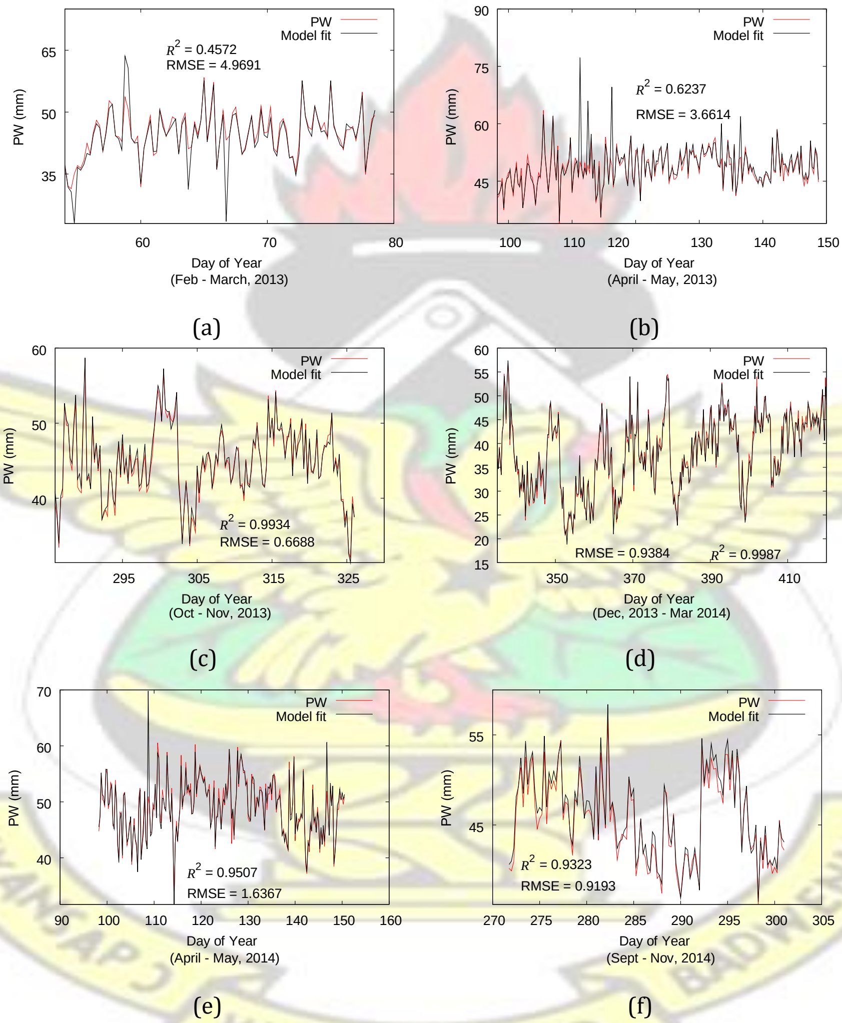

Figure 5.7: PW values against Days of the Year grouped according to weather seasons

On the plots in Figure 5.7, the linear-model predicted PW perfectly for September to November rainy season and also December to March dry season. The regression analysis for the major rainy season of April to June gave very good R^2 but high RMSE values. This can be due to the fact that no data was recorded in the months of June to August for the study period. Aside this small variations due to data gaps, the linear-model of $F(x) = 161.2 \cdot x - 360.7$ can predict the atmospheric water vapour over the Kumasi Station with an expected R^2 of 0.826 and *RMSE* of 2.132 mm. A study by Choy et al. (2013) indicated that there is strong spatial and temporal correlation between the variations of GPS-PWV and storm passages. Their report revealed uncertainties of 2–3mm in GPS derived PW. Vedel and Huang (2003) concluded that forecasts based on analyses including GPS ZTD data have higher precision when it comes to prediction of significant precipitation. Finally, Pollet et al. (2014), Dousa and Bennitt (2013), Chen et al. (2011) and Bender et al. (2008) all found higher correlations and smaller biases and root mean square errors between ZWD series provided by GPS and other water vapour sensing techniques. Their estimates correspond very well (≤ 1cm) and are consistent with NWP models at the centimetre level.

Table 5.3: Descriptive Statistics of PW grouped according to weather seasons

		Max	Min	Mean	σ	Rang
		63.533	20.794	44.290	7.291	42.73
Climatic Seasons	Feb - Mar 2013	58.375	31.454	45.053	5.581	26.921
	Apr - May 2013	63.533	33.924	48.395	4.401	29.609
	Oct - Nov 2013	58.360	32.070	44.721	4.834	26.290
	Dec - Mar 2014	56.747	20.794	38.065	7.722	35.953
	Apr - May 2014	60.545	32.052	49.003	4.932	28.493
	Sep - Nov	56.775	36.166	45.571	4.616	20.609

	201 4	

There are two rainy seasons in the study area: April through June and September through November

5.2 GNSS Tomography

The past decades have seen massive developments in GNSS atmospheric processing and soundings to provide integrated water vapour estimates. These integrated profiles lack a vertical discretization of the atmospheric processes because the atmosphere is assumed to be horizontally homogeneous. Mapping function are modelled based on this assumption for converting slant delays unto the zenith direction for PW or IWV retrieval (Bastin et al., 2007, Bender et al., 2011, Jones, 2010). For larger areas, this assumption does not hold hence individual slant delays must be considered to characterize vividly the atmospheric water vapour contents. The availability of a large number of data from different directions can be combined to spatially resolve atmospheric water vapour field by means of tomographic reconstruction techniques. Reconstructions of the observed slant delays allow for 3D analysis of the troposphere (Benevides et al., 2014). Troller et al. (2006) emphasized that the estimation of integrated water vapour contents amount is well established. However, the determination of the spatial water vapour distribution and its temporal variation in 3D field is still a major challenge.

The atmospheric water vapour observed in different directions are used to reconstruct its spatial distribution on a 3D grid using techniques called GNSS Tomography. GNSS tomography utilizes small deviation caused by the atmospheric layers between existing infrastructure of GNSS satellites and networks of geodetic reference stations to evaluate the amount of water vapour above the ground station (Wickert, 2014). This leads to temporally and spatially resolved field of the atmospheric water vapour. Slant delays are the basic information required to perform the GNSS tomography. Tomography works on a spatial grid and tries to partition the integral slant delays on the different grid cells

Figure 5.8. If sufficient data are available a spatially resolved field can be obtained. The major challenge in GNSS tomography is data availability as compared with huge volume of the atmosphere.

Other limitations identified by Rohm et al. (2012) are:

- the best approach to deliver more reliable slant delays;
- development of robust algorithms that will be precise and accurate in order to account for outliers in observations; and
- provision of effective channels to link meteorological agencies for near real-time processing of data

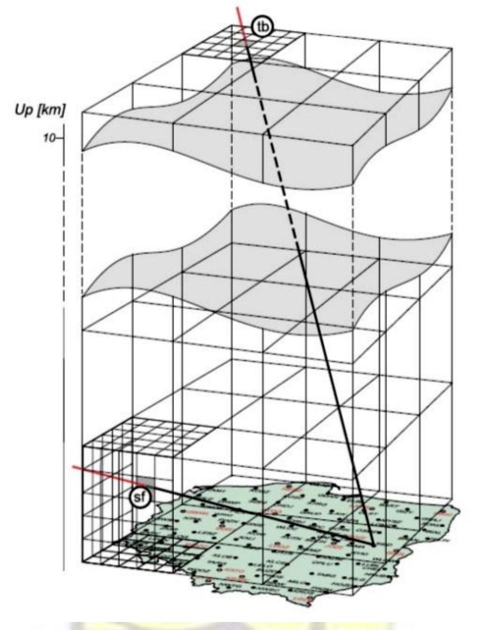

Figure 5.8: GNSS Tomographic concepts showing rays through vertical layers called voxels (Bosy et al., 2010)

5.2.1 GNSS Tomography Formulation

To retrieve the 3D water vapour density structure, a discretization of the troposphere on the study area has to be performed, where it is spatially divided into a finite number of boxes or cells (usually called voxels). Constant values are assigned to each cell [refer Figure 5.8] (Bender et al., 2011, Flores et al., 2000, Troller et al., 2006). A tomographic reconstruction of the atmospheric state is made possible based on these factors identified by Bender and Raabe (2007), Gradinarsky and JarLemark (2004) and Bastin et al. (2007):

(i) a large number of observations from a dense distribution of stations,

(ii) wide-area coverage and

(iii) availability of slant delays from wide angular range.

The reconstruction of a spatially resolved field from such integrated information (i.e. slant tropospheric delays (STD)) requires the solution of an inverse ill-posed problem with incomplete data (Bender and Raabe, 2007). To simulate realistic STD observations for tomographic imaging, a high resolution 3D refractivity field is required and NWP models can provide 3D fields of temperature, pressure and humidity or from a nearby

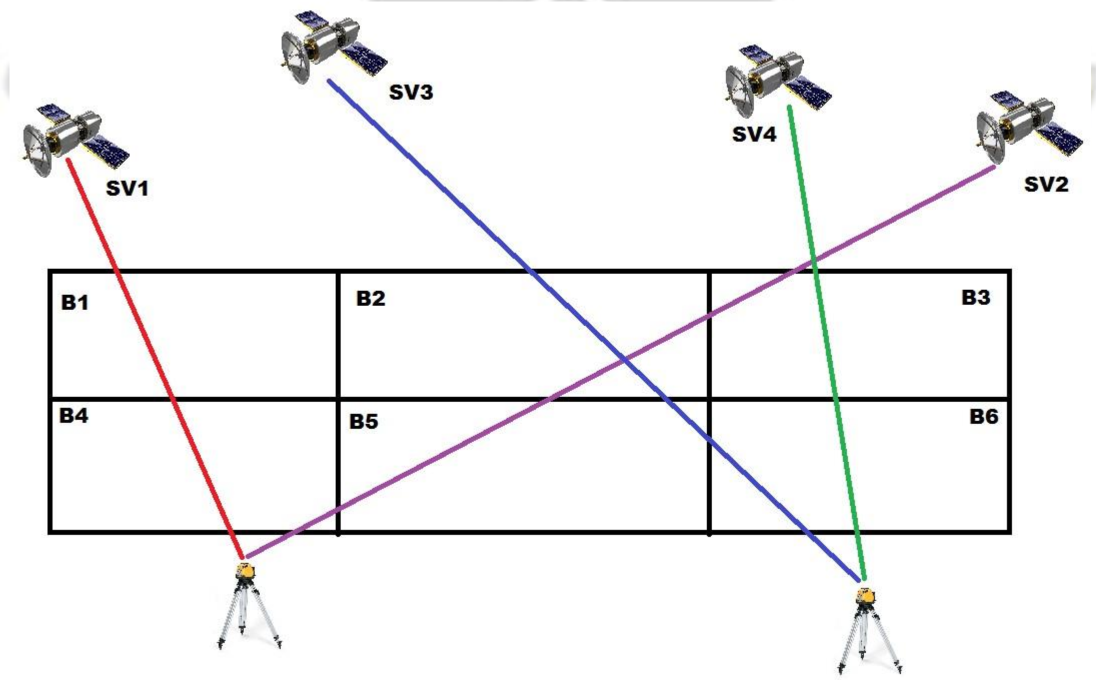

Figure 5.9: Conceptual view of signals through voxels

weather station. For numerical computations the 3D fields need to be discretized, i.e. the physical quantities are defined on the nodes of a spatial grid.

$$N(\mathbf{r}) \Rightarrow N_i, i = 1, 2, ..., q \qquad grid\ nodes$$

$$STD = 10^{-6} \cdot \sum_{j=1}^{u} N_j \Delta s_j \qquad with$$

$$\Delta s_j = f(N)$$

The general problem is non-linear as the signal path **S** is a function of the refractivity field **N**. It can then be linearized by assuming a straight signal path with small segments l_j

$$STD = 10^{-6} \cdot \sum_{j=1}^{u} N_j \cdot l_j \Rightarrow N_j \text{ and } l_j \text{ are independent} \tag{5.1}$$

Considering Equations (5.1), $j = 1,...,u$, where j is volumetric pixels (voxels). The 3D field, N, is mapped on a vector **x:** $N \rightarrow x$, where $\mathbf{x} = (x_1,x_2,...,q) = (N_1,N_2,...,N_q)$. Combining all slant delays in an observation vector, **m**, where $\mathbf{m} = (m_1,m_2,...,m_p) = (STD_1,STD_2,...,STD_p)$. A system of linear equation can be formed using the observation vector and 3D field vector, the resultant equation becomes $A \cdot x = m$.

$$\begin{bmatrix} l_{11} & 0 & 0 & l_{14} & 0 & 0 \\ 0 & l_{22} & l_{23} & l_{24} & l_{25} & 0 \\ 0 & l_{32} & 0 & 0 & l_{35} & l_{36} \\ 0 & 0 & l_{33} & 0 & 0 & l_{46} \end{bmatrix} \cdot \begin{bmatrix} B_1 \\ B_2 \\ B_3 \\ B_4 \\ B_5 \\ B_6 \end{bmatrix} = \begin{bmatrix} STD_1 \\ STD_2 \\ STD_3 \\ STD_4 \end{bmatrix}$$

In general, a solution **x** with **Ax = m** does not exist, hence we find $\tilde{\mathbf{x}}$ which minimizes the normal equations

$$min\{\|Ax - m\|\}$$

Standard techniques for solving linear inverse problems in tomographic techniques are: a) Weighted least-squares solution, b) Kalman-Filter, c) Algebraic reconstruction techniques, d) Conjugate gradient method, e) Singular value decomposition, et cetera.

A Case for GNSS Tomography in Ghana: Using the KNUST GPS Base Station, satellite coverage and visibility analysis were done to compute possible slant tropospheric delays, for GNSS Tomography refer Figure 5.10. The base station equipment is a 12channel Sokkia dual frequency receiver which is capable of tracking L1P, L2P, C1C and C2P observables for slant delay computations. Setting an elevation mask of 5^o, at an instance of observation the receiver tracks averagely 10 SVs logging 40 slant delays at an epoch. The processing interval used in the gLAB software was 300 secs and with 86400 secs in a day translating to 11520 STDs available for tomographic processing. With the exception of SV PRN30 all the GPS satellites were tracked and on the average 10 SVs were visible at any instance during the day. Satellites with PRN 28, 02, 14 and 18 were tracked for over 10 hours, whereas PRN 04, 16 and 31 were the ones with the least times of a little over 5 hours. Satellites with PRN12, 14, 17, 21, 22, 24, 25, 29 & 31 made two passes in the study area.

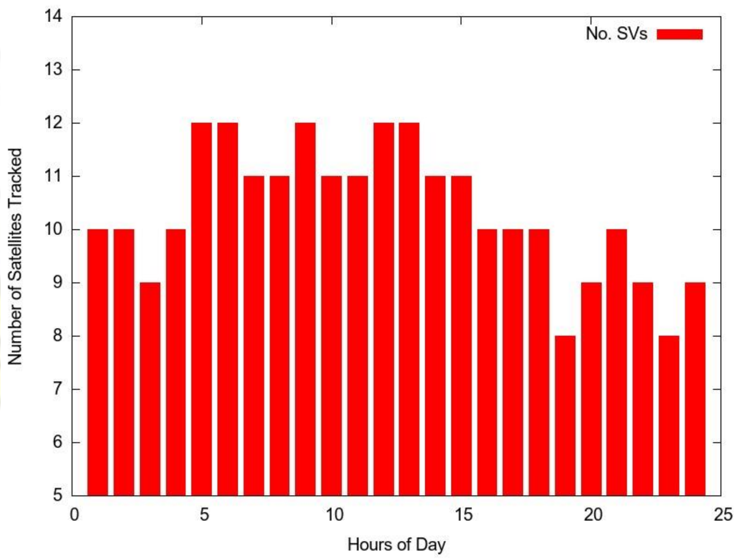

(a)

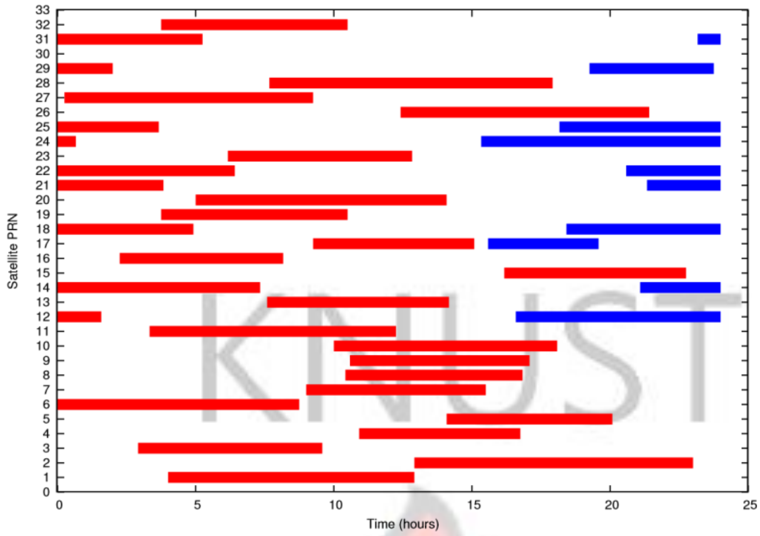

(b)

Figure 5.10: Number of Observed Satellites and visibility times above the horizon

5.3 Proposed GNSS Meteorological Set-up in Ghana

To improve weather prediction and most importantly precipitation forecasting, this study proposes a collaborative effort between Ghana Meteorological Agency (GMet) and the Survey and Mapping Division of the Lands Commission of Ghana to adopt GNSS meteorology. This concept can serve dual purpose of providing precise coordinates and differential corrections for PNT applications as well as PW for uploads into

NWP servers. To deploy a system using a network of GNSS receivers to sense water vapour, a 1^o resolution in the horizontal plane (approximately 110km) for Ghana was considered. Again, GNSS meteorological concepts require surface variables (i.e. pressure and temperature), for computation of PW. Considering these two assumptions and using the locations of GMet synoptic stations and GNSS Continuously Operating Reference Stations (CORS) as shown in Figure 5.11. A minimum of 19 GNSS receivers will be enough to cover the whole country.

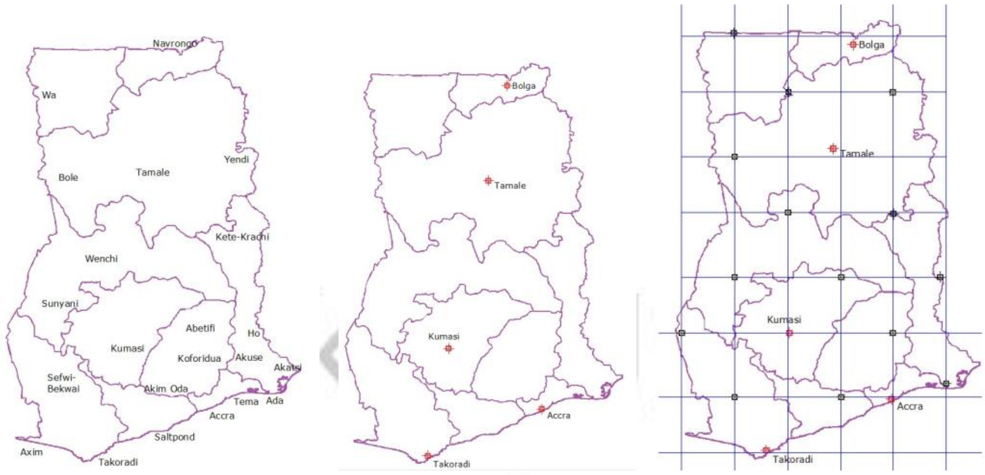

(a) GMet Synoptic stations (b) Current CORS locations (c) Proposed GNSS CORS location for Nationwide water vapour sensing

Figure 5.11: GNSS Meteorological Set-up in Ghana

Concluding Remarks: this chapter dealt with various tests and computations done to retrieve PW, and analysis run to compare results with Global Reanalysis models. Strong correlations were found between computed PW and the TCWV downscaled from the global models with results tilting in favour of ERA-Interim. Additional computations were done to derive correlation coefficients table for all parameters and quantities used in the study. It was found that ZTD and PW had an *r* value of 0.944. With this result, three (3) linear trendline models were computed and tested for ZTD and PW values.

The Linear model performed best and could predict PW with an R^2 of 0.826 and an *RMSE* of 2.132 mm. Seasonal variation tests too were conducted to access how the PW values change with the country's meteorological seasons. The findings show perfect agreement with our weather seasons.

Again, based on the findings, this study has proposed a 19-station GNSS CORS set-up to fully explore the capabilities of GNSS Meteorology to sense atmospheric water vapour for improved precipitation forecasting.

Chapter 6 Conclusions

6.1 Summary

The critical role atmospheric water vapour plays in the Earth's climate system requires its quantities both spatially and temporally to be sensed accurately using sensors that offer long-term stabilities. The work presented in this dissertation showed that the concepts of GNSS Meteorology have been well-developed with enhanced algorithms for meeting the needed accuracy and precision of ≤ 1cm for inferring water vapour sensing. It has been shown from this thesis that two approaches can be used for the retrieval of Integrated Water Vapour or Precipitable Water from GNSS signals. They are Double-Differenced (DD) techniques from baselines/vectors using network of GNSS stations or Precise Point Positioning (PPP) from single stations using IGS precise clocks and orbital products.

Zenith Total Delays (ZTD) were measured accurately by processing raw GPS datasets from the KNUST base station using the gLAB software. The processing parameters set in gLAB were an elevation mask of 5^o, data decimation of 300secs and an L1-C1 difference cycle-slip detection. Zenith Wet delays were obtained by subtracting computed zenith hydrostatic delays (ZHD) from ZTD using surface pressure and station orthometric height. We found the conversion of ZWD to IWV was straightforward using

the dimensionless constant (Π) and mean surface temperature (T_m). Aside the use of surface variables, there are models used to infer IWV with no weather data. Findings in the study showed that models with no weather data under-sampled PW or IWV though positive correlation were recorded with all three reanalysis data used. The correlation values, *r*, for computed PW from weather-free model and Reanalysis data were 0.541 for JRA, 0.598 for ERA-Interim and 0.458 for NCEP-R1.

Further PW comparisons were made with reanalysis data using models that incorporated surface variables. Resultant values from the correlation analysis indicated that retrieved PW correlates better with ERA-Interim, with an r–value of 0.8345 whilst JRA and NCEP-R1 gave 0.7729 and 0.6491 respectively. Three (3) curve-fitting models were tested on computed ZTD and retrieved PW, the linear model [$F(x) = 161.2(x) - 360.7$] gave the highest R^2 and the least *RMSE* values on predictions. Computed PW with the linear model gave standard errors of 6.0139 for JRA, 5.398 for ERA-Interim and 6.338 for NCEP reanalysis data. This goes to confirm that retrieved IWV or PW from GNSS signals using gLAB correlates better with ERA-Interim. However these findings are not to rate one reanalysis model ahead of other reanalysis in totality but in terms of atmospheric water vapour sampling in Ghana, ERA-Interim ranks higher. Seasonal variation analysis were done to determine how best inferred PW vary with weather patterns in Ghana. It was found that PW increases in the rainy seasons of April to June and also from September to November whereas there were decreases in the water vapour contents in the dry seasons.

On the issue of tropospheric delays (TD) estimates for precise positioning and other geodetic applications, descriptive statistics were run based on computed slant delays that were analysed for 3D GNSS tomographic construction. The maximum TD was 23.022m for satellites with 5^o elevations and minimum of 2.324m recorded at 87^o elevations. When mapped unto the zenith using the modified Niell mapping function (§2.2.3.6 on page 31), maximum and minimum delays of 2.576 and 2.047m with σ of 0.037 were recorded. Hence applications and works reliant on tropospheric delays should estimate

a maximum of 2.6m in their error budgets.

Finally, for enhanced weather prediction and precipitation forecasting, the proposed collaborative effort between Ghana Meteorological Agency and the Survey and Mapping Division of the Lands Commission of Ghana should be hasten to explore space weather applications. Considering the initial 1^o resolution proposed in this study, 20 GNSS base stations will be enough to cover the whole nation with surface variables being provided by the 22 GMet synoptic stations.

6.2 Outlook

The reviews done on atmospheric applications using GNSS signals showed numerous prospects; areas like IWV retrieval, tropospheric density profiles and ionospheric electron contents are in advanced and implementation stages. On the other hand, Earth's surface monitoring using multipath delayed reflections and IWV retrievals on moving platforms are emerging. The fullest potential of GNSS Meteorology and Space Weather can be tapped when there is a network of GNSS base stations. However, the concepts of PPP and GNSS signal simulators can be used in these areas for further research.

The dissertation utilised a single station for all data processing and only temporal analysis of IWV were carried out. Data from a network of receivers processed simultaneously with the IGS rapid orbits can deliver near-realtime IWV estimates for assimilating NWP models. An increased knowledge in spatial variations of atmospheric water vapour using tomographic techniques can be used in nowcasting and validating downscaled NWP models.

International Terrestrial Reference System (ITRS) continental reference frame realizations, improved quality and timely provision of orbit and clock products from IGS are making processing Multi-GNSS signals easier . These progressions coupled with the modernization of GNSS specifically the coming on board BeiDou, Galileo and additional civil signals (LC2) will make higher order ionospheric effects easier to handle. With less noisy ionospheric free linear combinations being implemented, the estimation of tropospheric delays can be made with high precision. Under the assumption of no multipath effects and systematic biases, these improvements will translate into increased accuracy of the ZWDs.

6.3 Recommendations

From this study, the following recommendations regarding the adoption and further investigations of GNSS Meteorology can be made:

(i) use of other scientific software applying baselines and double differencing techniques for ZTD computations using the Base stations in golden triangle of Ghana

(ii) different mapping functions be considered in mapping slant tropospheric delays unto the zenith for onward IWV retrieval

(iii) further GNSS data must be logged to monitor ZTD behaviour under intense precipitation during the rainy seasons for the months of May to August

Bibliography

Acheampong, A. A. (2009). Developing a Differential GPS service in Ghana. Master's thesis, Department of Geomatics Engineering, KNUST, Ghana. http://ir.knust.edu.gh/bitstream/123456789/667/1/Thesis.pdf.

Acheampong, A. A. (2012). Monitoring and predicting climate variability by estimating total electron content and integrated water vapor from gnss base stations in ghana. PhD Proposal Plan (Refined) to Building Stronger Universities Environment and Climate Platform. http://bsuec.org/fileadmin/user upload/bsuec/PhD Grant/Students/Acheampong KNUST 30 March 2012.pdf.

Adegoke, A. S. and Onasanya, M. A. (2008). Effect of propagation delay on signal transmission. *Pacific Journal of Science and Technology*, 9:13–19.

Ahrens, C. D. (2012). *Meteorology today: an introduction to weather, climate, and the environment*. Cengage Learning.

Allaby, M. (2009). *Atmosphere: A Scientific History of Air, Weather, and Climate*. Infobase Publishing.

Allen, R. L. (2015). Observational data and model output statistics: The challenges in creating high-quality guidance. Website, Accessed on May, 2015. http://www.nws.noaa.gov/mdl/synop/amspapers/18thwafobs.pdf.

Altamimi, Z., Collilieux, X., and M´etivier, L. (2011). ITRF2008: an improved solution of the international terrestrial reference frame. *Journal of Geodesy*, 85(8):457–473.

Andrews, D. G. (2010). *An introduction to atmospheric physics*. Cambridge University Press.

APPS (2015). Automatic precise positioning service of the global differential gps (GDGPS) system. http://apps.gdgps.net/. Jet Propulsion Laboratory, California Institute of Technology.

Ashby, N. (2003). Relativity in the global positioning system. *Living Rev. Relativity*, 6(1).

Atkins, N. (2006). Survey of meteorology – weather forecasting. Website, Accessed on May, 2015. http://apollo.lsc.vsc.edu/classes/met130/notes/chapter13/index.html.

AUSPOS (2015). AUSPOS - online GPS processing service. http://www.ga.gov.au/cgiperl/auspos/gps.pl. Geoscience Australia, Department of Resources, Energy and Tourism.

Bader, D., Covey, C., Gutowski, W., Held, I., Kunkel, K., Miller, R., Tokmakian, R., and Zhang, M. (2008). Climate models: An assessment of strengths and limitations. *US Department of Energy Publications*, page 8.

Baede, A. P. M., Ahlonsou, E., Ding, Y., and Schimel, D. S. (2001). The climate system: an overview. In *Climate Change 2001: impacts, adaptation and vulnerability*, pages 87–98. Cambridge University Press.

Banville, S., Marcelo, S., and Others (2014). The precise point positioning software center. Website, Accessed on Jan, 2014. http://www2.unb.ca/gge/Resources/PPP/OnlinePPPs.html.

Barthelmes, F. (2013). Definition of functionals of the geopotential and their calculation from spherical harmonic models. www.gfz-potsdam.de - News - GFZ Publications. GFZ German Research Centre for Geosciences Scientific Technical Report STR09/02.

Bastin, S., Champollion, C., Bock, O., Drobinski, P., and Masson, F. (2007). Diurnal cycle of water vapor as documented by a dense GPS network in a coastal area during ESCOMPTE IOP2. *Journal of Applied Meteorology and Climatology*, 46(2):167–182.

Bauer, P., Lopez, P., Moreau, E., Chevallier, F., Benedetti, A., and Bonazzola, M. (2007). The european centre for medium-range weather forecasts global rainfall data assimilation experimentation. In *Measuring Precipitation From Space*, pages 447–457. Springer.

Bender, M., Dick, G., Ge, M., Deng, Z., Wickert, J., Kahle, H.-G., Raabe, A., and Tetzlaff, G. (2011). Development of a GNSS water vapour tomography system using algebraic reconstruction techniques. *Advances in Space Research*, 47(10):1704–1720.

Bender, M., Dick, G., Wickert, J., Schmidt, T., Song, S., Gendt, G., Ge, M., and Rothacher, M. (2008). Validation of GPS slant delays using water vapour radiometers and weather models. *Meteorologische Zeitschrift*, 17(6):807–812.

Bender, M. and Raabe, A. (2007). Preconditions to ground based GPS water vapour tomography. *Annales Geophysicae*, 25(8):1727–1734.

Benevides, P., Catalao, J., and Miranda, P. M. A. (2014). Experimental GNSS tomography study in Lisbon (Portugal). *F´ısica de la tierra*, 26:65–79.

Berrada, B. H., Gole, P., and Lavergnat, J. (1988). A model for the tropospheric excess path length of radio waves from surface meteorological measurements. *Radio science*, 23(6):1023–1038.

Berrisford, P., Dee, D., Poli, P., Brugge, R., et al. (2011). *The* ERA-I*nterim archive. version 2.0*. ECMWF Publications.

Bevis, M., Businger, S., Chiswell, S., Herring, T. A., Anthes, R. A., Rocken, C., and Ware, R. H. (1994). GPS meteorology: Mapping zenith wet delays onto precipitable water. *Journal of Applied Meteorology*, 33(3):379–386.

Bevis, M., Businger, S., Herring, T., Rocken, C., Anthes, R., and Ware, R. (1992). GPS meteorology- remote sensing of atmospheric water vapor using the global positioning system. *Journal of Geophysical Research*, 97(D14):15787–15801.

Black, H. D. and Eisner, A. (1984). Correcting satellite doppler data for tropospheric effects. *Journal of Geophysical Research: Atmospheres (1984–2012)*, 89(D2):2616–2626.

Bock, O., Bosser, P., Bourcy, T., David, L., et al. (2013). Accuracy assessment of water vapour measurements from in situ and remote sensing techniques during the DEMEVAP 2011 campaign at OHP. *Atmospheric Measurement Techniques*, 6(10):2777– 2802.

Bokoye, A. I., Royer, A., O'Neill, N. T., Cliche, P., McArthur, L. J. B., Teillet, P. M., Fedosejevs, G., and Th´eriault, J.-M. (2003). Multisensor analysis of integrated atmospheric water vapor over Canada and Alaska. *Journal of Geophysical Research: Atmospheres (1984–2012)*, 108(D15).

Boos, D. D. et al. (2003). Introduction to the bootstrap world. *Statistical science*, 18(2):168–174.

Bosilovich, M. G., Rixen, M., Oevelen, v. P., Asrar, G., and Others (2012). Atmospheric reanalyses. In *Conference Report of the 4th World Climate Research Programme International Conference on Reanalyses*. WCRP Report 12/2012, http://www.wcrpclimate.org/documents/ICR4 Report.pdf.

Bosy, J., Rohm, W., and Sierny, J. (2010). The concept of the near real time atmosphere model based on the GNSS and the meteorological data from the ASG-EUPOS reference stations. *Acta Geodyn. Geomater*, 7(1):157.

Brammer, D., Wojtowicz, D., Hall, S. E., and Others (2010). Precipitation. Department of Atmospheric Sciences (DAS) at the University of Illinois at Urbana-Champaign. http://ww2010.atmos.uiuc.edu/(Gh)/guides/mtr/hyd/prcp.rxml.

Brunner, F. K. and Welsch, W. M. (1993). Effect of the troposphere on GPS measurements. *GPS World*, 4:42–51.

Buizza, R. (2002). Chaos and weather prediction. *European Centre for Medium-Range Weather, Internal Report; Meteorological Training Course*, pages 1–28.

Burhanpurwala, H., Fitzgerald, J., Hendriken, L., Mistry, D., and Others (2008). Surveying and Global positioning techniques. Geometric and Intelligent Computing Laboratory WiKi, http://gicl.cs.drexel.edu/index.php/Group9.

Businger, S., Chiswell, S. R., Bevis, M., Duan, J., Anthes, R. A., Rocken, C., Ware, R. H., Exner, M., VanHove, T., and Solheim, F. S. (1996). The promise of GPS in atmospheric monitoring. *Bulletin of the American Meteorological Society*, 77(1):5–18.

Caissy, M., Agrotis, L., Weber, G., Hernandez-Pajares, M., and Hugentobler, U. (2012). The international GNSS real-time service. *GPS World*, 23(6):52.

Carter, J. R. (2004). Gases, including water vapor. earth's dynamic weather. http://lilt.ilstu.edu/jrcarter/geo211/webpage-211/mod5-p4.htm, Accessed on Feb, 2013.

Chahine, M. T. (1992). The hydrological cycle and its influence on climate. *Nature*, 359(6394):373–380.

Chen, Q., Song, S., Heise, S., Liou, Y.-A., Zhu, W., and Zhao, J. (2011). Assessment of ZTD derived from ECMWF/NCEP data with GPS ZTD over China. *GPS solutions*, 15(4):415–425.

Choy, S., Wang, C., Zhang, K., and Kuleshov, Y. (2013). GPS sensing of precipitable water vapour during the March 2010 Melbourne storm. *Advances in Space Research*, 52(9):1688–1699.

CIRES (2014). Advancing reanalysis. Retrieved from http://www.reanalyses.org. Accessed on 30-11-2014 and maintained by the Cooperative Institute for Research in Environmental Sciences.

Clark, J. S., Carpenter, S. R., Barber, M., et al. (2001). Ecological forecasts: an emerging imperative. *Science*, 293(5530):657–660.

Coiffer, J. (2004). Weather forecasting technique considered as a sequence of standard processes from the forecaster's point of view. World Meteorological Organization Workshop On Severe And Extreme Events Forecasting. http://www.wmo.int/pages/index en.html.

Collins, P. and Langley, R. B. (1999). Tropospheric delay. *GPS WORLD*, page 53.

Courcoux, N. and Schr¨oder, M. (2015). The CM SAF ATOVS tropospheric water vapour and temperature data record: overview of methodology and evaluation. *Earth System Science Data Discussions*, 8(1):127–171.

Cross, P. A., Hollwey, J. R., and Small, L. G. (2002). Geodetic appreciation, working paper no. 2. School of Computing and Technology, University of East London.

CSRS (2015). Canadian spatial reference system precise point positioning. http://webapp.geod.nrcan.gc.ca/geod/tools-outils/ppp.php. Natural Resources Canada.

Dach, R., Hugentobler, U., Fridez, P., Meindl, M., et al. (2007). Bernese GPS software version 5.0. *Astronomical Institute, University of Bern*, 640:114.

Dattore, B. et al. (2015). NCEP climate forecast system version 2 (CFSv2). Computational and Information Systems Laboratory at the National Center for Atmospheric Research in Boulder, Colorado. http://rda.ucar.edu/datasets/ds094.0/ Accessed on May 2015.

Davis, J. L., Herring, T. A., Shapiro, I. I., Rogers, A. E. E., and Elgered, G. (1985). Geodesy by radio interferometry: Effects of atmospheric modeling errors on estimates of baseline length. *Radio science*, 20(6):1593–1607.

De Haan, S. (2008). *Meteorological applications of a surface network of Global Positioning System receivers*. PhD thesis, Wageningen University. http://edepot.wur.nl/121994.

Deblonde, G., Macpherson, S., Mireault, Y., and H´eroux, P. (2005). Evaluation of gps precipitable water over canada and the igs network. *Journal of Applied Meteorology*, 44(1):153–166.

Dee, D., Fasullo, J., Shea, D., Walsh, J., and Others. (2014). The climate data guide: Atmospheric reanalysis: Overview & comparison tables. Retrieved from https://climatedataguide.ucar.edu/climate-data/atmospheric-reanalysisoverview-comparison-tables. Last modified 05 Nov 2014.

Dee, D., Simmons, A., and Others (2011a). Developments in climate reanalysis at ECMWF. WCRP Open Science Conference, Denver Colorado. http://conference2011.wcrp-climate.org/.

Dee, D. P., Uppala, S. M., Simmons, A. J., Berrisford, P., Poli, P., Kobayashi, S., et al. (2011b). The ERA-Interim reanalysis: Configuration and performance of the data assimilation system. *Quarterly Journal of the Royal Meteorological Society*, 137(656):553–597.

Dousa, J. and Bennitt, G. V. (2013). Estimation and evaluation of hourly updated global GPS zenith total delays over ten months. *GPS solutions*, 17(4):453–464.

Dow, J. M., Neilan, R. E., and Rizos, C. (2009). The international GNSS service in a changing landscape of global navigation satellite systems. *Journal of Geodesy*, 83(3-4):191–198.

Dunn, L. B. (2003). Historical overview of numerical weather prediction. In *Handbook of Weather, Climate, and Water, Edited by Potter, T. D. and Colman, B. R.*, pages 677–688. John Wiley & Sons, Inc., Hoboken, New Jersey.

Ebita, A., Kobayashi, S., Ota, Y., Moriya, M., Kumabe, R., Onogi, K., Harada, Y., Yasui, S., Miyaoka, K., Takahashi, K., et al. (2011). The Japanese 55-year reanalysis JRA-55: an interim report. *Scientific Online Letters on the Atmosphere*, 7:149–152.

El-Rabbany, A. (2002). *Introduction to GPS: the global positioning system*. Artech House Publishers, Norwood.

Emanuel, K. (1995). Report of the first prospectus development team of the u.s. weather research program to NOAA and the NSF. *Bulletin of the American Meteorological Society*, 76:1194–1208.

Enderle, W. (2003). Galileo: Impact on spacecraft navigation system. *Journal of Global Positioning Systems*, 2(2):135–138.

Estey, L. H. and Meertens, C. M. (1999). TEQC: the multi-purpose toolkit for GPS/-GLONASS data. *GPS Solutions*, 3(1):42–49.

FAA-Editors (2015). GNSS – frequently asked questions – GPS. Satellite Navigation http://www.faa.gov/about/office org/headquarters offices/ato/service units/techops/navservices/gn

Flamant, C., Chaboureau, J.-P., Parker, D. J., et al. (2007). Airborne observations of the impact of a convective system on the planetary boundary layer thermodynamics and aerosol distribution in the inter-tropical discontinuity region of the West African monsoon. *Quarterly Journal of the Royal Meteorological Society*, 133(626):1175–1189.

Flores, A., Ruffini, G., and Rius, A. (2000). 4D tropospheric tomography using GPS slant wet delays. *Annales Geophysicae*, 18(2):223–234.

Gaglione, S. (2015). How does GNSS receiver estimate position. InsideGNSS March,April Ed. http://www.insidegnss.com/auto/marapr15-SOLUTIONS.pdf.

Gall, T. L. and Hobby, J. M. (2007). *Worldmark Encyclopedia of the Nations - Africa, 12th Ed*, volume 2. Thomson Gale.

Gao, Y. and Chen, K. (2004). Performance analysis of precise point positioning using rea-time orbit and clock products. *Journal of Global Positioning System*, 1:95–100.

GAPS (2015). GAPS- GPS analysis and positioning software v5.5.0. http://gaps.gge.unb.ca/. Dept of Geodesy and Geomatics Engineering, University of New Brunswick.

Ghoddousi-Fard, R. and Dare, P. (2006). Online GPS processing services: an initial study. *GPS Solutions*, 10(1):12–20.

Gleason, S. and Gebre-Egziabher, D. (2009). *GNSS Applications and Methods*. Artech House.

Goad, C. and Goodman, L. (1974). Modified hopfield tropospheric refraction correction model. In *TRANSACTIONS-AMERICAN GEOPHYSICAL UNION, Vol: 55 No. 12*, pages 1106–1106.

Google (2015). Google map of West Africa. Retrieved from https://www.google.com.gh/maps/@7.8918524,-2.7944333,6z?hl=en.

GPSWorld-Editors (2014). The almanac - orbit data and resources on active GNSS satellites. *GPSWorld Magazine*, 25(1):77–73.

Grace, L. (2015). Earth’s atmosphere – the troposphere. Website, Accessed on Jan, 2015. http://web.physics.ucsb.edu/ lgrace/chem123/troposphere.htm.

Gradinarsky, L. P. and JarLemark, P. (2004). Ground-based GPS tomography of water vapor: Analysis of simulated and real data. *Journal of the Meteorological Society of Japan. Ser. II*, 82(1B):551–560.

Grinter, T. and Roberts, C. (2011). Precise point positioning: where are we now? IGNSS Society 2011 Symposium Proceedings. Menay P/L, New South Wales, Australia.

Guerova, G. (2003). *Application of* GPS *derived water vapour for Numerical Weather Prediction in* Switzerland. PhD thesis, Faculty of Philosophy and Science, University of Bern.

Gullish, J. and Vaccaro, D. (2009). The top ten in PNT. InsideGNSS November/December Ed. http://www.insidegnss.com/node/1714.

Gupta, S. K. (2011). *Modern hydrology and sustainable water development*. John Wiley & Sons.

Gurtner, W. and Estey, L. (2007). RINEX-the receiver independent exchange format version 2.11. Astronomical Institute, University of Bern. ftp://igscb.jpl.nasa.gov/igscb/data/format/rinex211.txt.

Gutman, S. I., Sahm, S. R., Stewart, J., Benjamin, S., Smith, T., and Schwartz, B. (2003). A new composite observing system strategy for ground-based GPS meteorology, paper presented at the 12th symposium on meteorological observations and instrumentation. *Am. Meteorol. Soc., Boston, Mass.*

Hagemann, S., Bengtsson, L., and Gendt, G. (2003). On the determination of atmospheric water vapor from GPS measurements. *Journal of Geophysical Research: Atmospheres*, 108(D21).

Hallett, J. (2003). Measurements is the atmosphere. In *Handbook of Weather, Climate, and Water, Edited by Potter, T. D. and Colman, B. R.*, pages 711–720. John Wiley & Sons, Inc., Hoboken, New Jersey.

Harada, Y., Kamahori, H., Kobayashi, C., Endo, H., et al. (2015). The JRA-55 reanalysis: Representation of atmospheric 3 circulation and climate variability. The Second Weather Magazine, Meteorological Society of Japan. http://jmsj.metsoc.jp/EOR/2016-015.pdf DOI:10.2151/jmsj.2016-015.

Harmon, K. (2009). Satellites used to predict infectious disease outbreaks. Scientific American. http://www.scientificamerican.com/article/satellites-predict-infectiousdisease/.

Hartmann, G. K. and Leitinger, R. (1984). Range errors due to ionospheric and tropospheric effects for signal frequencies above 100 mhz. *Bulletin g´eod´esique*, 58(2):109– 136.

Haub, C., Gribble, J., and Jacobsen, L. (2015). 2015 world population datasheet. Population Reference Bureau. http://www.prb.org/pdf15/2015-world-population-datasheet eng.pdf.

Heiskanen, W. A. and Moritz, H. (1993). *Physical geodesy*. Institute of Physical Geodesy, Technical University Graz, Austria.

Hernandez-Pajares, M., Juan, J. M., Sanz, J., Ramos-Bosch, P., Rovira-Garcıa, A., Salazar, D., Ventura-Traveset, J., L´opez-Echazarreta, C., and Hein, G. (2010). The ESA/UPC GNSS-lab tool (glab). In *Proc. of the 5th ESA Workshop on Satellite Navigation Technologies (NAVITEC'2010), ESTEC, Noordwijk, The Netherlands*.

Herring, T. A. (1992). Modeling atmospheric delays in the analysis of space geodetic data. *Proceedings of Refraction of Transatmospheric signals in Geodesy, eds. J. C. De Munck and T. A. Spoelstra, Netherlands Geodetic Commission Publications on Geodesy*, 36.

Hieb, M. (2007). Global warming: A closer look at the numbers. http://www.geocraft.com/WVFossils/greenhouse data.html. Accessed on Jan 2013.

Hoffman, D. L. (2010). It's the water vapor, stupid! The Resilient Earth.

http://theresilientearth.com/?q=content/its-water-vapor-stupid. Accessed on Jan 2013.

Hofmann-Wellenhof, B., Lichtenegger, H., and Collins, J. (2012). *Global positioning system: theory and practice*. Springer Science & Business Media.

Hofmann-Wellenhof, B., Lichtenegger, H., and Wasle, E. (2007). GNSS–*global navigation satellite systems:* GPS*,* GLONASS*,* G*alileo, and more*. Springer.

Hopfield, H. S. (1969). Two-quartic tropospheric refractivity profile for correcting satellite data. *Journal of Geophysical research*, 74(18):4487–4499.

Hoque, M. M. and Jakowski, N. (2010). Higher order ionospheric propagation effects on GPS radio occultation signals. *Advances in Space Research*, 46(2):162–173.

Hordyniec, P. (2014). Modeling zenith delays and integrated water vapour. *Geodesy.– 2014.–6.–P*, pages 1–7.

Hu, G. (2009). Analysis of regional GPS campaigns and their alignment to the international terrestrial reference frame (ITRF). *Journal of Spatial Science*, 54(1):15–22.

Huffman, G. (2015). Weather forecasting. Website, Accessed on March, 2015. http://www.scholastic.com/teachers/article/weather-forecasting.

Ifadis, I. (1986). The atmospheric delay of radio waves: modeling the elevation dependence on a global scale. Technical Report no. 38L, School of Electrical and Computer Engineering, Chalmers University of Technology, G¨oteborg, Sweden.

IGS-Webmasters (2015). GPS satellite ephemerides / satellite station clocks. International GNSS Service (IGS) Products. http://igs.org/products/data.

Iribarne, J. V. and Godson, W. L. (1981). *Atmospheric thermodynamics; Geophysics and Astrophysics monographs*, volume 6. Springer Science.

Ishihara, M. (2005). GPS meteorology at Japan Meteorological Agency. CIMO Expert Team on Remote Sensing Upper-Air Technology and Techniques. http://www.wmo.int/pages/prog/www/IMOP/meetings/UpperAir/RemoteSensing/ Doc.3.1(3) JMA.pdf Accessed Feb 2013.

Isioye, O. A., Combrinck, L., Botai, J. O., and Munghemezulu, C. (2015). The potential for observing african weather with GNSS remote sensing. *Advances in Meteorology*, 2015.

Jade, S., Vijayan, M. S. M., Gaur, V. K., Prabhu, T. P., and Sahu, S. C. (2005). Estimates of precipitable water vapour from GPS data over the Indian subcontinent. *Journal of atmospheric and solar-terrestrial physics*, 67(6):623–635.

Januszewski, J. (2013). How the troposphere affects positioning solution using satellite navigation systems. In *Activities of Transport Telematics*, pages 275–283. Springer.

Jekeli, C. (2006). Geometric reference systems in geodesy. Div of Geodesy and Geospatial Science, School of Earth Sciences, Ohio State Univ.

Jin, S., Cardellach, E., and Xie, F. (2010). GNSS *Remote Sensing*. Springer.

Jin, S. and Komjathy, A. (2010). GNSS reflectometry and remote sensing: New objectives and results. *Advances in Space Research*, 46(2):111–117.

Jones, J. (2010). *An Assessment Of The Quality Of* GPS *Water Vapour Estimates And Their Use In Operational Meteorology And Climate Monitoring*. PhD thesis, Institute of Engineering Surveying and Space Geodesy, University of Nottingham.

Jones, J., Eric Pottiaux, E., Guerova, G., Dousa, J., Dick, G., Bock, O., Pacione, R., Elgered, G., Vedel, H., and deHaan, S. (2010). Advanced GNSS tropospheric products for the monitoring of severe weather events and climate (GNSS4SWEC). EU COSTAction Es1206.
http://www.gnss.be/communications/public/pospres IGS 3.pdf.

Jounot, L. (1998). Methane and carbon monoxide in the Troposphere. http://www.atmosp.physics.utoronto.ca/people/loic/chemistry.html Website Accessed on March 2013.

Juan, J. M., Hern´andez-Pajares, M., Sanz, J., Ramos-Bosch, P., Aragon-Angel, A., Orus, R., Ochieng, W., Feng, S., Jofre, M., Coutinho, P., et al. (2012). Enhanced precise point positioning for GNSS users. *IEEE Transactions on Geoscience and Remote Sensing*, 50(10):4213–4222.

Jutze, G. A. and Foster, K. E. (1967). Recommended standard method for atmospheric sampling of fine particulate matter by filter media—high-volume sampler. *Journal of the Air Pollution Control Association*, 17(1):17–25.

Kalnay, E. (2003). Historical overview of numerical weather prediction. In *Handbook of Weather, Climate, and Water, Edited by Potter, T. D. and Colman, B. R.*, pages 95–115. John Wiley & Sons, Inc., Hoboken, New Jersey.

K¨ampfer, N. (2013). Monitoring atmospheric water vapour. *ISSI Scientific Report Series*, 10:326.

Kann, D. (2005). The many users and uses of weather data. Weather Data Awareness Week, Albuquerque. http://www.srh.noaa.gov/srh/dad/coop/USEWX.pdf Accessed Jul 2012.

Kaplan, E. D. and Hegarty, C. J. (2005). *Understanding GPS: principles and applications*. Artech house.

Karabati´c, A. (2011). *Precise Point Positioning (*PPP*) - an alternative technique for ground based* GNSS *troposphere monitoring*. PhD thesis, Technische Universit¨at Wien, Austria.

Karabati´c, A. and Weber, R. (2009). Use of PPP to derive troposphere zenith wet delays of GNSS signals to support weather forecast models. 10th Osterreichischer¨ Geod¨atentag.

Karabati´c, A., Weber, R., and Haiden, T. (2011). Near real-time estimation of tropospheric water vapour content from ground based GNSS data and its potential contribution to weather now-casting in Austria. *Advances in Space Research*, 47(10):1691–1703.

Karney, C. (2014). Online geoid calculations using the geoideval utility. http://geographiclib.sourceforge.net/cgi-bin/GeoidEval.

Kaufman, Y. J. and Gao, B.-C. (1992). Remote sensing of water vapor in the near IR from EOS/MODIS. *Geoscience and Remote Sensing, IEEE Transactions on*, 30(5):871–884.

Kiehl, J. T. and Trenberth, K. E. (1997). Earth's annual global mean energy budget. *Bulletin of the American Meteorological Society*, 78(2):197–208.

Kistler, R., Collins, W., Saha, S., White, G., Woollen, J., Kalnay, E., Chelliah, M., Ebisuzaki, W., Kanamitsu, M., Kousky, V., et al. (2001). The NCEP-NCAR 50-year reanalysis: Monthly means CD-ROM and documentation. *Bulletin of the American Meteorological society*, 82(2):247–267.

Kleijer, F. (2004). *Troposphere Modeling and Filtering for Precise GPS Leveling*. PhD thesis, Technische Universiteit Delft, Netherlands.

Klobuchar, J. (1996). Ionospheric effects on GPS. *Global Positioning System: Theory and applications.*, 1:485–515.

Klobuchar, J. A. (1987). Ionospheric time-delay algorithm for single-frequency GPS users. *IEEE Transactions on Aerospace and Electronic Systems*, 3:325–331.

Kobayashi, S., Ota, Y., Harada, Y., Ebita, A., Moriya, M., Onoda, H., et al. (2015). The JRA-55 reanalysis: General specifications and basic characteristics. *Journal of Meteorological Society of Japan*, 93(1):5–48.

Kouba, J. (2009). A guide to using International GNSS service (IGS) products. International GNSS. ftp://ww.igs.org/igscb/resource/pubs/UsingIGSProductsVer21.pdf.

Kouba, J. and H´eroux, P. (2001). Precise point positioning using igs orbit and clock products. *GPS solutions*, 5(2):12–28.

Lai, L. L., Braun, A., Zhang, Q. P., Wu, Q., Ma, Y. N., Sun, W. C., and Yang, L. (2004). Intelligent weather forecast. In *Machine Learning and Cybernetics, 2004. Proceedings of 2004 International Conference on*, volume 7, pages 4216–4221. IEEE.

Langley, R. B. (1996). Propagation of the gps signals. In *GPS for Geodesy*, pages 103–140. Springer.

Leick, A. (2004). GPS *satellite surveying*. John Wiley & Sons, New York.

Leinweber, R. (2010). *Remote sensing of atmospheric water vapor over land areas using* MERIS *measurements and application to numerical weather prediction model validation*. PhD thesis, Freie Universit¨at Berlin, Germany.

Lichten, S. M., Bar-Sever, Y. E., Bertiger, W. I., Heflin, M., Hurst, K., Muellerschoen, R. J., Wu, S. C., Yunck, T. P., and Zumberge, J. (2005). Gipsy-Oasis II: A high precision gps data processing system and general satellite orbit analysis tool. *Technology*, pages 24–26.

Liou, Y.-A., Teng, Y.-T., Van Hove, T., and Liljegren, J. C. (2001). Comparison of precipitable water observations in the near tropics by GPS, microwave radiometer, and radiosondes. *Journal of Applied Meteorology*, 40(1):5–15.

Lynch, P. (2008). The origins of computer weather prediction and climate modeling. *Journal of Computational Physics*, 227(7):3431–3444.

MacDonald, A. E., Xie, Y., and Ware, R. H. (2002). Diagnosis of three-dimensional water vapor using a GPS network. *Monthly weather review*, 130(2):386–397.

Manzanas, R., Amekudzi, L. K., Preko, K., Herrera, S., and Guti´errez, J. M. (2014). Precipitation variability and trends in Ghana: An intercomparison of observational and reanalysis products. *Climatic Change*, 10.

Marini, J. W. (1972). Correction of satellite tracking data for an arbitrary tropospheric profile. *Radio Science*, 7(2):223–231.

MATLAB (2015). Two-sample t-test. Matlab R2015a Documentation, The MathWorks Inc. http://www.mathworks.com/help/stats/ttest2.html?searchHighlight=ttest Accessed on March 2015.

McSweeney, C., Lizcano, G., New, M., and Lu, X. (2010). The undp climate change country profiles: Improving the accessibility of observed and projected climate information for studies of climate change in developing countries. *Bulletin of the American Meteorological Society*, 91(2):157–166.

Mendes, V. B. (1999). *Modeling the neutral-atmosphere propagation delay in radiometric space techniques*. PhD thesis, University of New Brunswick, Frederiction, Canada.

Mims, F. M., Chambers, L. H., and Brooks, D. R. (2011). Measuring total column water vapor by pointing an infrared thermometer at the sky. *Bulletin of the American Meteorological Society*, 92(10).

Mireault, Y., T´etreault, P., Lahaye, F., H´eroux, P., and Kouba, J. (2008). Online precise point positioning: A new, timely service from natural resources canada. *GPS World, September*, pages 59–64.

Misra, P. and Enge, P. (2011). *Global Positioning System: Signals, Measurements and Performance Revised 2nd Ed.* Massachusetts: Ganga-Jamuna Press.

Motell, C., Porter, J., Foster, J., Bevis, M., and Businger, S. (2002). Comparison of precipitable water over Hawaii using AVHRR-based split-window techniques, GPS and radiosondes. *International Journal of Remote Sensing*, 23(11):2335–2339.

MSI (2012). Weather observations, a marine safety information publication. chapter 36. Marine Safety Information Publication Website, Accessed on Dec, 2014. http://msi.nga.mil/MSISiteContent/StaticFiles/NAV PUBS/APN/Chapt-37.pdf.

Muthike, W. (2014). The importance of weather and climate data: A perspective from an agricultural insurance provider. Climate Innovations Network Forum – UNDP blogspot. http://undp-cirda.blogspot.com/2014/11/the-importance-of-weather-andclimate.html.

Nave, C. R. (2012). Hyperphysics: Relative humidity. Website, Accessed on March, 2015. http://hyperphysics.phy-astr.gsu.edu/hbase/kinetic/relhum.html#c2.

Niell, A. E. (1996). Global mapping functions for the atmosphere delay at radio wavelengths. *Journal of Geophysical Research: Solid Earth (1978–2012)*, 101(B2):3227–3246.

Nilsson, T., B¨ohm, J., Wijaya, D. D., Tresch, A., Nafisi, V., and Schuh, H. (2013). Path delays in the neutral atmosphere. In *Atmospheric Effects in Space Geodesy, J. B¨ohm and H. Schuh (eds.)*, pages 73–136. Springer-Verlag Berlin Heidelberg.

Ning, T. (2012). *GPS Meteorology: With Focus on Climate Application*. PhD thesis, Chalmers University of Technology. http://publications.lib.chalmers.se/records/fulltext/157389.pdf.

Noll, C., Bock, Y., Habrich, H., and Moore, A. (2009). Development of data infrastructure to support scientific analysis for the international GNSS service. *Journal of Geodesy*, 83(3-4):309–325.

Notarpietro, R., Cucca, M., and Bonafoni, S. (2012). GNSS signals: A powerful source for atmosphere and earth's surface monitoring. In *Remote Sensing of Planet Earth, Edited by Yann Chemin*, pages 181–210. Intech.

NWS-Editors (2010). *National Weather Service Observing Handbook No. 1*. Marine Surface Weather Observations, a Publication of the National Oceanic and Atmospheric Administration.

Odumosu, J. O., Ajayi, O. G., Idowu, F. F., and Adesina, E. A. (2015). Evaluation of the various orthometric height systems and the nigerian scenario–a case study of lagos state. *Journal of King Saud University-Engineering Sciences*.

Olynik, M. C. (2002). Temporal characteristics of GPS error sources and their impact on relative positioning. *University of Calgary Reports No. 20162*.

Oppong, J. R. and Oppong, E. D. (2003). *Modern World Nations - Ghana*. Chelsea House Publishers. A Haights Cross Communcations.

Owusu, K. and Waylen, P. (2009). Trends in spatio-temporal variability in annual rainfall in ghana (1951-2000). *Weather*, 64(5):115–120.

Oyediran, O. F. and Adeyemo, A. B. (2013). Performance evaluation of neural network mlp and anfis models for weather forecasting studies. *African Journal of Computing & ICT*, 6(1):147–164.

Pasini, A. (2005). *From observations to simulations: a conceptual introduction to weather and climate modelling*. World Scientific Publishing, Singapore.

Pavlis, N. K., Holmes, S. A., Kenyon, S. C., and Factor, J. K. (2012). The development and evaluation of the earth gravitational model 2008 (EGM2008). *Journal of Geophysical Research: Solid Earth (1978–2012)*, 117(B4).

Petrov, L. (2014). Modeling of path delay in the neutral atmosphere: a paradigm shift. 12th European VLBI Network Symposium and Users Meeting, Proceedings of Science. http://arxiv.org/pdf/1502.06678.pdf.

Poku-Gyamfi, Y. (2009). *Establiment of* GPS *Reference Network in Ghana*. PhD thesis, Univ. der Bundeswehr Mu¨nchen.

Pollet, A., Coulot, D., Bock, O., and Nahmani, S. (2014). Comparison of individual and combined zenith tropospheric delay estimations during CONT08 campaign. *Journal of Geodesy*, 88(11):1095–1112.

P¨oschl, U. (2005). Atmospheric aerosols: composition, transformation, climate and health effects. *Angewandte Chemie International Edition*, 44(46):7520–7540.

Pottiaux, E. (2010). *Sounding the Earth's Atmospheric Water Vapour Using Signals Emitted by Global Navigation Satellite Systems*. PhD thesis, Department of Physics, Earth and Life Institute, Catholic University of Louvain.

PSD (2013). NCEP-DOE reanalysis (R2). Physical Sciences Division of Earth System Research Laboratory.
http://www.esrl.noaa.gov/psd/data/gridded/data.ncep.reanalysis2.html Accessed on August 2013.

Rahemi, N., Mosavi, M. R., Abedi, A. A., and Mirzakuchaki, S. (2014). Accurate solution of navigation equations in GPS receivers for very high velocities using pseudorange measurements. *Advances in aerospace engineering*, 2014.

Raju, P. L. N. (2013). Fundamentals of GPS. Satellite Remote Sensing and GIS Applications in Agricultural Meteorology http://www.wamis.org/agm/pubs/agm8/Paper7.pdf.

Ramanathan, V., Barkstrom, B. R., and Harrison, E. F. (1989). Climate and the earth's radiation budget. *Physics Today*, page 20.

Richardus, P. (1984). *Project Surveying*. 2nd Edition. Balkema, Rotterdam-Boston.

Rienecker, M. M., Suarez, M. J., Gelaro, R., Todling, R., Bacmeister, J., and Others (2011). MERRA: NASA's modern-era retrospective analysis for research and applications. *Journal of Climate*, 24(14):3624–3648.

Rizos, C. (2008). Multi-constellation GNSS/RNSS from the perspective of high accuracy users in Australia. *Journal of Spatial Science*, 53(2):29–63.

ROB-Editors (2010). GNSS. Royal Observatory of Belgium GNSS Research Group, http://gnss.be/gnss tutorial.php.

Rocken, C., VanHove, T., Johnson, J., Solheim, F., Ware, R., Bevis, M., Chiswell, S., and Businger, S. (1995). GPS/STORM—GPS sensing of atmospheric water vapor for meteorology. *Journal of Atmospheric and Oceanic Technology*, 12:468–478.

Rogers, L. (2008). A brief history of time measurement. Website, Accessed on May, 2015. Enriching Mathematics https://nrich.maths.org/6070.

Rohm, W. and Bosy, J. (2009). Local tomography troposphere model over mountains area. *Atmospheric Research*, 93(4):777–783.

Rohm, W., Gaiger, A., Brenot, H., Bender, M., Shangguan, M., and Bosy, J. (2012). GNSS tomography, assembled multi model solution, initial results from first experiment of IAG GNSS tomography working group. In *AGU Fall Meeting Abstracts*, volume 1, page 0913.

Rothacher, M. and Schmid, R. (2010). ANTEX: The antenna exchange format version 1.4. Forschungseinrichtung Satellitengeod¨asie, TU Mu¨nchen. ftp://igscb.jpl.nasa.gov/pub/station/general/antex14.txt.

Russell, R. (2010). The troposphere. Window to the Universe, National Earth Science Teachers Association. http://www.windows2universe.org/earth/Atmosphere/troposphere.html.

Saastamoinen, J. (1972). Atmospheric correction for the troposphere and stratosphere in radio ranging satellites. *Geophysical Monograph Series*, 15:247–251.

Salby, M. (2003). Foundamental forces and governing equaions. In *Handbook of Weather, Climate, and Water, Edited by Potter, T. D. and Colman, B. R.*, pages 7–20. John Wiley & Sons, Inc., Hoboken, New Jersey.

Scarda, S. (2010). EGNOS and Africa: design of an institutional set upy. In *3rd AfricaIndian Ocean (AFI) Regional Air Navigation Services Providers Meeting*. WORLDAIROPS http://www.worldairops.com/AFI/AFI index.html#4.

Schu¨ler, T. (2001). *On Ground-Based GPS Tropospheric Delay Estimation*. PhD thesis, Universit¨at der Bundeswehr Mu¨nchen, Germany.

Schulzweida, U., Kornblueh, L., and Quast, R. (2009). Climate data operators (CDO), user guide, version 1.4.0. https://code.zmaw.de/projects/cdo.

Seeber, G. (2003). *Satellite geodesy: foundations, methods, and applications*. de Gruyter.

Seidel, D. J. (2002). Water vapor: Distribution and trends. *Encyclopedia of Global Environmental Change, John Wiley & Sons, Ltd, Chichester*.

Seidel, D. J., Berger, F. H., Immler, F., Sommer, M., V¨omel, H., Diamond, H. J., Dykema, J., Goodrich, D., Murray, W., Peterson, T., et al. (2009). Reference upperair observations for climate: Rationale, progress, and plans. *Bulletin of the American Meteorological Society*, 90(3):361–369.

Shakhashiri, B. (2011). Water. Chemical of The Week, An scifun.org portal. http://scifun.chem.wisc.edu/chemweek/PDF/COW-Water-Jan2011.pdf.

Shrestha, S. M. (2003). Investigations into the estimation of tropospheric delay and wet refractivity using GPS measurements. Master's thesis, Department of Geomatics Engineering, UCGE Reports Number 20180, University of Calgary.

Shuman, F. G. (1978). Numerical weather prediction. *Bulletin of the American Meteorological Society*, 59:5–17.

Smart, C. L. (2015). Weather systems. Website, Accessed on July, 2015. http://www.kean.edu/ csmart/Observing/09.%20Weather%20sytems.pdf.

Soden, B. J., Wetherald, R. T., Stenchikov, G. L., and Robock, A. (2002). Global cooling after the eruption of mount pinatubo: A test of climate feedback by water vapor. *Science*, 296(5568):727–730.

Soler, T. and Snay, R. A. (2004). Transforming positions and velocities between the international terrestrial reference frame of 2000 and north american datum of 1983. *Journal of surveying engineering*, 130(2):49–55.

Solheim, F. S., Vivekanandan, J., Ware, R. H., and Rocken, C. (1999). Propagation delays induced in GPS signals by dry air, water vapor, hydrometeors, and other particulates. *Journal of geophysical research*, 104(D8):9663–9670.

Solheim, F. S. and Ware, R. H. (1997). Atmospheric water vapor sensing system using global positioning satellites. US Patent 5,675,081.

Solomon, S., Qin, D., Manning, M., Chen, Z., Marquis, M., Averyt, K. B., Tignor, M., and Miller, H. L. (2007). Climate change 2007: The physical science basis. contribution of working group i to the fourth assessment report of the intergovernmental panel on climate change. *Climate Change: the IPCC scientific assessment*, page 996.

Soos, A. (2010). Global warming and climate models. Oilprice.com. http://oilprice.com/The-Environment/Global-Warming/Global-Warming-AndClimate-Models.html Accessed on Jan 2013.

Spilker, J. J. (1996). Tropospheric effects on gps. *Global Positioning System: Theory and applications.*, 1:517–546.

Stankov, B. B. (1998). Multisensor retrieval of atmospheric properties. *Bulletin of American Meteorological Society*, 79:1835–1839.

Stanturf, J. A., Warren, M. L., Charnley Jr, S., Polasky, S. C., Goodrick, S. L., Armah, F., and Nyako, Y. A. (2011). Ghana climate change vulnerability and adaptation assessment.

Technical Report by USDA Forest Service for United States Agency for International Development.

Starr, D. and Melfi, S. (1991). The role of water vapor in climate. a strategic research plan for the proposed GEWEX water vapor project(GVaP). NASA Conference Publication, 60pp.

Stepaniak, D. et al. (2013). JRA-55: Japanese 55-year reanalysis, daily 3hourly and 6-hourly data. Research Data Archive at the National Center for Atmospheric Research, Computational and Information Systems Laboratory. http://rda.ucar.edu/datasets/ds628.0/ Accessed March, 2014.

Stimac, J. P. (2006). Weather forecasting. http://www.ux1.eiu.edu/ cfjps/1400/forecasting.html.

Subriana, J. S., Zornoza, J. M. J., and Hern´andez-Pajares, M. (2011). GNSS signal. ESA Navipedia. http://navipedia.net/index.php/GNSS signal.

Subriana, J. S., Zornoza, J. M. J., and Hern´andez-Pajares, M. (2013). GNSS *Data Processing, Vol 1: Fundamentals and Algorithms*. ESA Communications, Noordwijk, the Netherlands.

Sultan, B. and Janicot, S. (2003). The West African monsoon dynamics. part ii: The ’preonset’ and ’onset’ of the summer monsoon. *Journal of Climate*, 16(21):3407–3427.

Tao, W. (2008). Near real-time GPS PPP-inferred water vapor system development and evaluation. Master’s thesis, Department of Geomatics Engineering, UCGE Reports Number 20275, University of Calgary.

Taylor, J. W. and Buizza, R. (2006). Density forecasting for weather derivative pricing. *International Journal of Forecasting*, 22(1):29–42.

Tegedor, J., Øvstedal, O., and Vigen, E. (2014). Precise orbit determination and point positioning using GPS, Glonass, Galileo and BeiDou. *Journal of Geodetic Science*, 4(1).

T´etreault, P., Kouba, J., H´eroux, P., and Legree, P. (2005). Csrs-ppp: an internet service for gps user access to the canadian spatial reference frame. *Geomatica*, 59(1):17–28.

Teunissen, H. (2003). Global climate observing system (GCOS). *Global Atmosphere Watch*, page 140.

GMet editors (2013). Climatology of Ghana. http://www.meteo.gov.gh/website/index.php, Accessed on Jan, 2014.

Thayer, G. D. (1974). An improved equation for the radio refractive index of air. *Radio Science*, 9(10):803–807.

Torge, W. (2001). *Geodesy, 3rd Ed.* Walter de Gruyter.

Troller, M., Geiger, A., Brockmann, E., Bettems, J.-M., Bu¨rki, B., and Kahle, H.-G. (2006). Tomographic determination of the spatial distribution of water vapor using gps observations. *Advances in Space Research*, 37(12):2211–2217.

UCAR (2008). Earth's atmosphere- overview. University Corporation for Atmospheric Research, Center for Science Education. http://scied.ucar.edu/shortcontent/thermosphere-overview. Accessed on Nov 2014.

Uppala, S. M., K˚allberg, P. W., Simmons, A. J., Andrae, U., et al. (2005). The ERA-40 re-analysis. *Quarterly Journal of the Royal Meteorological Society*, 131(612):2961– 3012.

USACE-Editors (2003). NAVSTAR GPS surveying. US Army Corps of Engineers Manual, EM 1110-1-1003. http://www.publications.usace.army.mil/Portals/76/Publications/EngineerManuals/EM 11101-1003.pdf.

USGS-Eds (2011). Greenhouse gases. Science Education Handout, http://education.usgs.gov/lessons/gases.pdf. Accessed on Feb 2013.

Vedel, H. (2000). *Conversion of WGS84 geometric heights to NWP model HIRLAM geopotential heights*. Danish Meteorological Institute.

Vedel, H. (2006). Targeting optimal use of GPS humidity measurements in meteorology. web.dmi.dk/pub/tough/deliverables/d14-final-rep.pdf Accessed on July 2012.

Vedel, H., de Haan, S., and Jones, J. (2010). E-GVAP and the use of ground based GNSS data in meteorology. http://www.igs.org/event/newcastle2010/ Accessed on Aug 2012.

Vedel, H. and Huang, X.-Y. (2003). A NWP impact study with ground based GPS data. Danish Meteorological Institute. http://www2.mmm.ucar.edu/people/huang/publications/ztdda-tsukuba-proc.pdf.

Vogelmann, H., Sussmann, R., Trickl, T., and Reichert, A. (2015). Spatiotemporal variability of water vapor investigated using lidar and FTIR vertical soundings above the Zugspitze. *Atmospheric Chemistry and Physics*, 15(6):3135–3148.

Wallace, J. M. and Hobbs, P. V. (2006). *Atmospheric science: an introductory survey*, volume 92. Academic press.

Wang, H., Wei, M., Li, G., Zhou, S., and Zeng, Q. (2013). Analysis of precipitable water vapor from GPS measurements in chengdu region: Distribution and evolution characteristics in autumn. *Advances in Space Research*, 52(4):656–667.

Wang, Z. (2007). Weather forecasting – introduction. Website, Accessed on July, 2015. http://www-das.uwyo.edu/ zwang/atsc2000/Ch14.pdf.

Ware, R. H., Fulker, D. W., Stein, S. A., Anderson, D. N., Avery, S. K., Clark, R. D., Droegemeier, K. K., Kuettner, J. P., Minster, J. B., and Sorooshian, S. (2000). Suominet: A real-time national gps network for atmospheric research and education. *Bulletin of the American Meteorological Society*, 81(4):677–694.

Watson, R. T., Rodhe, H., Oeschger, H., and Siegenthaler, U. (1990). Greenhouse gases and aerosols. *Climate Change: the IPCC scientific assessment*, 1:17.

Weast, R. C., Lide, D. R., Astle, M. J. K., and Beyer, W. H. (1989). Handbook of chemistry and physics. –1989–1990.

Wells, D. E., Beck, N., Delikaraoglou, D., Kleusberg, A., Krakiwsky, E. J., Lachapelle, G., Langley, R. B., Nakiboglu, M., Schwarz, K. P., Tranquilla, J. M., et al. (1999). Guide to GPS positioning. Geodesy & Geomatics Lecture Notes; 58, http://www2.unb.ca/gge/Pubs/LN58.pdf.

Wickert, J. (2014). GNSS water vapour tomography. Website, Accessed on Feb, 2015. http://www.gfz-potsdam.de/en/section/gps-galileo-earthobservation/projects/gnss-tomography/.

Wolfe, D. E. and Gutman, S. I. (2000). Developing an operational, surface-based, GPS, water vapor observing system for naoo: Network design and results. *Atmospheric and Oceanic Technology*, 17(4):426–440.

Wu, J. T., Wu, S. C., Hajj, G. A., Bertiger, W. I., and Lichten, S. M. (1993). Effects of antenna orientation on gps carrier phase. *Manuscripta Geodaetica*, 18:91–91.

WW2010 (2015). Geopotential height. Website, Accessed on March, 2015. Department of Atmospheric Sciences (DAS) http://ww2010.atmos.uiuc.edu/%28Gh%29/guides/mtr/cyc/upa/hght.rxml.

Yilmaz, N. (2008). Comparison of different height systems. *Geo-spatial Information Science*, 11(3):209–214.

Yoshihara, T., Tsuda, T., and Hirahara, K. (2000). High time resolution measurements of precipitable water vapor from propagation delay of GPS satellite signals. *EARTH, PLANETS AND SPACE*, 52(7):479–494.

Appendix A

Plots and Charts

A.1 Curve Fitting and Model

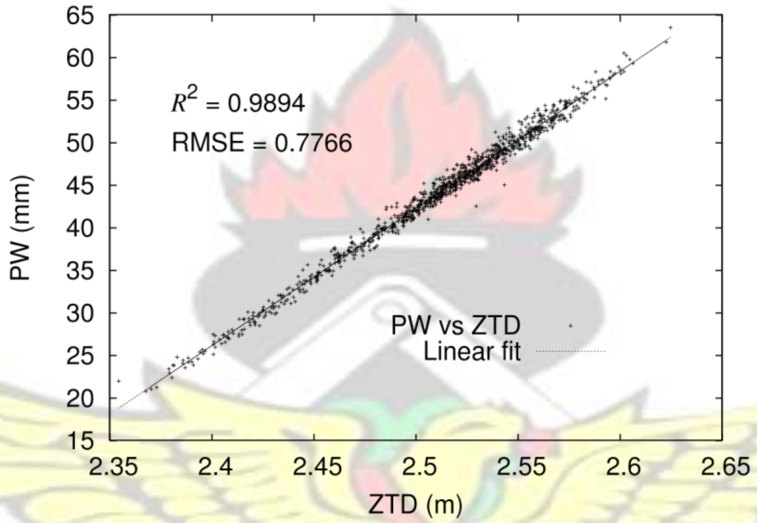

(a) Linear fit with $R^2 = 0.9894$ and $RMSE = 0.7766$ yielding $F(x) = 161.2(x) - 360.7$

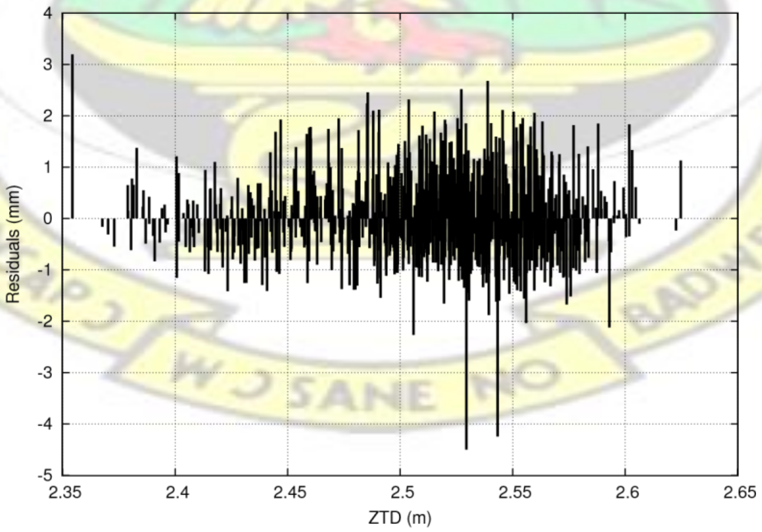

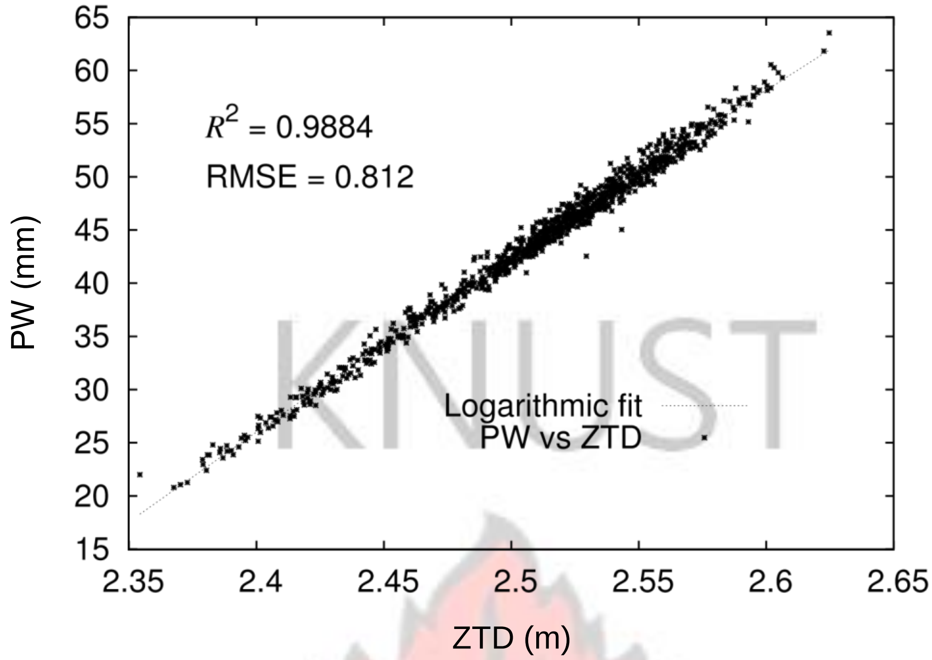

(a) Logarithmic fit with $R^2 = 0.9884$ and $RMSE = 0.812$ yielding $F(x) = 401.35 \cdot ln(x) - 325.37$

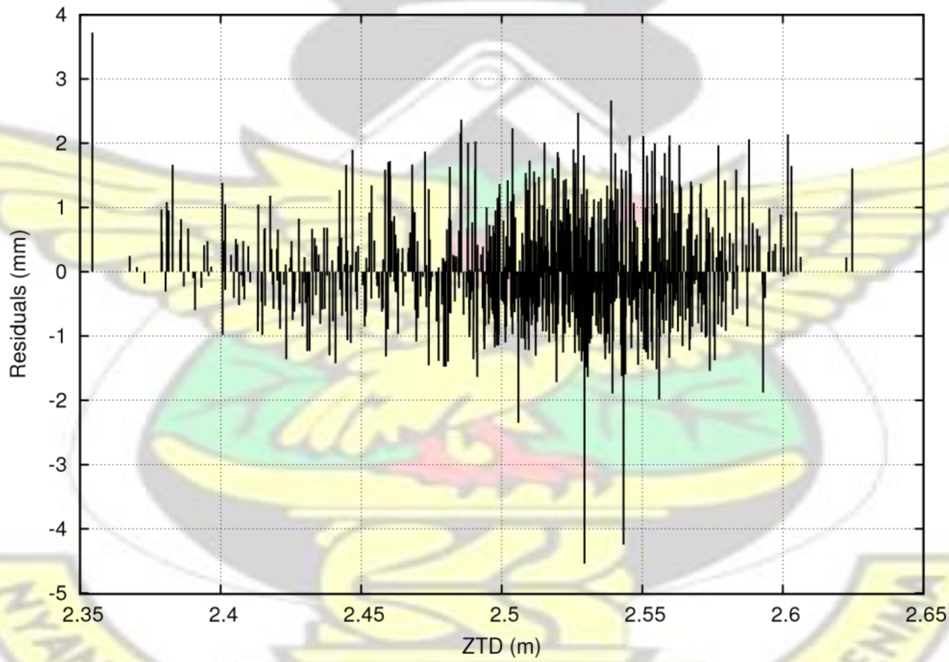

(b)

Figure A.2: Linear-fitting models: Logarithmic fit

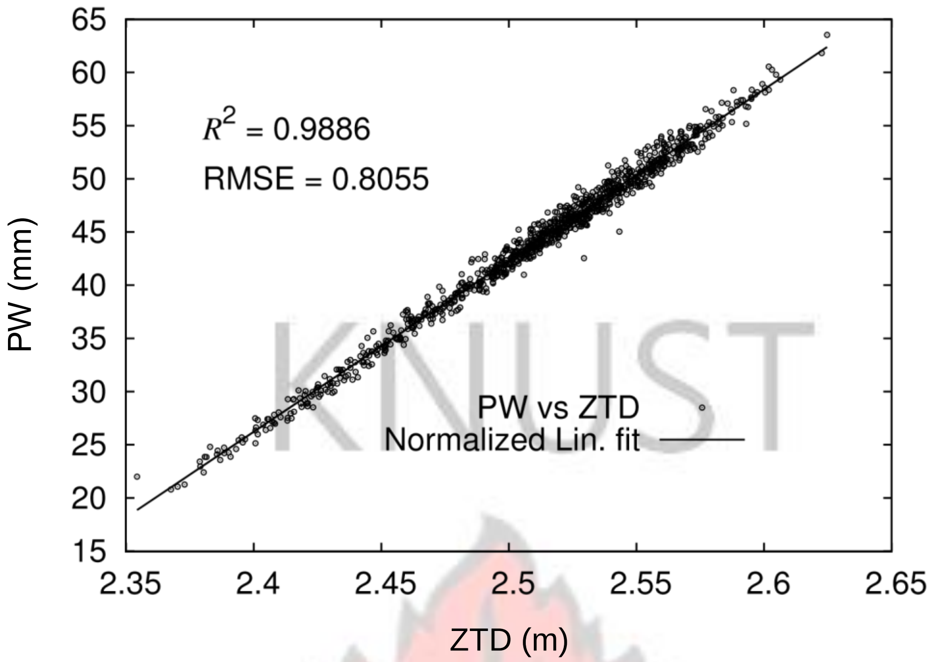

(a) Normalized-Linear fit with $R^2 = 0.9886$ and $RMSE = 0.8055$ yielding $F(x) = 7.49(z) + 44.09$, where $z = \frac{x-\mu}{\sigma}$, $\mu = 2.511$ & $\sigma = 0.04653$

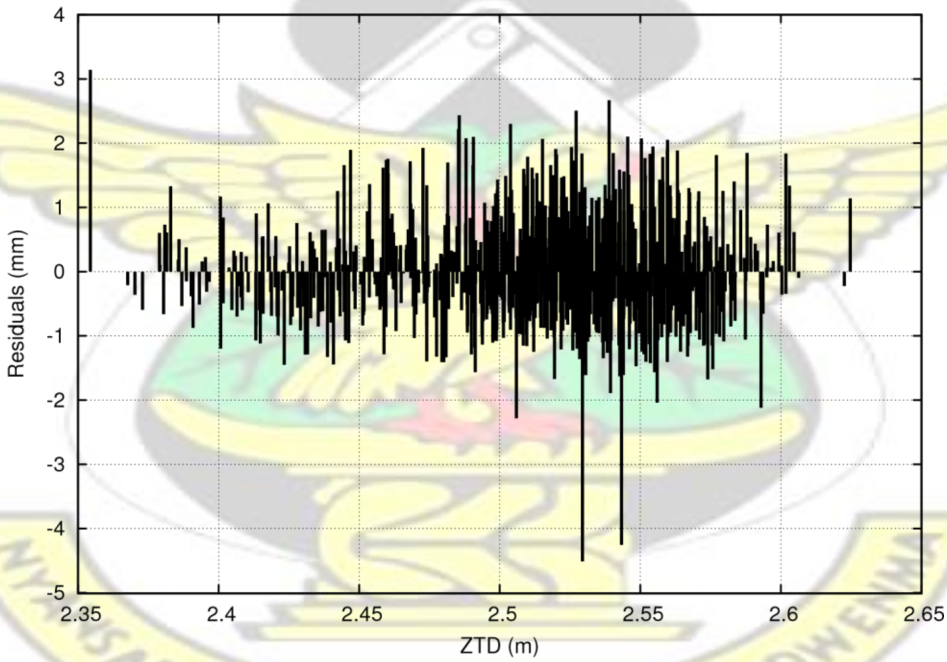

(b)

Figure A.3: Linear-fitting models: Normalized Linear fit

A.2 Linear Model and Reanalysis Data Comparison

Linear model trendline with 95% C.I. bounds and JRA Reanalysis Data comparison

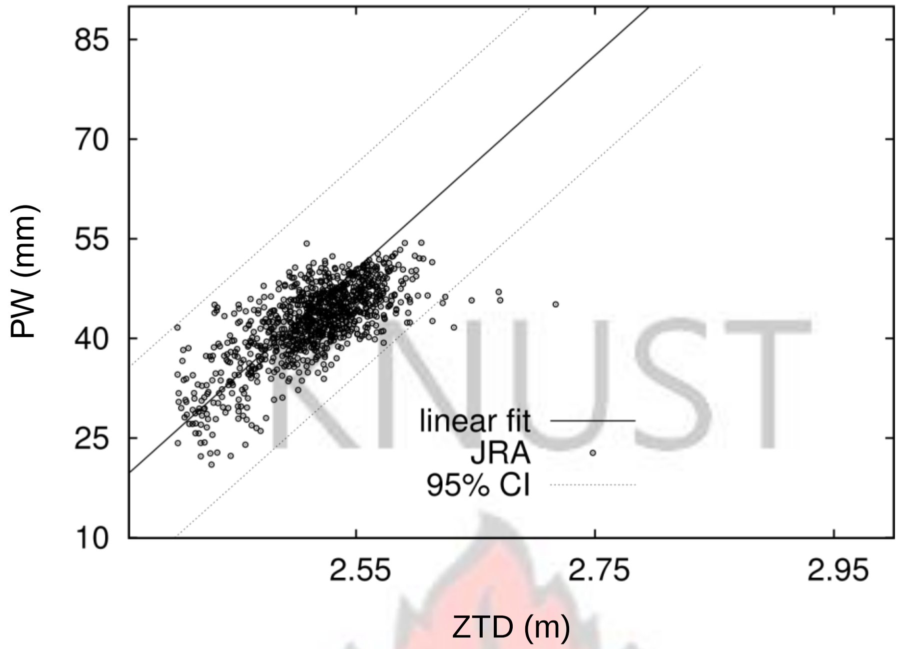

(a) Linear fit with JRA

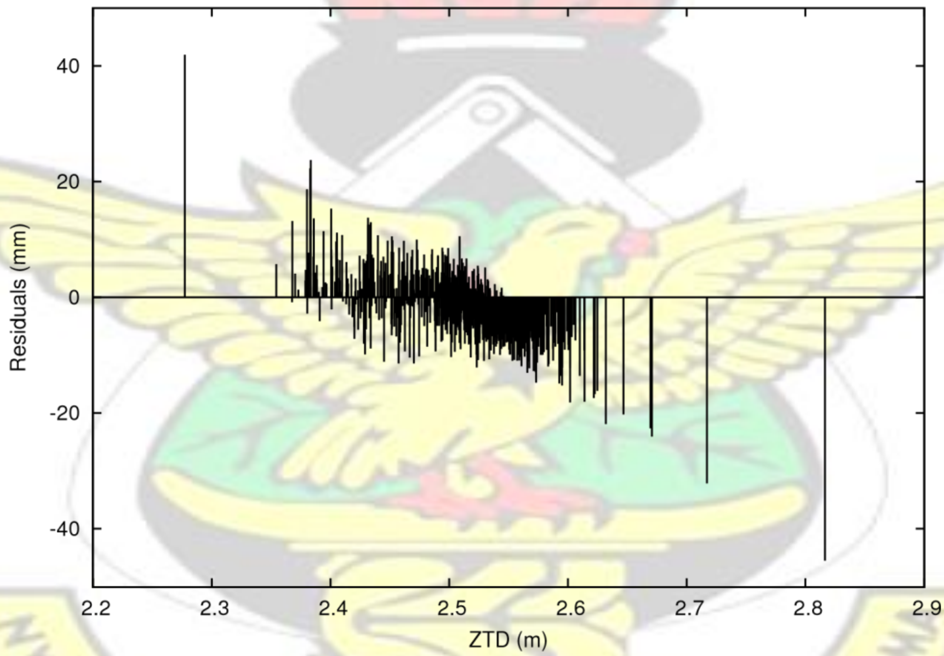

(b) SE of Estimate = 6.0139

Figure A.4: Linear model Trendline and JRA comparison
Linear model trendline with 95% C.I. bounds and ERA-Interim Reanalysis Data comparison

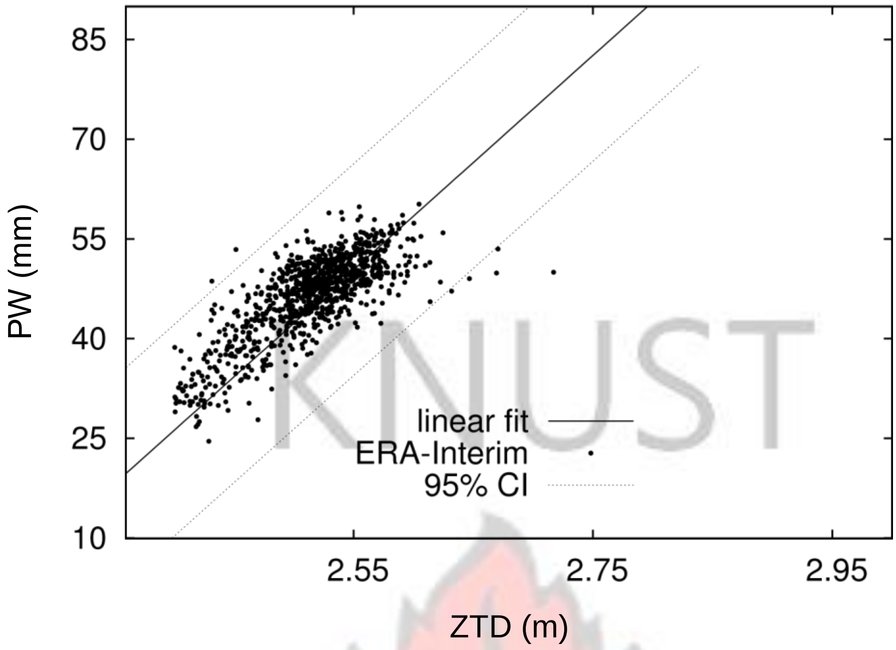

(a) Linear fit with ERA-Interim

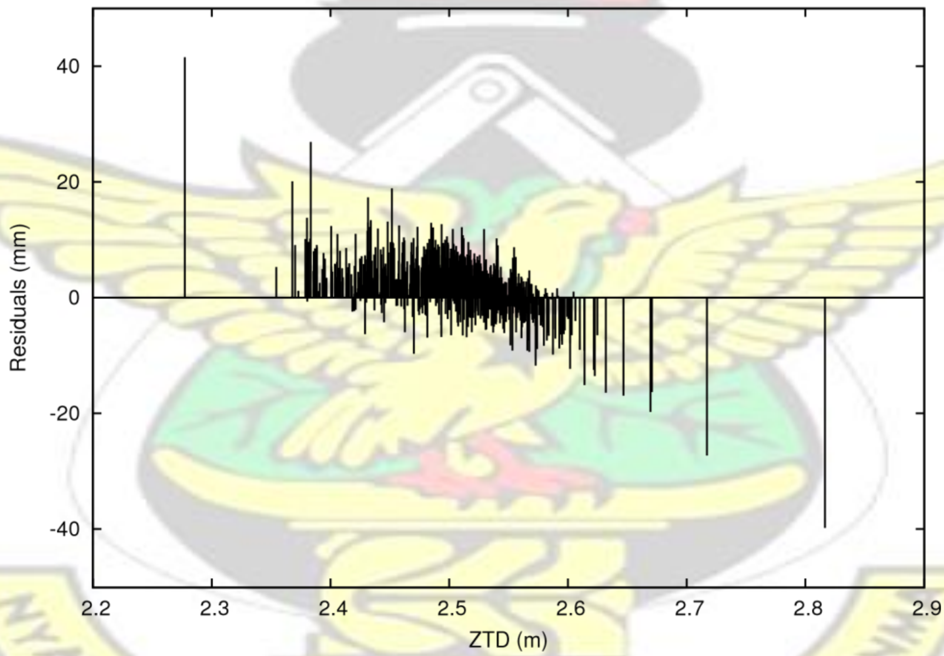

(b) SE of Estimate = 5.398

Figure A.5: Linear model Trendline and ERA-Interim Comparison

Linear model trendline with 95% C.I. bounds and NCEP-R1 Reanalysis Data comparison

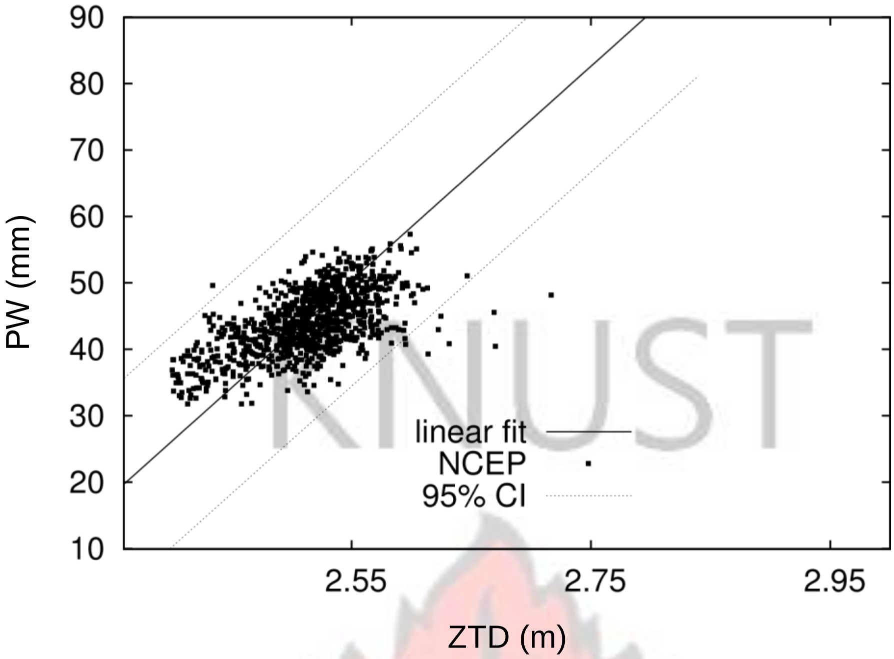

(a) Linear fit with NCEP-R1

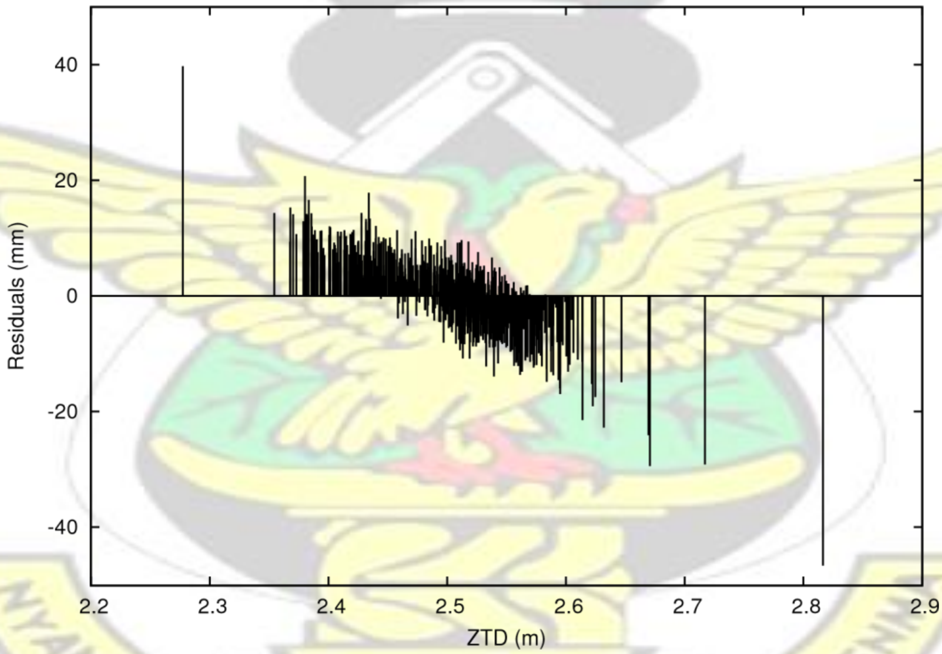

(b) SE of Estimate = 6.338

Figure A.6: Linear model Trendline and NCEP-R1 Comparison

A.3 Seasonal Variations of PW

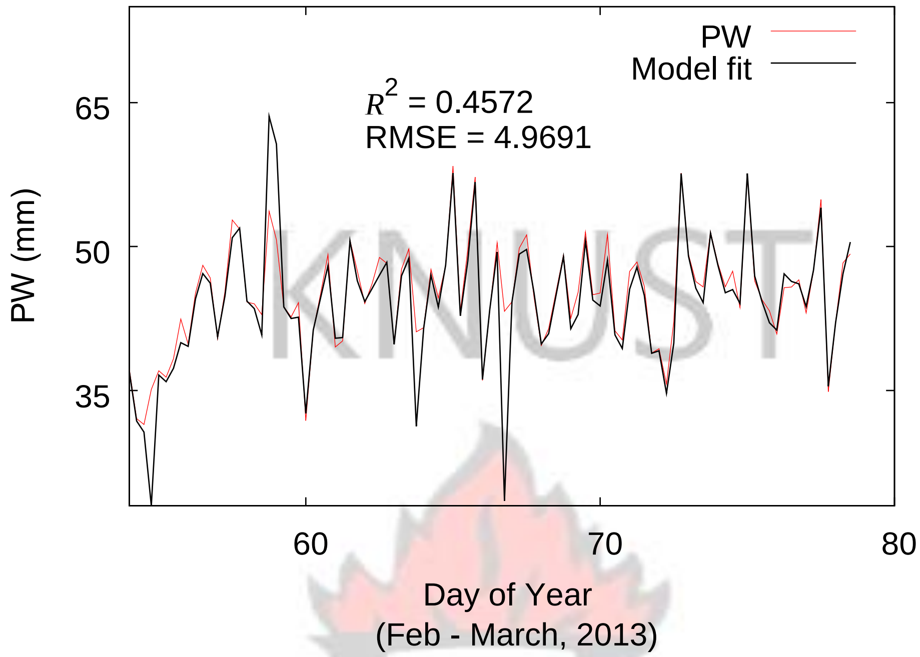

(a)

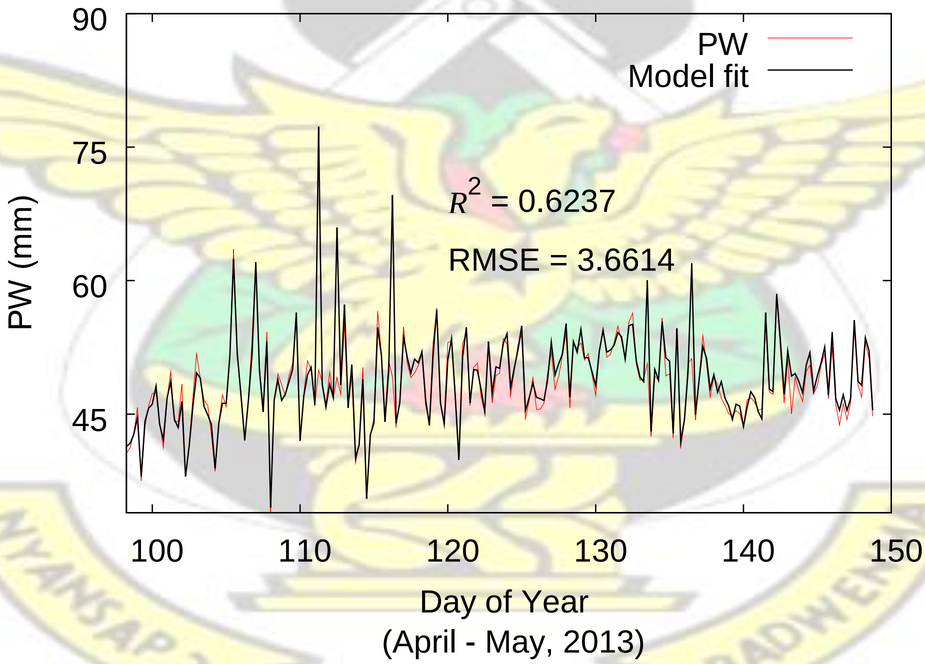

(b)

Figure A.7: PW values against DoY grouped according to weather seasons (a)

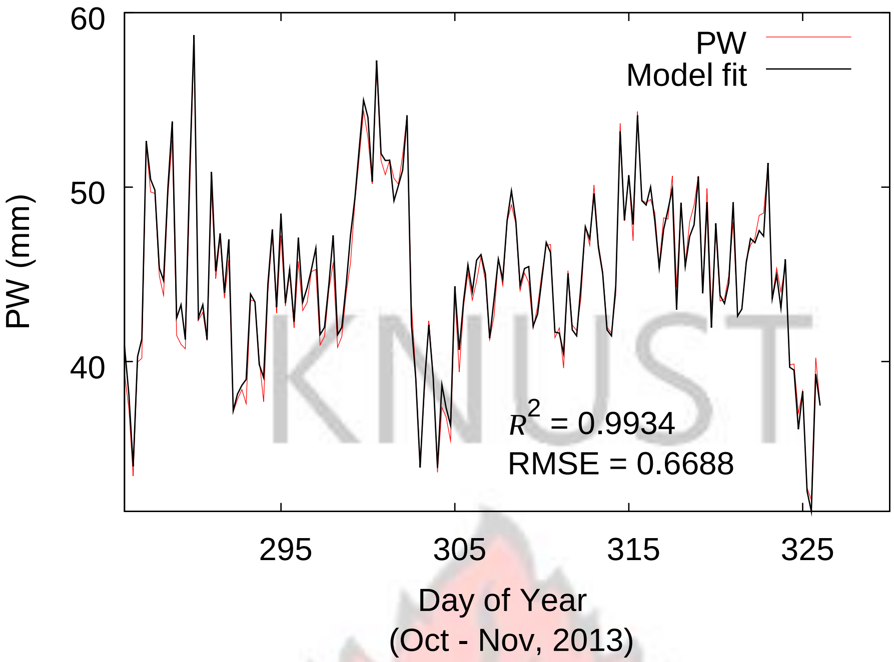

(a)

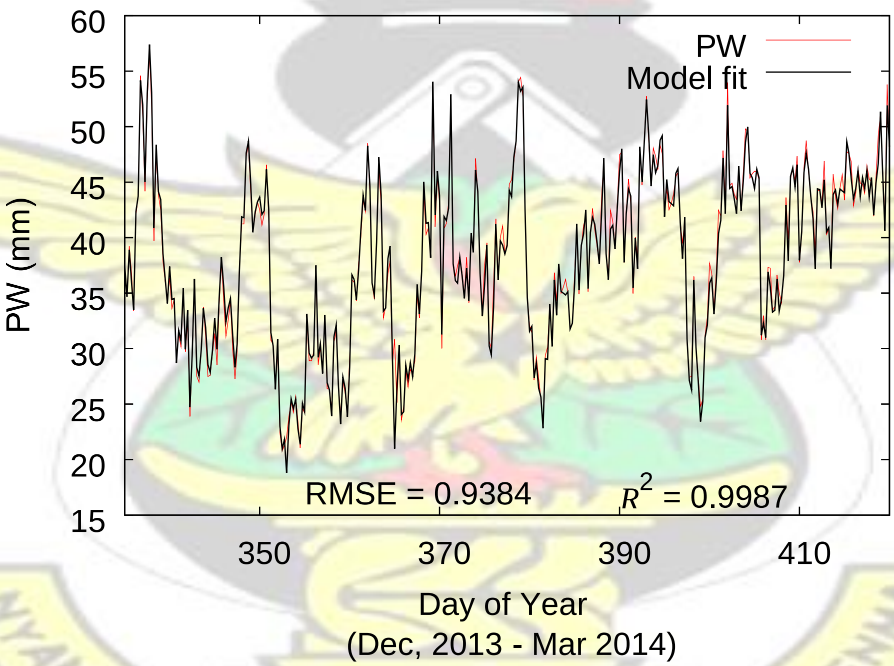

(b)

Figure A.8: PW values against DoY grouped according to weather seasons (b)

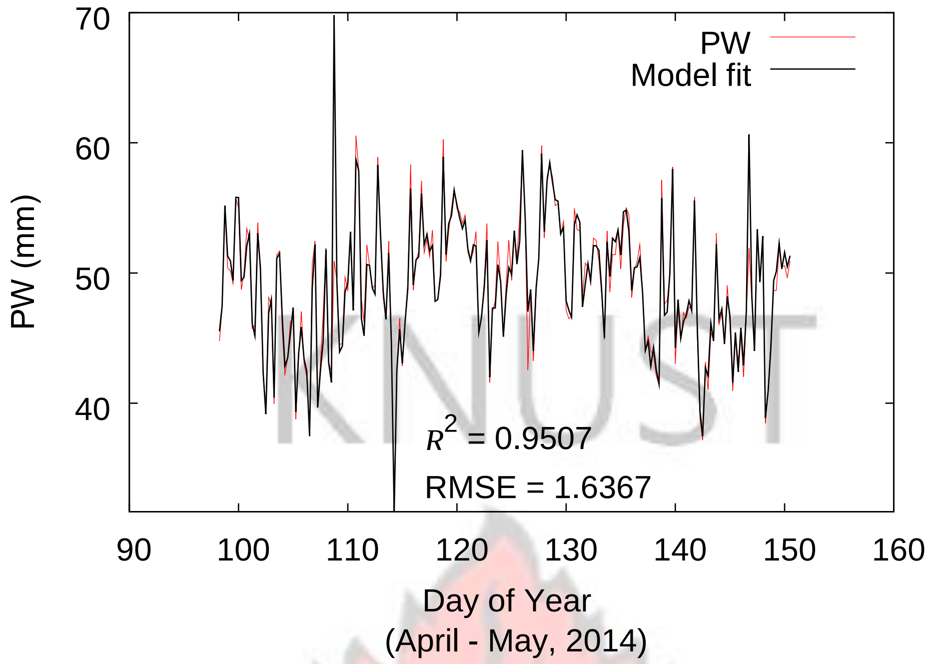

(a)

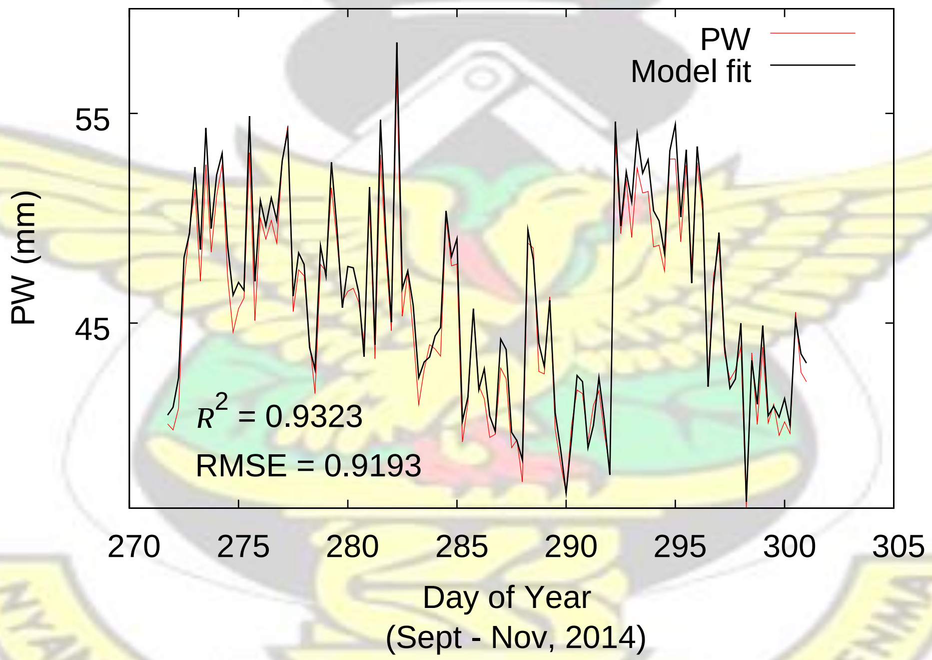

(b)

Figure A.9: PW values against DoY grouped according to weather seasons (c)

Appendix B

Processed Coordinates for Antenna Position

B.1 Results from GLAB using PPP

	Mean Antenna Position: gLAB
X	6333147.8021 m ± 0.0023
Y	-173104.3697 m ± 0.0012
Z	736230.3934 m ± 0.0010

Table B.1: gLAB Processed Coordinates of the Antenna Position

	ITRF08 Coordinates		
Date	X	Y	Z
Oct 01	6333147.7970	-173104.3656	736230.3849

Oct 02	6333147.7869	-173104.3694	736230.3892
Oct 04	6333147.8033	-173104.3680	736230.3898
Oct 05	6333147.7960	-173104.3615	736230.3870
Oct 06	6333147.7890	-173104.3656	736230.3849
Oct 08	6333147.7950	-173104.3740	736230.3857
Oct 30	6333147.7936	-173104.3735	736230.3909
Nov 02	6333147.8040	-173104.3792	736230.3908
Nov 03	6333147.8051	-173104.3718	736230.3963
Nov 04	6333147.8051	-173104.3718	736230.3963
Nov 05	6333147.7855	-173104.3673	736230.3915
Nov 06	6333147.8140	-173104.3661	736230.3945
Nov 07	6333147.7990	-173104.3675	736230.3919
Nov 08	6333147.7997	-173104.3578	736230.3960
Nov 09	6333147.7841	-173104.3648	736230.3901
Dec 01	6333147.8220	-173104.3677	736230.3967
Dec 02	6333147.8155	-173104.3793	736230.3945
Dec 03	6333147.8138	-173104.3758	736230.4011
Dec 04	6333147.8119	-173104.3679	736230.3972
Dec 05	6333147.8110	-173104.3763	736230.3952
Dec 06	6333147.8006	-173104.3718	736230.3939
Dec 07	6333147.8149	-173104.3715	736230.4006

B.2 Results from CSRS-PPP online PPP

Mean Antenna Position

X 6333147.8198 m ± 0.0014

Y -173104.3677 m ± 0.0008

Z 736230.3927 m ± 0.0008

Table B.2: CSRS-PPP Processed Coordinates of the Antenna Position

Date	ITRF08 Coordinates X	Y	Z
Oct 01	6333147.8177	-173104.3670	736230.3883
Oct 02	6333147.8159	-173104.3711	736230.3907
Oct 04	6333147.8191	-173104.3697	736230.3899
Oct 05	6333147.8164	-173104.3656	736230.3885
Oct 06	6333147.8090	-173104.3683	736230.3856
Oct 08	6333147.8116	-173104.3735	736230.3878
Oct 30	6333147.8172	-173104.3602	736230.3921
Nov 02	6333147.8233	-173104.3675	736230.3934
Nov 03	6333147.8217	-173104.3644	736230.3911
Nov 04	6333147.8175	-173104.3605	736230.3952
Nov 05	6333147.8063	-173104.3691	736230.3925

Nov 06	6333147.8217	-173104.3683	736230.3925
Nov 08	6333147.8230	-173104.3655	736230.3933
Dec 01	6333147.8282	-173104.3659	736230.3950
Dec 02	6333147.8297	-173104.3662	736230.3942
Dec 03	6333147.8185	-173104.3703	736230.3964
Dec 04	6333147.8251	-173104.3687	736230.3958
Dec 05	6333147.8183	-173104.3703	736230.3942
Dec 07	6333147.8283	-173104.3707	736230.3987
Dec 29	6333147.8274	-173104.3721	736230.3997

B.3 Results from GAPS online PPP

Mean Antenna Position X

6333147.8545 m ± 0.0018

Y -173104.3671 m ± 0.0007

Z 736230.3986 m ± 0.0009

Table B.3: GAPS Processed Coordinates of the Antenna Position

	ITRF08 Coordinates		
Date	X	Y	Z
Oct 01	6333147.8459	-173104.3646	736230.3943
Oct 02	6333147.8497	-173104.3697	736230.3940
Oct 04	6333147.8543	-173104.3699	736230.3938
Oct 05	6333147.8503	-173104.3673	736230.3960
Oct 06	6333147.8440	-173104.3688	736230.3921
Oct 08	6333147.8430	-173104.3714	736230.3972
Oct 30	6333147.8504	-173104.3620	736230.3936
Nov 02	6333147.8481	-173104.3617	736230.3992
Nov 03	6333147.8514	-173104.3679	736230.3970
Nov 04	6333147.8511	-173104.3633	736230.3966
Nov 05	6333147.8403	-173104.3732	736230.3966
Nov 06	6333147.8535	-173104.3708	736230.3991
Nov 08	6333147.8673	-173104.3693	736230.4021
Nov 08	6333147.8585	-173104.3677	736230.4000
Dec 01	6333147.8620	-173104.3648	736230.4010
Dec 02	6333147.8627	-173104.3699	736230.4040
Dec 03	6333147.8605	-173104.3634	736230.4045
Dec 04	6333147.8616	-173104.3653	736230.4013
Dec 05	6333147.8585	-173104.3626	736230.4012
Dec 07	6333147.8660	-173104.3677	736230.4039
Dec 29	6333147.8652	-173104.3671	736230.4048

B.4 Results from APPS online PPP

Mean Antenna Position X

6333147.8099 m ± 0.0018

Y -173104.3702 m ± 0.0005

Z 736230.3899 m ± 0.0005

Table B.4: APPS Processed Coordinates of the Antenna Position

	ITRF08 Coordinates		
Date	X	Y	Z
Oct 01	6333147.8074	-173104.3703	736230.3870
Oct 02	6333147.8121	-173104.3697	736230.3887
Oct 04	6333147.8079	-173104.3716	736230.3869
Oct 05	6333147.8181	-173104.3747	736230.3903
Oct 06	6333147.8012	-173104.3727	736230.3859
Oct 10	6333147.8316	-173104.3717	736230.3913
Oct 30	6333147.8066	-173104.3678	736230.3899
Nov 02	6333147.8206	-173104.3682	736230.3914
Nov 03	6333147.8087	-173104.3710	736230.3911
Nov 04	6333147.8040	-173104.3656	736230.3861
Nov 05	6333147.8041	-173104.3704	736230.3886
Nov 06	6333147.8131	-173104.3697	736230.3913
Nov 08	6333147.7971	-173104.3712	736230.3899
Dec 01	6333147.8169	-173104.3704	736230.3898
Dec 02	6333147.8040	-173104.3665	736230.3907
Dec 03	6333147.8085	-173104.3677	736230.3940
Dec 04	6333147.8132	-173104.3710	736230.3896
Dec 05	6333147.7974	-173104.3713	736230.3903
Dec 07	6333147.8127	-173104.3700	736230.3926
Dec 29	6333147.8141	-173104.3732	736230.3940

B.5 Results from AUSPOS online PPP

Mean Antenna Position X

6333147.8185 m ± 0.0018

Y -173104.3626 m ± 0.0005

Z 736230.3862 m ± 0.0005

Table B.5: AUSPOS Processed Coordinates of the Antenna Position

	ITRF08 Coordinates		
Date	X	Y	Z
Oct 01	6333147.8210	-173104.3620	736230.3840
Oct 02	6333147.8210	-173104.3600	736230.3890
Oct 04	6333147.8120	-173104.3660	736230.3830
Oct 05	6333147.8260	-173104.3670	736230.3880
Oct 06	6333147.8020	-173104.3600	736230.3840
Oct 08	6333147.8130	-173104.3690	736230.3860
Nov 02	6333147.8170	-173104.3720	736230.3890
Nov 03	6333147.8160	-173104.3570	736230.3860
Nov 04	6333147.8170	-173104.3580	736230.3830
Nov 05	6333147.8120	-173104.3640	736230.3860
Nov 06	6333147.8180	-173104.3570	736230.3830
Nov 07	6333147.8160	-173104.3610	736230.3850
Nov 08	6333147.8350	-173104.3640	736230.3910
Nov 08	6333147.8200	-173104.3640	736230.3880
Dec 01	6333147.8100	-173104.3570	736230.3860
Dec 02	6333147.8280	-173104.3660	736230.3870
Dec 03	6333147.8400	-173104.3660	736230.3900
Dec 04	6333147.8160	-173104.3620	736230.3880
Dec 05	6333147.8130	-173104.3640	736230.3900
Dec 06	6333147.8140	-173104.3610	736230.3900
Dec 07	6333147.8180	-173104.3610	736230.3900
Dec 29	6333147.8210	-173104.3600	736230.3890

Appendix C

The gLAB GNSS Processing

Software

C.1 Interfaces of the gLAB Software

Figure C.1: gLAB start-up page

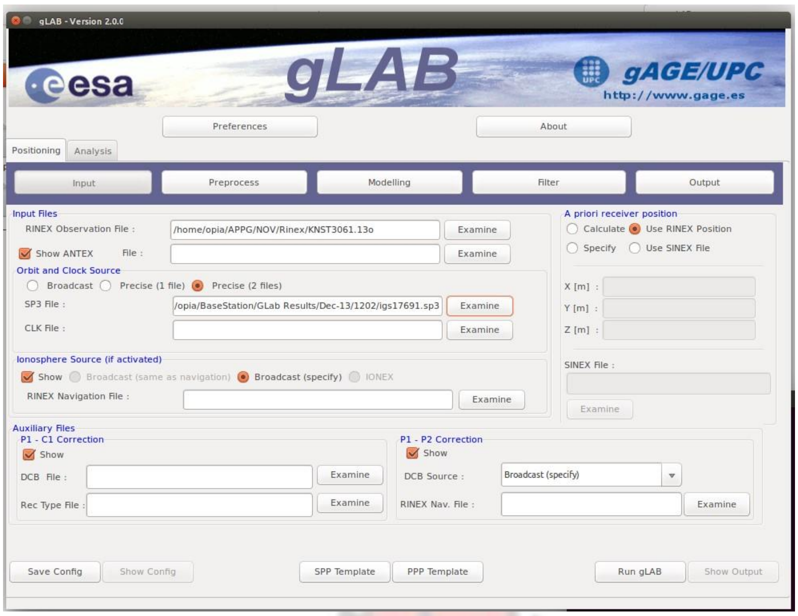

Figure C.2: gLAB: data input page

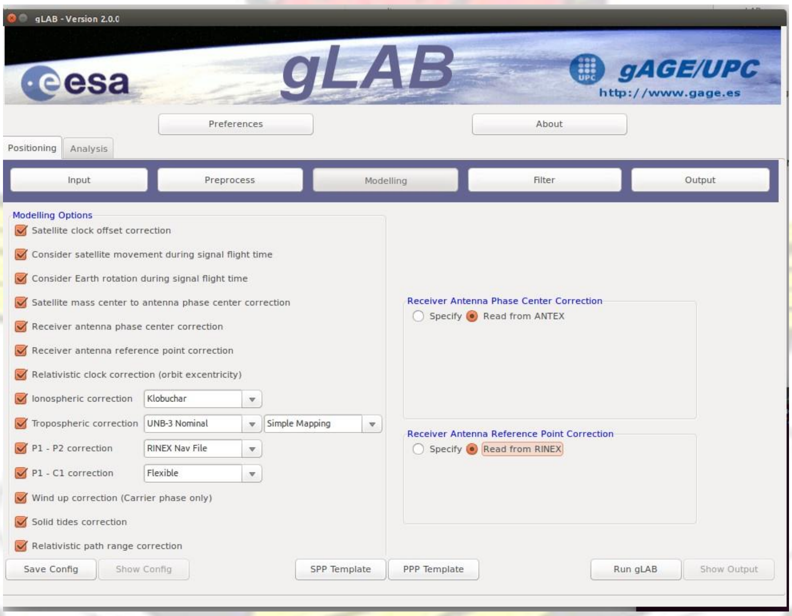

Figure C.3: gLAB: data pre-process and parameter settings page

Below are links to the developers main website, user manual, data and tutorial slides (Hernandez-Pajares et al., 2010):

Main page:- http://gage14.upc.es/gLAB/

The User Manual:- http://gage14.upc.es/gLAB/docs/EDUNAV-SUM-gAGE UPC.pdf Tutorial Slides:- http://gage14.upc.es/gLAB/GNSS _Data Processing _Lab Exercises

C.2 RINEX

Receiver Independent Exchange Format (RINEX) is a data interchange format that works on all GNSS processing software irrespective of the receiver used to log the data. Detailed information on RINEX can be found in Gurtner and Estey (2007). The version used for the study was 2.11.

```
     2.11           OBSERVATION DATA    G (GPS)             RINEX VERSION / TYPE
teqc  2013Mar15                         20140211 13:00:39UTCPGM / RUN BY / DATE
Linux2.4.20-8|i386|gcc|Win32-MinGW32|=                      COMMENT
teqc  2013Mar15                         20140211 12:19:59UTCCOMMENT
Planning v4.21      Geomatic Eng. Dept  10-Feb-14 12:07     COMMENT
KNUST                                                       MARKER NAME
Akwasi A Acheampong KNUST                                   OBSERVER / AGENCY
SVA05180005                             2.111               REC # / TYPE / VERS
                    SOK600                                  ANT # / TYPE
  6333147.8037  -173104.3720   736230.3861                  APPROX POSITION XYZ
        0.0000        0.0000        0.0000                  ANTENNA: DELTA H/E/N
     1     1                                                WAVELENGTH FACT L1/2
     7    L1    L2    C1    C2    P2    D1    D2            # / TYPES OF OBSERV
    30.0000                                                 INTERVAL
teqc windowed: start @ 2014 Feb  3 00:00:00.000             COMMENT
teqc windowed:  end  @ 2014 Feb  3 23:59:30.000             COMMENT
  2014     2     3     0     0    0.0000000     GPS         TIME OF FIRST OBS
                                                            END OF HEADER
 14  2  3  0  0  0.0000000  0 10G22G29G06G25G18G14G24G21G12G31
 127785419.113    99573093.551    24316742.688                    24316749.039
       747.164         582.215
 115510132.180    90007947.090    21980820.984                    21980823.062
     -2516.641       -1961.023
 128615149.969   100219637.105    24474651.734                    24474661.578
      1988.801        1549.723
 120250336.008    93701683.035    22882848.516                    22882854.641
```

Figure C.4: Sample Rinex header for Observation session on 3rd Feb, 2014

C.3 APPS Final Output

APPS Summary file for site 0015. Produced from RINEX file KNST3361.13O on Fri Jun 20 11:53:03 UTC 2014

The reference frame is ITRF 2008 (with semi-major axis = 6378137 m; flattening factor = 1/298.257222101)

Output data rate is 300 seconds. Minimum elevation angle is 7.5 degrees.

Satellite antenna phase center offset and maps taken from IGS Standards igs08 1740.atx.

Receiver antenna phase center offset and maps taken from IGS Standards igs08 1740.atx.

Receiver antenna phase center offset relative to the antenna reference is 0 m

The antenna reference point offset from the monument reference, based on the RINEX file header, is 0 m

Product used to process KNST3361.13O: JPL Final

Static point positioning mode (a single set of site coordinates are estimated):

Total number of Phase measurements: 2428. RMS post-fit Phase residuals: 0.013 m. Number of excluded Phase measurements: 30

Total number of Pseudorange measurements: 2458. RMS post-fit PRange residuals: 0.816 m. Number of excluded PRange measurements: 0

Estimated Cartesian coordinates: X = 6333147.8040 m Y = -173104.3665 m Z = 736230.3907 m

Sigmas of Cartesian coordinates: SigX = 0.0029 m SigY = 0.0008 m SigZ = 0.0008 m

Estimated Geodetic coordinates (WGS84/GRS80): Lat = 6.67270394 deg East Lon = -1.56567967 deg Height = 296.5295 m

Sigmas of Geodetic coordinates: SigLat = 0.0006 m SigLon = 0.0008 m SigHeight = 0.0029 m

Time variable estimated parameters:

Table C.1: Output from APPS

#Secs from start	GPS Time(yyyy:mm:dd:hh:mm:ss.ssss)	HZTrop(m)	WZTrop(m)	Sig(m)	Clock(m)	Sig(m)
0.0000	2013:12:02:00:00:0.0000	2.2213	0.2450	0.003	0.509	0.021
300.0000	2013:12:02:00:05:0.0000	2.2213	0.2452	0.002	0.597	0.021
600.0000	2013:12:02:00:10:0.0000	2.2213	0.2454	0.002	0.472	0.021
900.0000	2013:12:02:00:15:0.0000	2.2213	0.2454	0.002	0.276	0.021
1200.0000	2013:12:02:00:20:0.0000	2.2213	0.2453	0.002	0.754	0.021
1500.0000	2013:12:02:00:25:0.0000	2.2213	0.2447	0.002	0.563	0.021
1800.0000	2013:12:02:00:30:0.0000	2.2213	0.2441	0.002	0.532	0.021
2100.0000	2013:12:02:00:35:0.0000	2.2213	0.2436	0.002	0.375	0.021
2400.0000	2013:12:02:00:40:0.0000	2.2213	0.2432	0.002	0.560	0.021
2700.0000	2013:12:02:00:45:0.0000	2.2213	0.2430	0.002	0.383	0.021
3000.0000	2013:12:02:00:50:0.0000	2.2213	0.2427	0.002	0.477	0.021
3300.0000	2013:12:02:00:55:0.0000	2.2213	0.2426	0.002	0.508	0.021

C.4 CSRS-PPP Final Output

GPS Precise Point Positioning (CSRS-PPP ver. 1.05/34613/2013-12-12)

Natural Resources Canada, Geodetic Survey Division, Geomatics Canada
615 Booth Street, room 440, Ottawa, Ontario, Canada, K1A 0E9
Phone: (613) 995-4410, fax: (613) 995-3215
Email: information@geod.nrcan.gc.ca

————————————————————————————-

Processing Options

User dynamics	STATIC
Observation processed	CODE & PHASE
Frequency observed	L3
Satellite orbits	PRECISE
Satellite product input	CLK-RINEX
Ionospheric model	L1 & L2
Marker coordinates	ESTIMATED
Troposphere zenith delay (TZD)	ESTIMATED
Clock interpolation	YES
Parameter smoothing	NO
Reference frame	ITRF
Ellipsoid for lat, long, h	WGS84
Coordinate system	ELLIPSOIDAL
Satellite clock interval (s)	30
Pseudorange sigma (m)	2.000
Carrier phase sigma (m)	0.015
TZD random walk ($mm/hr^{1/2}$)	5.000
Marker to ARP distance (m)	0.000
Cutoff elevation (deg)	10.000

Table C.2: Output from CSRS-PPP

STN	YEAR-MM-DD	HR:MN:SS.SSS	NSV	DLAT(m)	DLON(m)	DHGT(m)	CLK(ns)	TZD(m)	STZD(m)
15	2013-12-01	00:00:00.000	9	-0.1190	-0.7560	-0.1520	0.8890	2.4323	0.0999
15	2013-12-01	00:00:30.000	9	-0.1440	-0.8030	0.3750	0.9150	2.4310	0.0997
15	2013-12-01	00:01:00.000	9	-0.0620	-0.5050	-0.3530	1.0190	2.4241	0.0992
15	2013-12-01	00:01:30.000	9	-0.1450	-0.7010	0.4370	2.0830	2.4270	0.0981
15	2013-12-01	00:02:00.000	9	-0.2180	-0.7050	0.6310	1.0880	2.4288	0.0964
15	2013-12-01	00:02:30.000	8	-0.2630	-0.7110	0.6760	2.4900	2.4265	0.0939
15	2013-12-01	00:03:00.000	9	-0.3080	-0.6610	0.7480	2.7690	2.4303	0.0908
15	2013-12-01	00:03:30.000	9	-0.2540	-0.5820	0.5840	2.4980	2.4253	0.0871
15	2013-12-01	00:04:00.000	9	-0.1850	-0.5650	0.6000	2.4780	2.4227	0.0830

C.5 gLAB Final Output

INFO Processing with precise products

INFO Forcing ionospheric model for this processing

INFO Forcing enabled tropospheric estimation for this processing

INFO RINEX observation input file:

INFO SP3 orbits file:

INFO Clocks file:

INFO RINEX navigation file for Klobuchar corrections:

INFO File for DCB corrections:

INFO ANTEX antenna input file:

INFO Making equivalence: P1==C1

INFO INPUT Station marker: 00151790

INFO INPUT Antenna type: SOK600

INFO INPUT Receiver type: 0-Unknown

INFO PREPROCESSING Prealign carrier phase measurements: ON

INFO PREPROCESSING Decimation 300

INFO PREPROCESSING Usable frequencies [GPS]: F1 F2

INFO PREPROCESSING Elevation mask: 5.00

INFO PREPROCESSING Discard satellites under eclipse conditions: YES

INFO PREPROCESSING Receiver apriori position: 6333147.8037 -173104.3720 736230.3861 [RINEX]

INFO PREPROCESSING CycleSlip Li: ON [Min:0.034 Max:0.080 t:60.000]

INFO PREPROCESSING CycleSlip BW: ON [Min:0.900 Max:18.000 Slope:9.000]

INFO PREPROCESSING CycleSlip L1C1: OFF

INFO MODELING Satellite clock offset correction: ON

INFO MODELING Consider satellite movement during signal flight time: ON

INFO MODELING Consider Earth rotation during signal flight time: ON

INFO MODELING Receiver Antenna Phase Center Offset (PCO): F1 -0.00072 -0.00007 0.07235

INFO MODELING Receiver Antenna Phase Center Offset (PCO): F2 0.00012 -0.00099 0.08415

INFO MODELING Receiver Antenna Reference Point (ARP): 0.0000 0.0000 0.0000

INFO MODELING Relativistic clock correction: ON

INFO MODELING Ionosphere model: Klobuchar

INFO MODELING Troposphere model: ON

INFO MODELING Troposphere model: Simple Nominal

INFO MODELING Troposphere model: Niell Mapping

INFO MODELING P1-C1 DCB model: Flexible

INFO MODELING P1-P2 DCB model: RINEX

INFO MODELING Wind up correction: ON

INFO MODELING Solid tides correction: ON

INFO MODELING Relativistic path range correction: ON

INFO MODELING Orbit interpolation degree: 10

INFO MODELING Clock interpolation degree: 0

INFO MODELING Use satellite 'SV Health' flag of navigation message: OFF

INFO FILTER Measurement: 1 PC StdDev:1.00

INFO FILTER Measurement: 2 LC StdDev:0.01

INFO FILTER Carrierphase is used: YES

INFO FILTER Estimate troposphere: ON

INFO FILTER Forward Processing

INFO FILTER Parameters [Phi,Q,P0] Position: 1.00e+000 0.00e+000 1.00e+008

INFO FILTER Parameters [Phi,Q,P0] Clock: 0.00e+000 9.00e+010 9.00e+010

INFO FILTER Parameters [Phi,Q,P0] Troposphere: 1.00e+000 1.00e-004 2.50e-001

INFO FILTER Parameters [Phi,Q,P0] Ambiguity: 1.00e+000 0.00e+000 4.00e+002

INFO OUTPUT Satellite Velocity: ITRF

Appendix D

Climate Data Operators

D.1 Installing CDO

How to download and install Climate Data Operator (CDO) with NetCDF, GRIB2 and HDF5 support Building CDO with Netcdf, HDF5 and GRIB2 support. CDO is a collection of command line Operators to manipulate and analyse Climate and NWP model data, there are more than 600 operators available in the software suite (Schulzweida et al., 2009).

Download **CDO** from https://code.zmaw.de/projects/cdo/files. On a Unix platform use the *wget* command.

“wget https://code.zmaw.de/attachments/download/10198/cdo-1.6.9.tar.gz”

Download **NetCDF** from http://www.unidata.ucar.edu/downloads/netcdf/index.jsp Use the C version.

“wget ftp://ftp.unidata.ucar.edu/pub/netcdf/netcdf-4.3.3.1.tar.gz”

Download **Grib API** from https://software.ecmwf.int/wiki/display/GRIB/Releases

https://software.ecmwf.int/wiki/download/attachments/3473437/grib api-1.13.1.tar.gz?api=v2

Download **Jasper** from http://www.ece.uvic.ca/~frodo/jasper/#download.

“wget http://www.ece.uvic.ca/~frodo/jasper/software/jasper-1.900.1.zip”

Download **HDF5** and **zlib** from

“wget https://www.hdfgroup.org/ftp/HDF5/current/bin/linux-centos7-x86 64/hdf5-1.8.15-linux-centos7x86 64-shared.tar.gz”

“wget http://zlib.net/zlib-1.2.8.tar.gz”

How to install **CDO** with **GRIB**, **NetCDF** and **HDF5** support. Note that the binaries are in */opt/cdo-install/bin*. This folder must be created and added to the path to make the binaries available everywhere.

Install zlib using

./configure –prefix =/opt/cdo-install

‘make’, ‘make check’ and ‘make install’

Install HDF5 using

./configure -with-zlib=/opt/cdo-install -prefix=/opt/cdo-install CFLAGS=-fPIC

’make’, ’make check’ and ’make install’

Install NetCDF using

CPPFLAGS=-I/opt/cdo-install/include LDFLAGS=-L/opt/cdo-install/lib ./configure –prefix=/opt/cdoinstall CFLAGS=-fPIC

’make’, ’make check’ and ’make install’

Install Jasper using

./configure -prefix=/opt/cdo-install CFLAGS=-fPIC

’make’, ’make check’ and ’make install’

Install grib using

./configure –prefix=/opt/cdo-install CFLAGS=-fPIC –with-netcdf=/opt/cdo-install –with-jasper=/opt/cdo-install

’make’, ’make check’ and ’make install’

Install cdo using

./configure -prefix=/opt/cdo-install CFLAGS=-fPIC -with-netcdf=/opt/cdo-install -with-jasper=/opt/cdoinstall -with-hdf5=/opt/cdo-install -with-grib api=/opt/cdo-install

’make’, ’make check’ and ’make install’

The commands above will install and set the Unix CC terminal to explore NMP weather data in either GRIB or NetCDF formats using CDO. Some common cdo scripts to view weather data with reference to Schulzweida et al. (2009) are as follows:

user@PC-name:~$ cdo info $\ll inputfile \gg$

This command writes information about the structure and contents of all input datasets to standard output. The parameters are 1) Date and Time, 2) Code number and Level 3) Size of the grid and number of Missing values and 4) Minimum, Mean and Maximum.

user@PC-name:~$ cdo griddes$\ll inputfile \gg$

This gives the description of the grid in the data file whether its a guassian, curvilinear, LatLon or cell. It also identifies the size, boundary and incremental constants.

user@PC-name:~$ cdo sellonlatbox lon1,lon2,lat1,lat2$\ll inputfile \gg \ll outputfile \gg$

Selects a longitude/latitude box. The user has to give the longitudes and latitudes of the edges of the box.

user@PC-name:~$ cdo remapbic $\ll inputfile \gg \ll outputfile \gg$

This module contains operators to *remap* all input fields to a new horizontal grid. Performs a bicubic interpolation on all input fields. This interpolation method only works on regular quadrilateral grids.